

**SPECTROSCOPIC ANALYSIS OF DNA STRANDS  
INFLUENCED BY MAGNETIC FIELD**

**SEYEDEH MARYAM BANIHASHEMIAN**

**FACULTY OF PHYSICS  
UNIVERSITY OF MALAYA  
KUALA LUMPUR**

**2014**

**SPECTROSCOPIC ANALYSIS OF DNA STRANDS  
INFLUENCED BY MAGNETIC FIELD**

**SEYEDEH MARYAM BANIHASHEMIAN**

**THESIS SUBMITTED IN FULFILLMENT OF THE  
REQUIREMENTS FOR THE DEGREE OF  
DOCTOR OF PHILOSOPHY**

**DEPARTMENT OF PHYSICS  
FACULTY OF SCIENCE  
UNIVERSITY OF MALAYA  
KUALA LUMPUR**

**2014**

**UNIVERSITI MALAYA**

# UNIVERSITI MALAYA

## ORIGINAL LITERARY WORK DECLARATION

Name of Candidate: **SEYEDEH MARYAM BANIHASHEMIAN**

I/C/Passport No: **T16284817**

Registration/Matric No.: **SHC100044**

Name of Degree: **DOCTOR OF PHILOSOPHY**

Title of Project Paper/Research Report/Dissertation/Thesis ("this Work"):

**"SPECTROSCOPIC ANALYSIS OF DNA STRANDS INFLUENCED BY MAGNETIC FIELD"**

Field of Study: **NANO BIOELECTRONICS-PHYSICS**

I do solemnly and sincerely declare that:

- (1) I am the sole author/writer of this Work,
- (2) This Work is original,
- (3) Any use of any work in which copyright exists was done by way of fair dealing and for permitted purposes and any excerpt or extract from, or reference to or reproduction of any copyright work has been disclosed expressly and sufficiently and the title of the Work and its authorship have been acknowledged in this Work,
- (4) I do not have any actual knowledge nor do I ought reasonably to know that the making of this work constitutes an infringement of any copyright work,
- (5) I hereby assign all and every rights in the copyright to this Work to the University of Malaya ("UM"), who henceforth shall be owner of the copyright in this Work and that any reproduction or use in any form or by any means whatsoever is prohibited without the written consent of UM having been first had and obtained,
- (6) I am fully aware that if in the course of making this Work I have infringed any copyright whether intentionally or otherwise, I may be subject to legal action or any other action as may be determined by UM.

(Candidate Signature)

Date:

Subscribed and solemnly declared before,

Witness's Signature

Date:

Name: **SAADAH ABDUL RAHMAN**

Designation: **PROFESSOR DATIN DR.**

Witness's Signature

Date:

Name:

Designation:

## LIST OF PUBLICATIONS

### Published

1. Banihashemian, S. M., Periasamy, V., Ritikos, R., Rahman, S. A. and Mousakazemi Mohammadi, S.M. (2013). Spectroscopy of Oligonucleotide DNA in Different Strength of Magnetic Field. *Molecules*, 18, 1797-11808.
2. Khatir, N. M., Banihashemian, S. M., Periasamy, V., Ritikos, R., Abd Majid, W. H. and Rahman, S. A. (2012). Electrical Characterization of Gold-DNA-Gold Structures in Presence of an External Magnetic Field by Means of I-V Curve Analysis. *Sensors*, 12(3), 3578-3586.
3. Khatir, N. M., Banihashemian, S. M., Periasamy, V., Abd Majid, W. H. and Rahman, S. A. (2012). Current-Voltage Characterization on Au-DNA-Au Junctions under the Influence of Magnetic Field. *Advanced Materials Research*, 535, 1350-1353.
4. Khatir, N. M., Banihashemian, S. M., Periasamy, V., Abd Majid, W. H. and Rahman, S. A. (2012). DNA Strand Patterns on Aluminium Thin Films. *Sensors*, 11(7), 6719-6727.

### Submitted

1. Banihashemian, S. M., Periasamy, V., Ritikos, R., Rahman, S. A. and Mousakazemi Mohammadi, S.M. (2013). Magnetic field effect on Optical band gap of Oligonucleotide DNA, (Submitted).
2. Banihashemian, S. M., Periasamy, V. and Rahman, S. A. (2013). Spectroscopic Analysis of Static Magnetic Field (Less Than 1000 mT) Effect on the Integrity of DNA, (Submitted).

## LIST OF CONFERENCES

1. Banihashemian, S. M., Periasamy, V. and Rahman, S. A. Magnetic Field Effect on DNA Temperature In Vitro, *International Conference on New and Advanced Materials (NAMIC)*, 13-15 August 2013, Islamic Azad University, Majlesi Branch, Isfahan, Iran (International).
2. Banihashemian, S. M., Periasamy, V. and Rahman, S. A. Spectroscopic analysis of DNA (Adenine-Thymine) Influenced by Magnetic field, *International Conference on New and Advanced Materials (NAMIC)*, 13-15 August 2013, Islamic Azad University, Majlesi Branch, Isfahan, Iran (International).
3. Khatir, N. M., Banihashemian, S. M., Periasamy, V., Abd Majid, W. H. and Rahman, S. Nano Scale Pattern of DNA Strands of Aluminium Thin Film, *4<sup>th</sup> International Congress on Nanoscience and Nanotechnology (ICNN)*, 8-10 September 2012, University of Kashan, Iran (International).
4. Khatir, N. M., Banihashemian, S. M., Periasamy, V., Abd Majid, W. H. and Rahman, S. Investigation of Magnetic Field Effect on DNA Chain by Current-Voltage Characterization, *26<sup>th</sup> Regional Conference on Solid State Science & Technology (RCSSST)*, 22-23 November 2011, University of Malaya, Malaysia (National).
5. Khatir, N. M., Banihashemian, S. M., Periasamy, V., and Abd Majid, W. H. Novel Method of Fabricating Nano-Gaps Using DNA Strands, *The 6<sup>th</sup> Mathematics and Physical Science Graduate Congress (6th MPSGC)*, 13-15 December 2010, University of Malaya, Malaysia (National).
6. Khatir, N. M., Banihashemian, S. M., Periasamy, V., Abd Majid, W. H. and Rahman, S. A New Method of Forming Nano Cracks Using DNA Strands, *National Physics Conference (PERFIK) Damai Laut*, Perak, 27-

30 October 2010, University Kebangsaan Malaysia, Malaysia (National).

7. Khatir, N. M., Banihashemian, S. M., Periasamy, V., and Abd Majid, W. H. Designing DNA sensor based on Contact Metal-Bio material, *1<sup>st</sup> Nanotechnology Conference (NTC)*, 2-3 June 2009, University of Malaya, Malaysia (International).

## **PATENT AND AWARD**

### **Patent**

1. A New Method of Fabricating Nano-Gaps on Aluminium/Silicon Structures using DNA Strands (2010), Malaysian Patent Number 2010700067.

### **Awards**

2. Silver Medal - Novel Method of Fabricating Nano-Gaps using DNA Strands, Persidangan DNA Ekspo Ciptaan Institusi Pengajian Tinggi Antarabangsa (PECIPTA), 13-15 September 2011, Pusat Konvensyen Kuala Lumpur (KLCC), Malaysia (International).

## ACKNOWLEDGEMENTS

Though only my name appears on the cover of this dissertation, a great many people have contributed to its production. I owe my gratitude to all those people who have made this dissertation possible and because of whom my postgraduate experience has been one that I will cherish forever.

My deepest gratitude goes to my supervisors, Dr. Vengadesh P. and Prof. Datin Dr. Saadah Abdul Rahman. Their patience and support helped me to overcome many crisis situations and complete this dissertation.

Most importantly, none of this would have been possible without the love and patience of my family. My darling daughter, Mohadeseh to whom this dissertation is dedicated, has been a constant source of love, concern, support and strength all these years. I would like to express my heart-felt gratitude to my Mother on earth and my Father in the sky, who prayed for me always.

Many friends have helped me to stay sane throughout these difficult years. Their support and care helped me overcome setbacks and stay focused on my postgraduate study. I greatly value their friendship and I deeply appreciate their belief in me.

I would like to acknowledge Dr. Mohammad Mahmoudian, who helped me improve my knowledge in the area.

I am thankful to the technical staffs that maintained all the machines in Low Dimensional Materials Research Centre's laboratory. I am also grateful to both the former and current staffs at University of Malaya.

Finally, I appreciate the financial support provided by University of Malaya, which was used to fund the research discussed in this dissertation and Brightspark Scholarship.



## ABSTRAK

Dalam tahun-tahun kebelakangan ini, jumlah penyelidikan berkaitan dengan penderiaan peranti biologi telah bertambah. Siasatan berkaitan dengan kesan alam sekitar ke atas DNA melibatkan pelbagai disiplin kajian dan dijalankan dengan aktif disebabkan keasliannya. Kajian tingkah laku beberapa parameter optik DNA di bawah pengaruh medan magnet luaran adalah sangat menarik kerana ia boleh menjurus kepada aplikasi penting di dalam bidang bioperubatan dan elektronik. Kajian-kajian ini telah dimungkinkan dengan adanya banyak sistem pengukuran optik canggih dan praktikal yang mana boleh didapati kini. Dalam kerja ini, pencirian spektroskopi ke atas DNA yang dicairkan di bawah medan magnet luaran telah diukur menggunakan teknik spektroskopi transmisi ultra-violet-cahaya nampak (UV-Vis) dan serakan Raman. Keamatan serapan, pekali pemupusan dan ketulenan bebenang berganda (diekstrak dari *Mimosa pudica*) dan oligonukleotida DNA telah diukur untuk mengkaji ciri-ciri berkaitan biologi terhadap kekuatan medan magnet yang digunakan. Segi sifat fizik optik DNA seperti jurang jalur, indeks biasan dan fungsi kehilangan DNA telah disiasat sebagai suatu fungsi pelbagai kekuatan medan magnet. Keputusan menunjukkan bahawa terdapat suatu peningkatan di dalam pekali pemupusan untuk dsDNA dengan peningkatan kekuatan medan magnet disebabkan pecahan dan belahan bebenang DNA. Pencirian terma dan rintangan juga telah dikaji untuk kesan pendedahan DNA kepada medan magnet. Keputusan menunjukkan bahawa pendedahan kepada medan magnet luaran ada sedikit pengaruh ke atas kerintangan, parameter optik, suhu dan ikatan hidrogen bebenang DNA. Jurang jalur yang besar DNA yang dikaji hanya menunjukkan suatu perubahan kecil apabila didedahkan

kepada medan magnet lebih kuat daripada 750 mT. Penyelidikan ini berkesimpulan bahawa ciri-ciri yang dikaji berkaitan dengan pendedahan DNA kepada medan magnet menunjukkan potensi kukuh untuk aplikasi di dalam bidang bioperubatan khasnya sebagai peralatan di dalam ujian diagnostik dan penyelidikan kejuruteraan bio.

## ABSTRACT

In recent years, the number of research related to biological sensing devices has increased tremendously. Investigations related to environmental effects on DNA involve multidisciplinary studies and are actively pursued due to its novelty. Studies on the behavior of some optical parameters of DNA under the influence of external magnetic field are therefore very interesting as it can lead to important applications in the biomedical field and electronics. These studies have been made possible with the availability and practicability of many high-end optical measurement systems, which are currently available. In this work, spectroscopic characterizations on diluted DNA under external magnetic field were measured using ultra-violet-visible (UV-Vis) transmission and Raman scattering spectroscopy techniques. The absorption intensity, extinction coefficient and purity of double strands (extracted from *Mimosa pudica*) and oligonucleotide DNA were measured to study the biological related properties with respect to the magnetic field strength applied. The Physics aspects of the optical properties of the DNA such as band gap, refractive index and loss function of DNA were investigated as a function of various magnetic field strengths. Results indicate that there is an increase in the extinction coefficient for dsDNA with increase in the magnetic field strength due to breakage and cleavage of DNA strands. Thermal and resistance characterization were also studied on the effects of DNA exposure to magnetic field. The results show that exposure to the external magnetic field has some influence on the resistivity, optical parameters, temperature and hydrogen bond of the DNA

strands. The large band gap of the DNA under study only shows a small change when exposed to magnetic fields stronger than 750 mT. This research concluded that the properties studied in relation to DNA exposure to the magnetic field shows strong potential for applications in the biomedical field particularly as tools in diagnostic testing and bio-engineering research.

## Table of Contents

LIST OF PUBLICATIONS .....	I
<b>Published</b> .....	i
<b>Submitted</b> .....	i
LIST OF CONFERENCES .....	II
PATENT AND AWARD .....	IV
<b>Patent</b> .....	iv
<b>Awards</b> .....	iv
ACKNOWLEDGEMENTS .....	V
ABSTRAK .....	VI
ABSTRACT .....	VIII
TABLE OF CONTENTS .....	X
LIST OF TABLES .....	XIV
LIST OF FIGURES .....	XVI
LIST OF ABBREVIATIONS .....	XXII
LIST OF SYMBOLS .....	XXIII
1    CHAPTER I: INTRODUCTION .....	1
1.1    Introduction .....	1
1.2    Motivations .....	5
1.3    Objectives .....	6
1.4    Thesis outline .....	7

2	CHAPTER II: REVIEW OF RELATED LITERATURE .....	9
2.1	Introduction .....	9
2.1.1	Biological perspective .....	12
2.2	DNA structure .....	21
2.2.1	Thymine .....	22
2.2.2	Cytosine .....	23
2.2.3	Adenine .....	25
2.2.4	Guanine .....	26
2.3	Types of DNA cleavage .....	28
2.3.1	DNA hydrolysis .....	28
2.3.2	Photochemical cleavage of DNA .....	29
2.4	UV-Vis spectroscopy .....	29
2.4.1	Biological perspective .....	30
2.4.2	Physics perspective .....	32
2.5	Magnetic field effect on materials.....	35
2.5.1	Classical mechanics .....	35
2.5.2	Quantum mechanics of the magnetic field effects on materials .....	37
3	CHAPTER III: DESIGN, METHODS AND PROCEDURE .....	46
3.1	Introduction .....	46
3.2	Materials.....	46
3.2.1	DNA extraction .....	47
3.2.2	Oligonucleotide .....	49
3.3	Fabrication of chip .....	49
3.3.1	Cleaning .....	49
3.3.2	Mask .....	50

3.3.3	Lithography .....	51
3.3.4	Deposition .....	59
3.4	Set up preparation .....	62
3.5	Analysis and measuring .....	64
4	CHAPTER IV: RESULTS AND DISCUSSIONS: BIOLOGICAL PERSPECTIVE.....	67
4.1	Introduction .....	67
4.2	Purity calculation .....	72
4.3	Extinction coefficient .....	74
4.4	Wavelength at maximum optical density (WMOP).....	81
4.5	Optical density .....	83
5	CHAPTER V: RESULTS AND DISCUSSIONS: PHYSICS PERSPECTIVE.....	85
5.1	Introduction .....	85
5.1.1	Optical parameter .....	85
5.1.2	Raman spectroscopy .....	102
5.1.3	Resistivity.....	105
5.1.4	Temperature .....	109
6	CHAPTER VI: CONCLUSIONS AND FUTURE WORKS.....	114
6.1	Introduction .....	114
6.1.1	Biological perspective .....	114
6.1.2	Physics perspective .....	115
6.1.3	Future works .....	116
6.2	Light as an electromagnetic wave motion.....	118
7	APPENDIX B .....	122

7.1	Kubelka-Munk .....	122
8	APPENDIX C .....	125
8.1	Kramers-Kronig Relations .....	125
8.1.1	Refractive indices.....	125
9	APPENDIX D .....	130
9.1	Selection rules in Raman spectroscopy.....	130
9.2	The atom mass, charge and position in the DNA bases.....	131
	REFERENCES .....	135



## List of Tables

Table 2-1 Published papers on work related to magnetic fields and DNA shown chronologically by year and the applications based on the biological perspective.....	14
Table 2-2 Published papers about magnetic fields and DNA by year and application from a Physics perspective. ....	17
Table 3-1 Oligonucleotide DNA feature used in this work.....	49
Table 3-2 Categorisation of popular photoresists used in micro-engineering (Banks, 2006). ....	53
Table 3-3 Current photoresists in several viscosities.....	55
Table 3-4 Soft bake times for different thicknesses of SU-8 photoresist. ....	56
Table 3-5 Exposure dose for different thicknesses of SU-8 photoresist.....	56
Table 3-6 Exposure dose for different substrates for SU-8 photoresist.....	57
Table 3-7 Post-exposure bake times for different thickness of SU-8 photoresist. ....	58
Table 3-8 Development times for different thicknesses of the SU-8 developer..	58
Table 3-9 The lithography parameters for the chip fabrication process. ....	59
Table 3-10 Deposition rates for DC Magnetron sputter system. ....	61
Table 4-1 The statistical regression analysis for the purity curve of AT-100, CG-100 and P-DNA exposed to the magnetic field.....	73
Table 4-2 Theoretical and experimental results of $\epsilon$ for AT 100 mer and CG 100 mer oligonucleotides (E-BC; Base composition method, E-NN; Nearest neighbour method, E-EX; Experimental result).....	76
Table 4-3 Statistical regression analysis for the extinction coefficient curve for various magnetic fields. ....	81

Table 4-4 Statistical regression analysis of the maximum wavelength in the absorption spectra of dilute DNA at various magnetic field strengths. ....	83
Table 4-5 Statistical regression analysis of the optical density at various magnetic field strengths. ....	84
Table 5-1 Comparison of the $E_g$ values determined using two methods; Beer-Lambert and Kubelka-Munk. ....	91
Table 5-2 Lorentz fit parameters for the loss function of AT-100, CG-100 and P-DNA. ....	101
Table 5-3 Statistical regression analysis of the resistivity of AT-100 A exposed to various magnetic fields. ....	107
Table 5-4 Statistical regression analysis of the resistivity of CG-100 exposed to various magnetic fields. ....	108
Table 5-5 Statistical regression analysis of the resistivity of P-DNA exposed to various magnetic fields. ....	108
Table 5-6 Statistical regression analysis of the temperature of AT-100 exposed to various magnetic fields. ....	112
Table 5-7 Statistical regression analysis of the temperature of CG-100 exposed to various magnetic fields. ....	112
Table 5-8 Statistical regression analysis of the temperature of P-DNA exposed to various magnetic fields. ....	113
Table 9-1 The atom mass, charge and position in thymine. ....	131
Table 9-2 The atom mass, charge and position in Cytosine ....	132
Table 9-3 The atom mass, charge and position in Adenine.....	133
Table 9-4 The atom mass, charge and position in Guanine.....	134

## List of Figures

Figure 1.1 A typical biosensor for sensing biomaterials consists of an electronic device that provides communication between biological samples and a display showing the data. ....	1
Figure 2.1 The total number of published documents in the magnetic field and DNA subject area. ....	10
Figure 2.2 Published documents on DNA and magnetic fields according to categories. ....	11
Figure 2.3 The total number, by year, of published documents about DNA and magnetic fields. ....	11
Figure 2.4 DNA molecules are made up of four bases; guanine (G), adenine (A), cytosine (C) and thymine (T). Each base is attached to a deoxyribose (sugar molecule) and phosphate groups (Cuniberti, Maciá, Rodriguez et al., 2007).....	21
Figure 2.5 (a) Geometry and positions of atoms in thymine. (b) The molecular orbital energy levels in thymine molecules (HOMO and LUMO levels) (Silaghi, 2005). ....	22
Figure 2.6 The UV-Vis spectrum of thymine calculated using density functional theory. ....	23
Figure 2.7 (a) Geometry and positions of atoms in cytosine. (b) The molecular orbital energy levels in cytosine molecules (HOMO and LUMO levels) (Silaghi, 2005). ....	24
Figure 2.8 The UV-Vis spectrum of cytosine calculated using density functional theory. ....	24

Figure 2.9 (a) Geometry and positions of atoms in adenine. (b) The molecular orbital energy levels in adenine molecules (HOMO and LUMO levels) (Silaghi, 2005).	25
Figure 2.10 The UV-Vis spectrum of adenine calculated using density functional theory.	26
Figure 2.11 (a) Geometry and positions of atoms in guanine. (b) The molecular orbital energy levels in guanine molecules (HOMO and LUMO levels) (Silaghi, 2005).	27
Figure 2.12 The UV-Vis spectrum of guanine calculated using density functional theory.	27
Figure 2.13 DNA and nucleophile hydroxide interaction. A hydroxide or activating water promotes the phosphate group by attaching to and splitting the DNA strain (viewing the picture from left to right shows a schematic of the cleavage mechanism).	28
Figure 2.14 The cleavage of DNA by oxidation in the guanine site.	29
Figure 2.15 The molecule with energy equal to $\Delta E$ , differences between the HOMO-LUMO levels (energy gap).	30
Figure 2.16 The angular momentum vector, $L$ , can lie along specific orientations with respect to the external magnetic field.	38
Figure 2.17 An atom is placed in a magnetic field with the convention that the South Pole is at the top and the North Pole is at the bottom.	38
Figure 2.18 The difference in energy between adjacent levels.	39
Figure 2.19 The splitting of the sodium D line when the amplitude of the magnetic fields increase from low to high shows this effect.	42
Figure 2.20 Raman scattering mechanism, including Stokes, anti-Stokes and Rayleigh scattering.	44

Figure 3.1 An image of <i>Mimosa pudica</i> commonly known as the sensitive plant.	47
Figure 3.2 DNA extraction protocol	48
Figure 3.3 Mask designed using AutoCAD 14 software. The left one is for the negative photoresist while the right one is for the positive photoresist.	51
Figure 3.4 Patterns fabricated using positive and negative photoresists, positive (left) and negative (right)	52
Figure 3.5 Schematic of the patterning mechanism	54
Figure 3.6 Procedure used to make a layer of SU-8 photoresist on a prepared substrate.	54
Figure 3.7 Deposition techniques; chemical and physical processes.	60
Figure 3.8 Thermal evaporation machine, belonging to the Department of Physics, University of Malaya, used in the present study.	61
Figure 3.9 A side view of the magnetic field generator used in this work. Two coils are located parallel to each other and separated by a small distance.	62
Figure 3.10 Magnetic field generated via current in the magnetic generator in various gap size between two coil pair (Helmholtz coil pair system).	63
Figure 3.11 Measurement set up, including AVO meter, Tesla meter, timer, thermometer , magnetic generator that included power supply and electromagnet and wire connections	65
Figure 3.12 Diluted DNA sample placed in the magnetic field region (a) Electromagnet; (b) Thermometer; (c) Multimeter; (d) Timer; (e) Teslameter; (f) Electromagnet power supply and (g) DNA sample.	65
Figure 4.1 Flow-chart showing the two perspectives of analyses done in this work based on the biological and Physics aspects.	67

Figure 4.2 UV-Vis spectra of diluted AT-100 DNA sample after exposure to magnetic fields of various strengths (250, 500, 750 and 1000 mT).....	70
Figure 4.3 UV-Vis spectrum of diluted CG-100 DNA sample after exposure to magnetic fields of various strengths (250, 500, 750 and 1000 mT).....	70
Figure 4.4 UV-Vis spectrum of diluted P-DNA sample after exposure to magnetic fields of various strengths (250, 500, 750 and 1000 mT).....	71
Figure 4.5 The measurement setup included a magnetic field generator for applying a uniform magnetic field, a thermometer to control and monitor the temperature and an AVO meter to calculate the resistance. A drop of diluted DNA placed between two metal electrode. ....	71
Figure 4.6 The variation in the purity of diluted DNA samples (P-DNA, AT-100 and CG-100) against the magnitude of magnetic field strengths.....	72
Figure 4.7 UV-Vis Spectrum for four different concentrations. Subfigure shows the optical density versus concentration for the AT-100 oligonucleotide DNA.....	76
Figure 4.8 UV-Vis Spectrum for four different concentrations. The subfigure shows the optical density versus concentration for CG-100 oligonucleotide DNA. ....	77
Figure 4.9 UV-Vis absorption at various wavelengths and four different concentrations. The subfigure shows the optical density versus concentration for the P-DNA.....	77
Figure 4.10 The variation in the extinction coefficients of diluted DNA exposed to magnetic fields. ....	79
Figure 4.11 Mechanism of the hydrolysis interaction in the DNA helix.....	80
Figure 4.12 Variation of the maximum wavelength in the absorption spectra of diluted DNA influenced by magnetic field exposure.....	82
Figure 4.13 Variation in the optical density of dilute DNA that was exposed to magnetic fields. ....	83

Figure 5.1 The absorption spectra of diluted AT-DNA exposed to magnetic field fitted by the equations for direct band gap transitions. ....	87
Figure 5.2 The absorption spectra of diluted CG-DNA exposed to magnetic field fitted by the equations for direct band gap transitions. ....	88
Figure 5.3 The absorption spectra of diluted P-DNA exposed to a magnetic field were fitted by the equations for direct band gap transitions. ....	88
Figure 5.4 Kubelka-Munk coefficients of the absorption spectra of AT-DNA exposed to various magnetic fields. ....	89
Figure 5.5 Kubelka-Munk coefficients of the absorption spectra of CG-DNA exposed to various magnetic fields. ....	90
Figure 5.6 Kubelka-Munk coefficients of the absorption spectra of P-DNA exposed to various magnetic fields. ....	90
Figure 5.7 Dispersion curves of real part of the refractive index of AT-100 DNA after exposure to different strengths of magnetic fields. ....	94
Figure 5.8 Dispersion curves of real part of the refractive index of CG-100 DNA after exposure to different strengths of magnetic fields. ....	94
Figure 5.9 Dispersion curves of real part of the refractive index of P-DNA after exposure to different strengths of magnetic fields. ....	95
Figure 5.10 Imaginary part of the refractive index of AT-100 DNA exposed to magnetic fields. ....	96
Figure 5.11 Imaginary part of the refractive index of CG-100 DNA exposed to magnetic fields. ....	97
Figure 5.12 Imaginary part of the refractive index of P-DNA exposed to magnetic fields. ....	97
Figure 5.13 Loss function of AT-100 DNA exposed to different magnetic field strengths. ....	99

Figure 5.14 Loss function of CG-100 DNA exposed to different magnetic field strengths. ....	99
Figure 5.15 Loss function of P-DNA exposed to different magnetic field strengths. ....	100
Figure 5.16 Comparison of the Raman spectra of AT-DNA before and after exposure to magnetic field. ....	102
Figure 5.17 Comparison of the Raman spectra of CG-DNA before and after exposure to magnetic field. ....	103
Figure 5.18 Comparison of the Raman spectra of P-DNA before and after exposure to magnetic field. ....	103
Figure 5.19 Resistivity of AT-DNA exposed to magnetic fields. ....	106
Figure 5.20 Resistivity of CG-DNA exposed to magnetic fields. ....	106
Figure 5.21 Resistivity of P-DNA exposed to magnetic fields.....	106
Figure 5.22 Temperature of AT-DNA exposed to magnetic fields.....	110
Figure 5.23 Temperature of CG-DNA exposed to magnetic fields.....	111
Figure 5.24 Temperature of P-DNA exposed to magnetic fields. ....	111
Figure 6.1 Potential applications of DNA strands and oligonucleotides in Physics and Biology .....	117
Figure 7.1 Two fluxes which are completely diffuse. One in the positive x-direction, $J$ , and one in the negative x-direction, $I$ . ....	122



## List of Abbreviations

A	Adenine
AFM	Atomic Force Microscopy
CVD	Chemical Vapor Deposition
I–V	Current-Voltage
C	Cytosine
DFT	Density Functional Theory
DNA	Deoxyribonucleic Acid
DC	Direct Current
dsDNA	Double Stranded DNA
$E_F$	Fermi Level
FTIR	Fourier Transform Infrared
G	Guanine
HOMO	Highest Occupied Molecular Orbital
IR	Infrared
K-K	Kramers-Kronig
K-M	Kubelka-Munk
LB	Lambert-Beer
LUMO	Lowest Unoccupied Molecular Orbital
MDM	Metal-DNA-Metal
MEMS	Micro-Electro Mechanical Systems
MO	Molecular Orbital
PVD	Physical Vapor Deposition
PECVD	Plasma Enhanced Chemical Vapor
PCR	Polymerase Chain Reaction
RF	Radio Frequency
SEM	Scanning Electron Microscopy
ssDNA	Single Stranded DNA
T	Thymine
UV	Ultraviolet
UV-Vis	Ultraviolet-Visible

## List of Symbols

$A$	Absorption.
$\sigma^*$	Anti bonding Molecular Orbital
$A$	Average cross-section
$E_g$	Band gap
$k$	Boltzmann's constant
$\sigma$	Bonding Molecular Orbital
$\tilde{n}$	Complex optical refractive index -
$\tilde{k}$	Complex optical refractive index- phase
$C$	Concentration
$\sigma$	Conductivity
$I$	Current
$J$	Current density
$\varepsilon(\omega)$	Dielectric Constant
$m^*$	Effective mass
$F_E$	Electric force
$q$	Electron charge
$\varepsilon$	Extinction Coefficient
$E_F$	Fermi Level
$\varepsilon''$	Imaginary dielectric constant
$n_i$	Imaginary part of Refractive index
$L$	Length of the DNA
$B$	Magnetic field
$F_B$	Magnetic force
$O.P$	Optical Density
$L$	Path length
$h$	Planck's constants
$K$	Propagation vector
$\varepsilon'$	Real part of dielectric constant
$n_r$	Real part of Refractive index
$n$	Refractive index
$R$	Resistance
$T$	Temperature
$V$	Velocity

$C$	Velocity of an electromagnetic wave
$c_0$	Velocity of an electromagnetic wave in
$\lambda$	Wave length

## CHAPTER I: INTRODUCTION

### 1.1 Introduction

In recent years, a lot of work has been conducted based on the use of biological specimens such as deoxyribonucleic acid (DNA), a low-dimensional form of nanomaterial for potential applications in photonics and electronics devices. Investigations related to the effects of various environmental conditions on DNA have been actively pursued in multidisciplinary studies due to its potential applications in the biomedical and electronics fields. This field of research is in its infancy with respect to potential applications in Physics and electronics. Most recent research on this aspect in the field of Physics has been focused on trapping and manipulating of DNA for use in biosensors and chips.

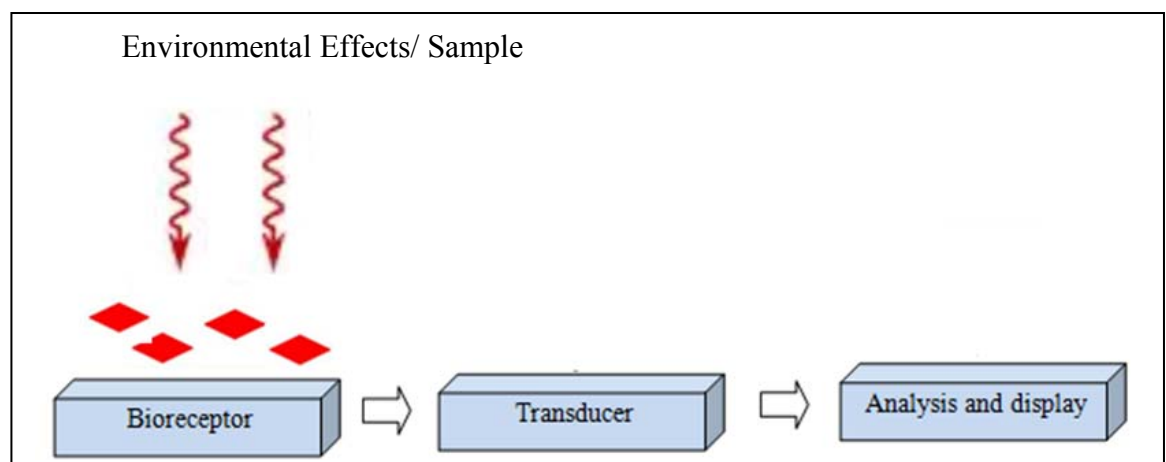


Figure 1.1 A typical biosensor for sensing biomaterials consists of an electronic device that provides communication between biological samples and a display showing the data.

Biosensors are sensing devices in which a biological element is linked to a transducer for sensing a target sample or environmental effect (Collings, Caruso, 1997). Generally, biosensors operate by converting a biological

parameter or response to an electronic signal or optical spectrum to recognise chemical and physical interactions. Components of biosensors include a target, bioreceptor, transducer and signal analyser as shown in Figure 1.1.

Bioreceptors contain a biological molecular system (e.g., an antibody, a protein, or a nucleic acid) and a living biological object (e.g., cells and tissue), which is utilised for recognition in biomedicine. A transducer can be in the form of the following common characterization techniques, 1) optical spectroscopy (e.g., ultraviolet-visible (UV-Vis), Fourier Transform Infrared Spectroscopy (FTIR), 2) electrochemical measurements (e.g., voltammetry), 3) mass analysis and 4) other similar measurements (thermal, electrical).

As shown as Figure 1.2, DNA is the most important components in bioreceptor and since it is the main building block of genetics, it has attracted growing interest in biosensor technologies (Vo-Dinh, Alarie, Isola et al., 1999). Optical activity (Teles, Fonseca, 2008) or the activity of an optical compound label (Bosch, Sanchez, Rojas et al., 2007) can be used in sensors for biorecognition (Marazuela, Moreno-Bondi, 2002) through applying common optical techniques, such as UV-Vis spectroscopy (Bosch, Sánchez, Rojas et al., 2007; Singh, Sariciftci, Grote, 2010). Indeed, recently visible and infrared spectroscopies have been used to develop DNA biosensors for diagnostics (Lindqvist, Graslund, 2001; Saito, Silva, Pungartnik et al., 2012).

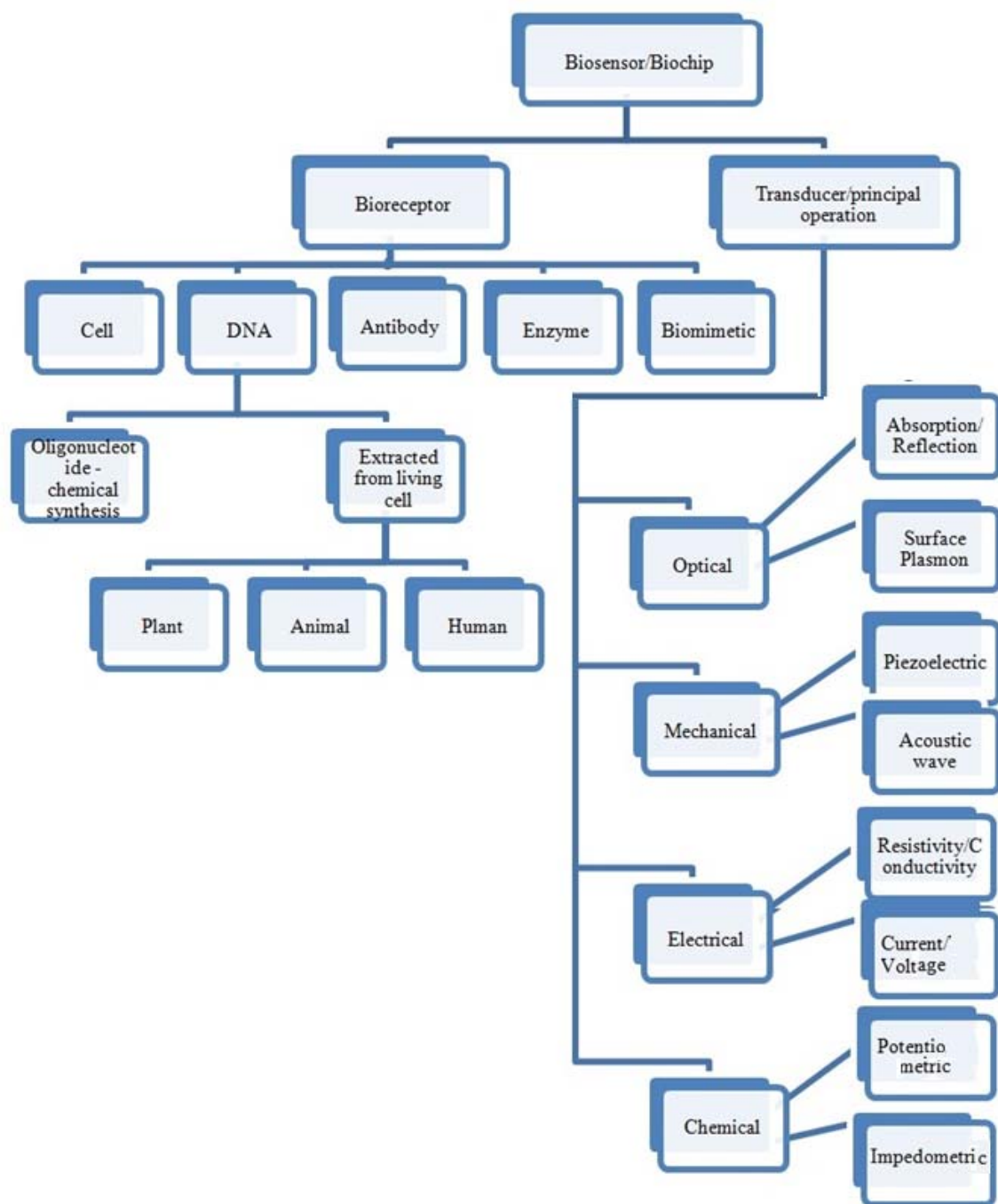


Figure 1.2 Schematic categories of Biosensors schemes

Interactions between DNA and the environment are not only interesting subjects in life sciences, which are related to the replication and mutation of genes and the origins of diseases, but also have attracted a lot of attention in studies related to Physics, Chemistry and Engineering. External magnetic fields

can be useful tools for manipulating and controlling material and physiochemical interactions remotely. The more interesting question is whether static magnetic fields can cause damage to DNA structure and alter its optical properties. There are many studies focused on this issue. Magnetic field can result in changes in the energy levels and thus causes movement of charges in DNA molecules and can have influence on the DNA responsiveness. Also, by controlling and manipulating the magnetic field remotely, this effect can be used to extend its application in the medical and biosensors area. As result of this, the effects of magnetic field exposure on biomaterials have gained a lot of attention in recent years in research. Biomaterials can be easily manipulated using an external magnetic field. For instance, magnetic particles that are tagged to a biomaterial can be made to move or stretch using magnetic force and magnetic treatments can be applied to tissue and blood (Dobson, 2008; Strick, Allemand, Bensimon et al., 1996). In the biomaterials category in general, the biological and scientific research interest in DNA strand manipulation using moderate-intensity magnetic fields has increased. Interesting studies involve immobilised DNA strands on small chips, mechanically manipulated DNA in a magnetic tweezers device (Haber, Wirtz, 2000) and magnetically arranged DNA in liquid crystals (Brandes, Kearns, 1986; Davidson, Strzelecka, Rill, 1988). Another interesting application, reported by our group, involves magnetic sensors in metal-DNA-metal structures (Khatir, Banihashemian, Periasamy, Ritikos, Abd Majid et al., 2012). Feasible electrical and medical applications of applying magnetic fields to DNA provided new perspectives for DNA manipulation and characterisations (Lan, Chen, Chang, 2011).

The in vivo effect of magnetic fields on DNA in rat brains was previously studied (Lai, Singh, 2004). However, in this work the effect of magnetic fields on DNA in vitro using an optical method is investigated for the first time.

In this work, spectroscopic characterizations of diluted DNA oligonucleotides AT (100mer) and CG (100mer) and DNA extracted from plant subjected to an external magnetic field are conducted using UV-Vis spectroscopy to determine their potential for use in electronic devices and biosensor applications. The optical spectra of the DNA are measured to study the optical parameter such as refractive index and band gap with respect to the strength of the applied magnetic field.

## 1.2 Motivations

Biosensors are powerful tools for identifying toxic compounds in industrial products, biological samples (e.g., virus, tissue and bacteria) and environmental systems (e.g., water). The effects of environmental pollution can be recognized and detected by applying optical and electrical detection tools to biological samples. The simplicity, speed, high selectivity and sensitivity in using the small geometry of biomaterial based micro- and nanochips for detecting molecules and environmental interactions make biomaterials as the current preferred tools for researchers in detectors.

DNA strands and short oligonucleotides with several tens of base pairs in large group of biomaterials are novel candidates for biochips and sensors because of their unique properties which can result in DNA-based sensing devices. The interest in hybrid structures of biomaterials and electronic elements (metal/semiconductor, biomaterial/DNA) has increased tremendously



recently (Braun, Eichen, Sivan et al., 1998; Richter, Mertig, Pompe et al., 2001).

Practical use of DNA and bio-components in micro- and nanoelectronics as sensors, including magnetic and opto-magnetic detectors has significantly created great interest in the investigation of magnetic field effects on DNA and short-length oligonucleotides. In this work, the optical absorption of diluted DNA exposed to external magnetic fields is investigated from the optical density measurements. The main purpose of this study is to investigate the possibility of using the effects of magnetic fields on DNA for medical and industrial applications. The possible applications include magnetic sensors, biochips, microfluidic devices, nanoparticle separation and virus detection.

### 1.3 Objectives

The main objectives of this study are measured from the analysis done on the results obtained from the optical and physical properties of DNA extracted from plants (*Mimosa pudica*) as a natural DNA that was available in our living area and of oligonucleotide DNA as a simplest artificial DNA, after exposure to different magnetic field strength. All measurements are performed before and after exposure to the magnetic field and analysed from the biological as well as the physical perspectives. The objectives of the work done in this research are highlighted below.

1. To determine the effects of exposure of DNA samples to different magnetic field strength from the biological perspective on the following parameters:
  - (i) DNA purity
  - (ii) The extinction coefficient of DNA

- (iii) The optical density of DNA.
  - (iv) The wavelength of the DNA absorption peak.
2. To determine the effects of exposure of DNA samples to different magnetic field strength from the physics perspective on the following parameters:
- (i) Band gap of DNA samples
  - (ii) Refractive index of DNA samples
  - (iii) The hydrogen bonds in the DNA helix.
  - (iv) The resistivity of DNA samples.
  - (v) DNA temperature variations.
  - (vi) The loss function of DNA samples.
3. To explain the effects of exposure to in vitro magnetic field on the above parameters both from the biological and physics perspective in relation to the structure of DNA.

#### 1.4 Thesis outline

The thesis is organized into 6 chapters. Chapter I begin with a brief introduction on biosensors and the classification of biosensors. Importance of studies related to biosensors and magnetic field influence on DNA is also highlighted. The research problems and significance of the studies are discussed, including the study features, analysis conditions and limitations. Aims and motivations of the work are presented and the objectives are outlined in this chapter.

Chapter II provides an organised literature review covering the various concepts used in this study. The highlighted studies featured in this review are

related to the objectives of this study. The theoretical background of this work is presented, discussed and categorised.

Chapter III describes the research methodology adopted in this work for data collection and processing. The materials, instruments and devices used in carrying out the research are described in the first part of the chapter followed by the fabrication process, extraction methods and analysis. Limitations and problems of the analysis are briefly mentioned in the final parts of this chapter.

Chapter IV presents the results with discussions and analysis of the data based on the biological aspects. The data analysis and calculation techniques are also described in this chapter. Similarly the results with discussions and analysis of the data based on the physics aspect are presented in Chapter V. In both these chapters, analysis of the data are presented in diagrams, charts and tables obtained from scientific software, such as Microsoft Excel, SPSS and ADF. The results are discussed using physical and chemical principles to relate the effects of magnetic field strength on the various parameters studied in this work and the accuracy of the hypothesis investigated.

Finally, Chapter VI presents the conclusions and recommendations for future works.

## CHAPTER II: REVIEW OF RELATED LITERATURE

### 2.1 Introduction

The effects of exposing biomaterials to magnetic fields have gained considerable attention in the past several decades. Biomaterials can be easily manipulated by an external magnetic field. Magnetic particles that are tagged to biomaterials for instance, can be moved and stretched using magnetic force (Chen, Fu, Zhu et al., 2011) and can be treated using magnetic fields (Elson, 2009). Magnetic fields can also be used to manipulate tissue and blood (blood cell separation using Magnetophoresis). As part of the general biomaterials category, biological and scientific research in manipulating DNA strands using moderate-intensity magnetic fields has increased. Immobilising DNA strands on small chips (Campàs and Katakis, 2004), mechanically manipulating DNA using a magnetic field in a magnetic tweezer device (Brogioli, 2009; Leuba, Wheeler, Cheng et al., 2009) and magnetically arranging liquid crystals (Morii, Kido, Suzuki et al., 2004) have been reported. Magnetic sensors in metal-DNA-metal structures are another interesting application reported by our group (Khatir, Banihashemian, Periasamy, Abd Majid et al., 2012).

To investigate the interest in magnetic fields and DNA, statistical analysis was performed using a database. The subjects that were published in this field were investigated by categorising the published papers by the type of document, the subject area and the number of papers. The pie chart in Figure 2.1 depicts the number of papers in the respective subjects. As depicted in this figure, 37.8% of the published papers and conference proceedings are from the Physics perspective, 17.2% are related to Engineering and 12.2% are in the

Materials Science field. Most of the remaining studies are in Medicine and Biochemistry.

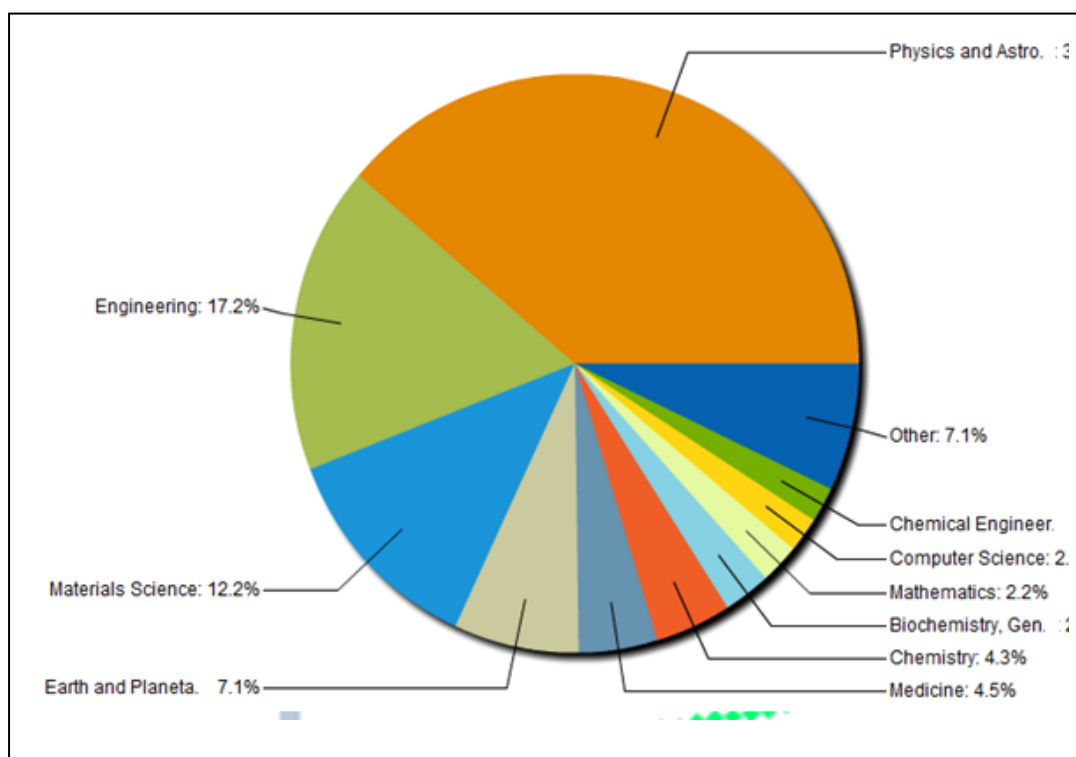


Figure 2.1 The total number of published documents in the magnetic field and DNA subject area.

Most (approximately 75.8 %) published documents about magnetic fields and DNA are original articles (as shown in Figure 2.2). The remaining documents include conference papers, papers in press and review papers.

The total number of published documents by year is shown in Figure 2.3. This figure illustrates that the number of studies in this area has exponentially increased because of the significant attention in recent decades. Overall, the results show that the largest increase in these documents cover the Physics and Engineering perspective of the research especially in the most recent years. Most of the documents are original articles and these have also gradually increased in the past few years. Published papers on the effect of magnetic fields on DNA can be statistically divided into two sections covering the biological and Physics perspectives of the studies. The literature regarding

the effects of static magnetic fields on DNA strands from biological and physical perspectives is reviewed by considering the application and characterisation methods.

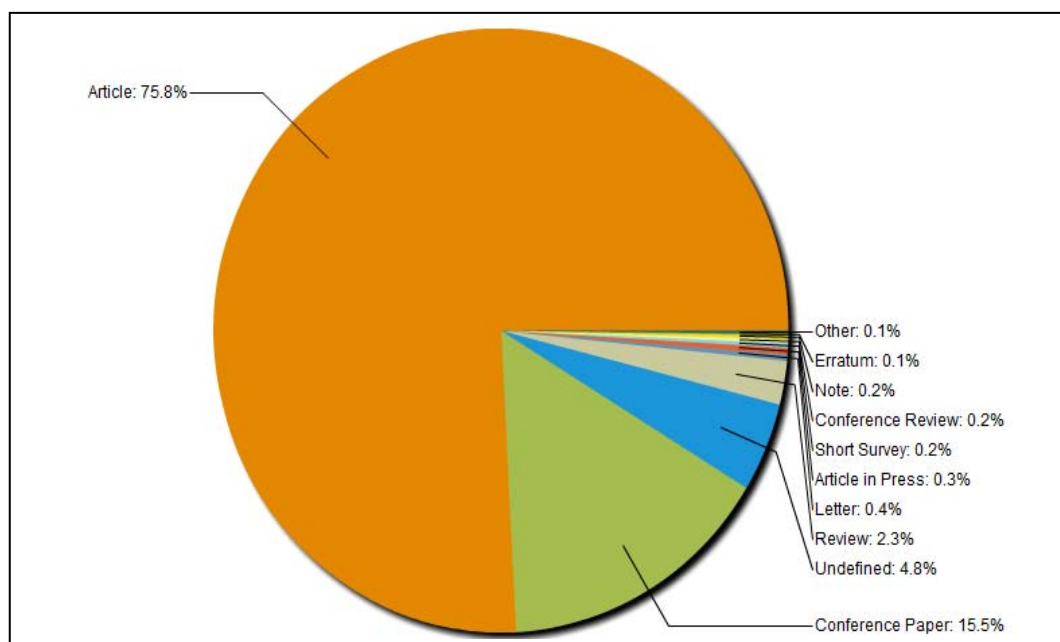


Figure 2.2 Published documents on DNA and magnetic fields according to categories.

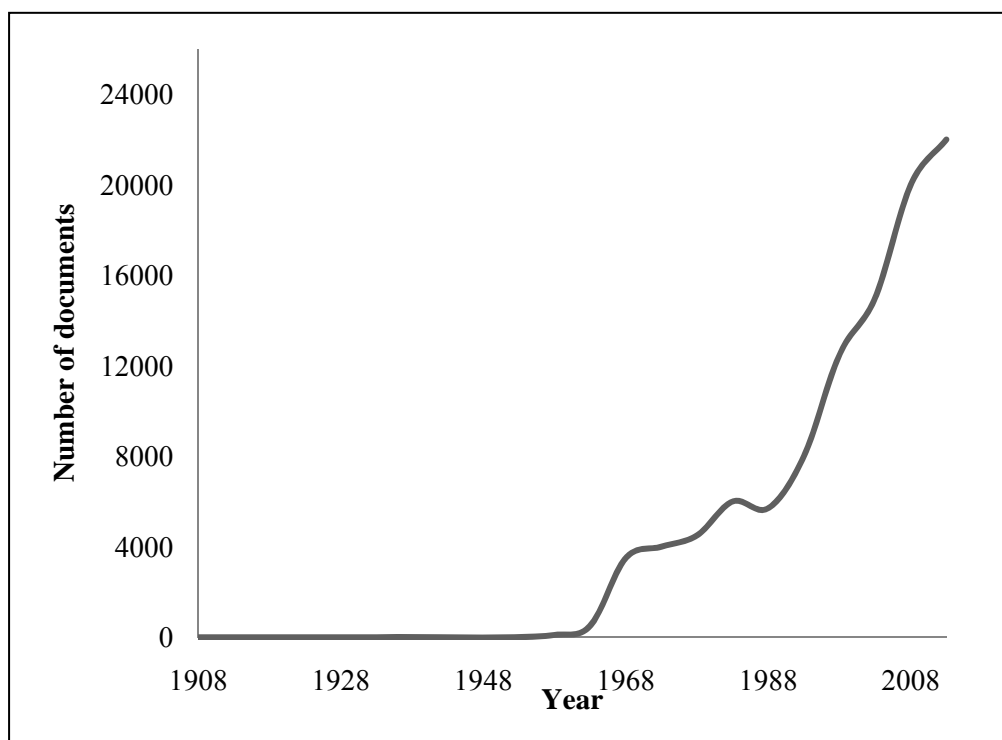


Figure 2.3 The total number, by year, of published documents about DNA and magnetic fields.

### 2.1.1 Biological perspective

Effect of magnetic fields on biomaterials and living cells is an interesting subject with numerous publications since more than 50 years. The more interesting question is whether static magnetic fields cause damage to DNA structure and alter its properties. There are many studies focusing on this issue. It has been reported that 50/60 Hz magnetic fields increase the damage via the effect on trace amounts of ions in cells (Jajte, Zmyślony, Palus et al., 2001; McNamee, Bellier, McLean et al., 2002). Strong static magnetic field can affect gene expression and charge transportation (Kimura, Takahashi, Suzuki et al., 2008). Furthermore, magnetic treatments have been reported in the treatment of Ehrlich carcinoma (El-Bialy and Rageh, 2013). The published papers on magnetic field effects on DNA are listed and categorized in Table 2-1. As shown in the table, one of the earliest studies on the effect of magnetic fields on a biological sample was performed by Barnothy in 1964 (Barnothy, 1964). Fox published similar research in 1966 (Fox, 1966) and many papers on this topic were published afterwards (Bodega, Forcada, Suárez et al., 2005; Eldashev, Shchegolev, Surma et al., 2010; Kirschvink, Kobayashi-Kirschvink Woodford, 1992; Leszczynski, 2005; Miyakoshi, 2006; Moore, 1979; Sekino, Tatsuoka, Yamaguchi et al., 2006). The broad range of studies on biomaterials and magnetic fields provided new applications in medicine. These includes treatment in muscle cells (Eldashev et al., 2010), cancer therapy (Raylman, Clavo Wahl, 1996), brain research, diseases (e.g., Parkinson's and Alzheimer's) (Ueno, 2012), magnetic resonance imaging (MRI) measurements of brain impedance (Leszczynski, 2005; Sakurai, Terashima Miyakoshi, 2009) and the control and growth of cells (Lucia Potenza, Ubaldi, De Sanctis et al., 2004), including those in specific orientations (Morii, Kido et al., 2005). The effects

of magnetic fields on DNA are more interesting than the effects of electric fields' because of the specific change in properties and roles of DNA in cells when exposed to magnetic field.

Published works addresses the in vivo magnetic field effects on DNA (Ichioka, Minegishi, Iwasaka et al., 2000) and in vitro (Blackman, Benane, Rabinowitz et al., 1985). Some of the research showed that high magnetic field exposure damages living cells in vivo. For instance, in rat brain, free radicals that are found in biological organisms created by magnetic fields damage the brain (Amara, Douki, Garrel et al., 2011; Lee, Johng, Lim et al., 2004; Pan and Liu, 2004; Theodosiou and Thomas, 2008; Villarini, Moretti, Scassellati-Sforzolini et al., 2006) showed cleaved double-stranded DNA (Kim, Ha, Lee et al., 2010). Studies about the effects of magnetic fields on DNA in vitro show reorientation of DNA in the direction of the magnetic field (Emura, Ashida, Higashi et al., 2001; Gamboa, Gutiérrez, Alcalde et al., 2007). Improvements in magnetic configurations also permit magnetic sorting, stretching and twisting of DNA strands using small volumes of biomaterial and various bioapplications (Al-Hetlani, Hatt, Vojtíšek et al., 2010; Thachappillya Mukundan, Tran Tuona Phan, 2013).

Various applications of magnetic field effects on DNA that have been reported are organised in Tables 2-1 and 2-2. The overwhelming majority of these researches were performed in vivo.



Table 2-1 Published papers on work related to magnetic fields and DNA shown chronologically by year and the applications based on the biological perspective.

Authors	Year	PCR	Magnetic bead	Micro fluid, Chanel	Drug and treatment	Separation, orientation	Deviation, Damage	in vivo
Barnothy and et al	1969						*	*
Fox, M. A.	1966						*	
Moore, R. L.	1979						*	*
Ueno, S.	1992						*	*
Lin H and et al	1995				*			*
Zannella, S.	1998						*	*
Emura R., and et al	2001					*		
Jandova A and et al	2001				*			
Curcio M and et al	2002	*	*					
Saunders, R. D.	2002						*	*
Hautot D and et al	2003				*			*
Codina A. and et al	2004				*	*		*
Laing T.D. and et al	2004					*		
Morii N. and et al	2004					*		
Woldansk and et al	2004				*			*
Wen J and et al	2004							*
Pan H and et al	2004				*			*
Morii N and et al	2005					*		*
Gamboa O.L and et al	2007					*		*
Ohashi T and et al	2008		*	*		*		*
Theodosiou E and et al	2008		*			*		*
Kimura T and et al	2008					*	*	*
Roberts C and et al	2008							*
Lhuillier S and et al	2009			*				*
Elson E.	2009				*			*
Sakurai T and et al	2009							*
Elson E.	2009				*			*
Boles D.J and et al	2011	*	*	*	*			
Higashi T and et al	2011	*						
Pozhidaeva and et al	2012		*		*			*
Cannon B and et al	2012	*						
Lim J and et al	2012	*						*
El-Bialy N.S and et al	2013				*			*

Of the wide range of analysis methods used in biological sciences to trace the variation, damage and interaction of DNA, UV-Vis spectroscopy is one of the most convenient and commonly used tools. Zai et al. in 1998 published research about the DNA and protein constituents of viruses that were characterised using UV-Vis spectroscopy (Zai Qing and Thomas G.J, 1998). Toyama et al. in 2001, reported the use of UV-Vis spectroscopy to analyse adenine residues in DNA (Toyama, Miyagawa, Yoshimura et al., 2001). In 2005, Zhou and co-researchers studied the interaction between CT-DNA and cytochrome C using electrochemistry and UV-Vis spectroscopy (Zhou, Feng, Wu et al., 2005). DNA that was functionalised by nanoparticles of gold was investigated using UV-Vis spectroscopy in the Witten research group (Witten, Bretschneider, Eckert et al., 2008).

Drug-DNA interactions are another subject that can be studied using UV-Vis analysis (Perveen, Qureshi, Ansari et al., 2011). Raman spectroscopy is another technique for analysing biomaterials and their interaction with other materials or the environment. Although this method is not as widely used as UV-Vis spectroscopy, Raman is a useful method for analysis in multidisciplinary studies. In 1999, Yiming X. et al. studied the microscopic damage of DNA using Raman spectroscopy (Yiming, Zhixiang, Hongying et al., 1999). In 2001, Ke et al. investigated the microscopic DNA damage caused by acetic acid using Raman spectroscopy (Ke, Yu, Gu et al., 2001). Shaw C.P. and Mallidis C. studied damaged DNA structures (Mallidis, Wistuba, Bleisteiner et al., 2011; Shaw C.P and Jirasek, 2009). Human sperm damage also can be investigated using Raman spectroscopy tools (Niederberger, 2012, 2013). Combining Raman and UV-Vis spectroscopy is a powerful tool that

provides complementary results using the parallel analysis techniques (Jangir, Dey, Kundu et al., 2012; Kang and Zhou, 2012).

### 2.1.2 Physics perspective

The influence of magnetic fields on DNA is analysed to utilise this material as a smart element in electronics. Lack of physical and industrial studies of this material encourages us to investigate the capability of this smart material by extending the monitoring of DNA variations. The application of this structure as a multidisciplinary material is clearly a subject that compels many scientists around the world to manipulate DNA structures.

This field of research is in its infancy in Physics and electronics. Most recent research from a Physics perspective is focused on manipulating and trapping DNA for its use as sensors and on chips. Combining nanoparticles with DNA molecules extends the capability of this material.

Piunno P.A.E. and his research group in 1999 published one of the first papers in which DNA was introduced to engineering. The researchers immobilised DNA using fibre optics (Piunno, Watterson, Wust et al., 1999). In the same year, several studies were published using DNA and oligonucleotide biosensors and by optimising parameters, such as immobilisation and hybridisation (Liu and Tan, 1999; Xu, Ma, Liu et al., 1999; Zhang, Zhou, Yuan et al., 1999). The original article in 2000 showing the use of DNA in sensors, such as those in fibre optics and piezoelectricity, attracted significant attention (Mehrvar, Bis, Scharer et al., 2000; Piunno, Hanafi-Bagby, Henke et al., 2000; K. R. Rogers, 2000; Tombelli, Mascini, Sacco et al., 2000; Walt, 2000; Wolfbeis, 2000). In 2001, Lin et al. published a review of fibre-optic DNA biosensors as a new developing technology that has high potential for detecting oligonucleotide patterns, diagnosing gene or DNA damage, and

identifying drugs and enzymes using fibre optics sensors (Lin and Jiang, 2001). The number of papers describing DNA applications in biosensors and fibre-optic sensors increased significantly since 2001 (Ahmad, Chang, King et al., 2005; Epstein, BiranWalt, 2002; Jiang, LeiGao, 2006; Martins, Prazeres, Fonseca et al., 2010; Peter, Meusel, Grawe et al., 2001; Kim R Rogers, Apostol, Madsen et al., 2001).

Table 2-2 Published papers about magnetic fields and DNA by year and application from a Physics perspective.

<b>Authors</b>	<b>Year</b>	<b>Nano/ Microparticle</b>	<b>Chip/ Sensor</b>	<b>Separation</b>	<b>Tweezers</b>
Sonti, et al	1997	*			
Iwasaka et al	1998	*		*	
Iwasaka, et al	1998			*	
Yan J et al	2004	*	*		*
Morii, N. et al	2004			*	
Graham D.L et al	2005				
Mykhaylyk, et al	2007	*			
Klaue D et al	2009				*
Leuba, S. H. et al	2009	*	*		*
Peng, H. et al	2009	*			*
Brogioli, D.	2009				*
Manosas, M. et al	2010				*
Chan, et al	2011		*		
Khatir et al	2012		*	*	
Lionnet, T. et al	2012				*
Lim, J.Dobson, J.	2012	*			
Chen, H. et al	2012				*
Mahmoudy et al	2012		*		
Medley, C. D. et al	2012	*			
De Vlaminck, I. et al	2013				*

Tables 2-1 and 2-2, shows that the number of papers published about the interaction between magnetic fields and DNA from a biological perspective is greater than that for the physical perspective. Most of the researches from the Physics perspective were performed in the past few years, indicating that

the research in this subject is still in its infancy. Recently, DNA strand manipulation and measurements in the presence of magnetic fields have attracted significant scientific research attention. Magnetic tweezers are used to study and manipulate individual DNA strands using a combination of magnetic fields and a microscope.

In 2004, Potenza L. et al. investigated the effects of a large static magnetic field on various DNA molecules in vivo and in vitro. The researchers analysed the magnetic field effect from a biological perspective. Their results showed that in vitro magnetic fields induce DNA mutations and that exposure to large magnetic fields perturbs the stability of DNA. However in vivo, this effect is not serious because of cellular protection (L. Potenza, Cucchiarini, Piatti et al., 2004).

As shown in Table 2-2, the number of studies that were performed using magnetic field as tweezer-like tools to control DNA has increased. In 2004, Yan et al. studied and manipulated single DNA molecules using magnetic fields (Static fields, 2006). In 2009, the research groups of Brogioli, Peng and Leuba separately released their results about using magnetic fields to control single DNA molecules (Peng and Ling, 2009). In 2010, Manosas, M. et al reported DNA tracking motors (Manosas, Meglio, Spiering et al., 2010). In 2012, Lionnet, T. et al reported using magnetic fields to trap a single DNA molecule (Lionnet, Allemand, Revyakin et al., 2012). All of this research focused on controlling DNA by using magnetic fields to capture and manipulate DNA to extend its application without limiting or altering its physical properties.

Using magnetic field is advantageous not only in sensors and manipulation but also in separating nanoparticles and ions. A magnetophoretic

force can separate ions and charged materials, including DNA and particles to which DNA are attached. In 1998, Iwasaka et al. investigated the use of magnetophoresis with macromolecules. The researchers studied proteins and DNA using optical transmittance analysis in a high magnetic field (8 T superconducting solenoid) (Iwasaka and Ueno, 1998).

Microfluidic-based approaches have been used to place specific types of forces on linear nucleic acids of various lengths and motilities. The nucleic acids are placed on a surface and are subjected to electrophoresis through micron-sized obstacles. Magnetic tweezers (Salerno, Brogioli, Cassina et al., 2010), microfluidics, molecular motors, and DNA-drug interactions are helping investigations for manipulating the behaviour of a DNA strand using magnetic fields and magnetic nanosized beads (Mosconi, Allemand, Bensimon et al., 2009).

The latest studies, by our own group, reported the effect of magnetic fields on DNA for use in sensors and chips (Khatir, Banihashemian, Periasamy, et al., 2012; Khatir, Banihashemian, Periasamy, et al., 2012). DNA deposited between metallic gaps was exposed to magnetic fields of various intensities. The analysis was based on electrical characterisation and physical parameters. In this thesis, previously unreported effects of magnetic fields on DNA features, from both biological and physical perspectives are investigated. The main purpose of this study is to investigate DNA in an external magnetic field. This situation can be applied to sensors and chips for detecting and distinguishing samples. Our reported work includes aspects of novel multidisciplinary studies continuing previous studies. This work includes additional studies of the potential of DNA as a sensor, specifically as a magnetic sensor and as a light sensor, and investigates environmental effects

on DNA. In vitro characterisations of the influence of magnetic fields on DNA strands are proposed, and these characterisations can be applied in Physics, Biology, Medicine and electronic devices. Studying the optical parameters of DNA molecules exposed to external magnetic fields, in both the general research area and in this paper, is interesting. This study provides a simplified physical picture of the effect of a magnetic field on DNA integrity in vitro. The optical absorption of diluted DNA under external magnetic fields was investigated by measuring the intensity of normally incident light that passes through a transparent quartz cuvette. The absorption, purity and extinction coefficient of DNA were measured using UV-Vis spectroscopy. To verify the results, a micro-Raman spectrum with a surface-enhanced Raman signal on a thin layer of Au was measured. Both the UV-Vis and Raman results indicate breakage of the DNA strands. Manipulation of DNA strands by magnetic fields is an interesting idea that has been suggested to be applied to DNA bioassays, microfluidic manipulation and nanoparticle capture. In conclusion, this research shows that these materials have potential in biomedical and electronic devices and are indispensable tools in diagnostics tests. Optical characteristics of DNA using UV-Vis spectroscopy are commonly studied in Physics by calculating the optical constant and the band gap. The Kubelka-Munk theory (Y. Yang, Celmer, Koutcher et al., 2002) and the Kramers-Kronig function are used as mathematics tools to analyse the refractive index and calculate the band gap (Pinchuk, 2004; Singh et al., 2010). Kramers-Kronig function is a powerful tool for analysing the optical constant of DNA (Houssier and Kuball, 1971; INAGAKI, Hamm, Arakawa et al., 1974). DNA optical analysis also includes band gap calculations (Iguchi, 2001; Wang, LewisSankey, 2004; Yousef, Abu El-Reash, El-Gammal et al., 2013). In this

work, UV-Vis and Raman spectroscopy are used to analyse the effects of magnetic field on DNA strands and oligonucleotide DNA for multidisciplinary applications.

## 2.2 DNA structure

Human and plant cells contain a nucleus, which provides genetic information. The nucleus includes long strands of DNA that carry and encode genetic information. All DNA molecules consist of four bases, guanine (G) and adenine (A), known as purines, and cytosine (C) and thymine (T), known as pyrimidines.

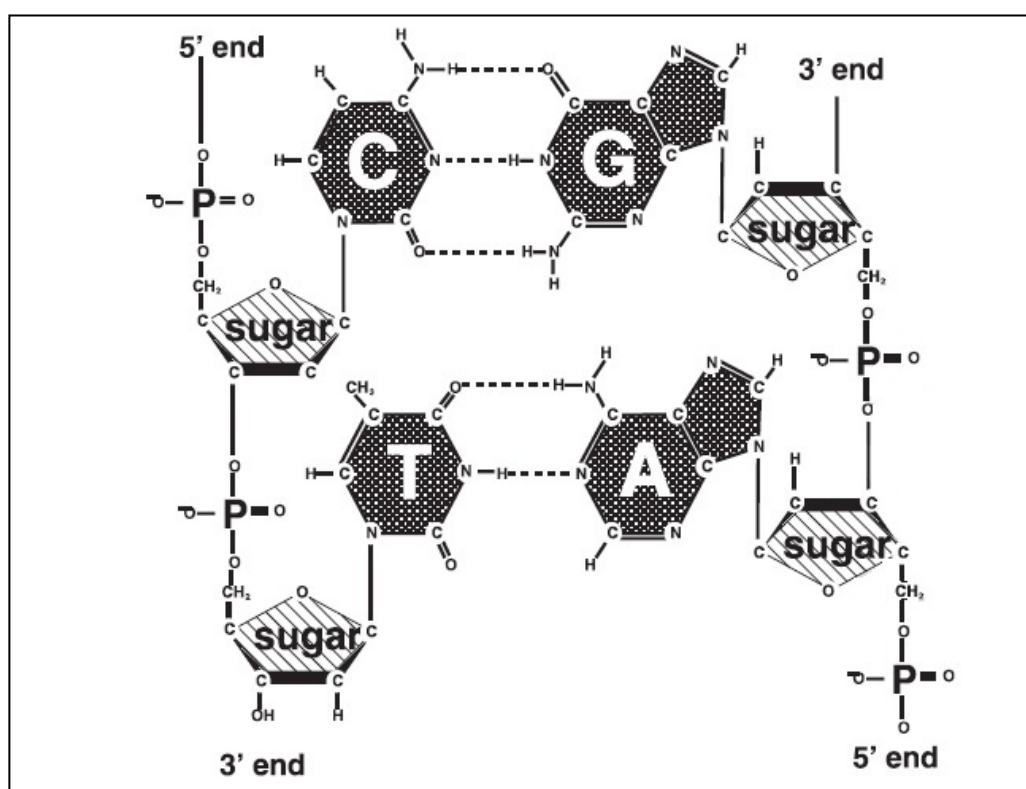


Figure 2.4 DNA molecules are made up of four bases; guanine (G), adenine (A), cytosine (C) and thymine (T). Each base is attached to a deoxyribose (sugar molecule) and phosphate groups (Cuniberti, Maciá, Rodríguez et al., 2007).

Each base has a specific combination and composition of nitrogen, oxygen, hydrogen and carbon. For the DNA structure, each base is attached to



a deoxyribose (sugar molecule) and phosphate groups (Figure 2.4), shown as P. Individual nucleotides are attached through the phosphate molecules, and the sequence of these nucleotides determines the product of the gene.

### 2.2.1 Thymine

Thymine is one of the four fundamental bases that form the DNA structure. This molecule is in the pyrimidine group, a category of molecules that each contains 15 atoms. In DNA, this molecule binds to an adenine molecule using hydrogen bridges. Figure 2.5 (a) indicates the atoms in the thymine base and their geometry. The blue spheres indicate nitrogen atoms, the grey ones represent carbon and the red is for oxygen. Charge and mass of each atom and their positions are shown in Appendix E.

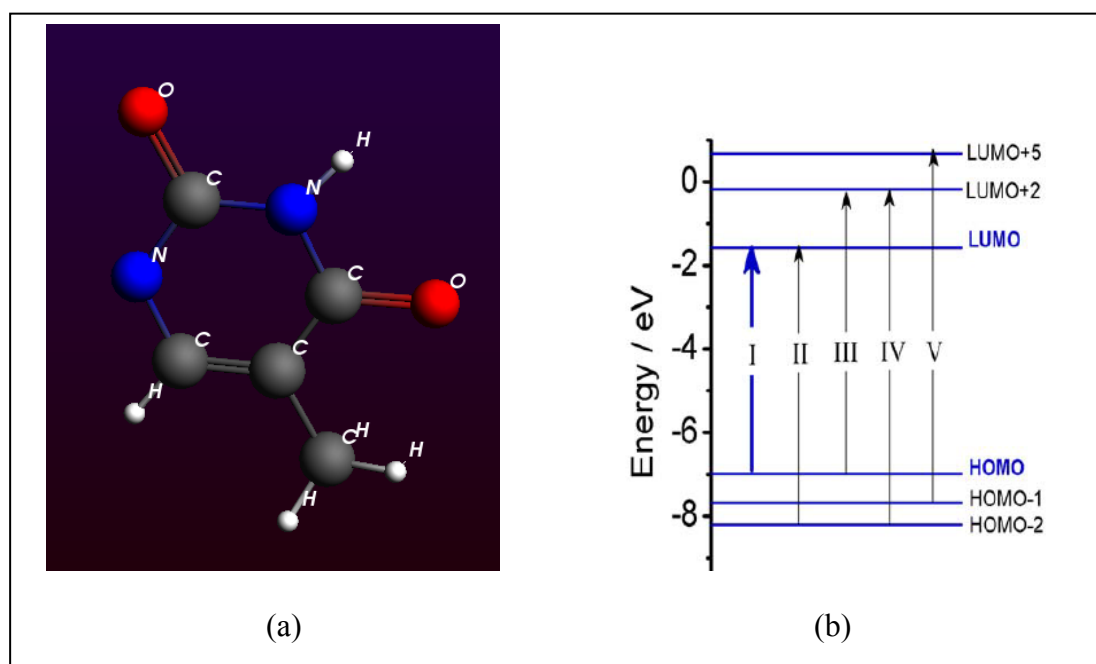


Figure 2.5 (a) Geometry and positions of atoms in thymine. (b) The molecular orbital energy levels in thymine molecules (HOMO and LUMO levels) (Silaghi, 2005).

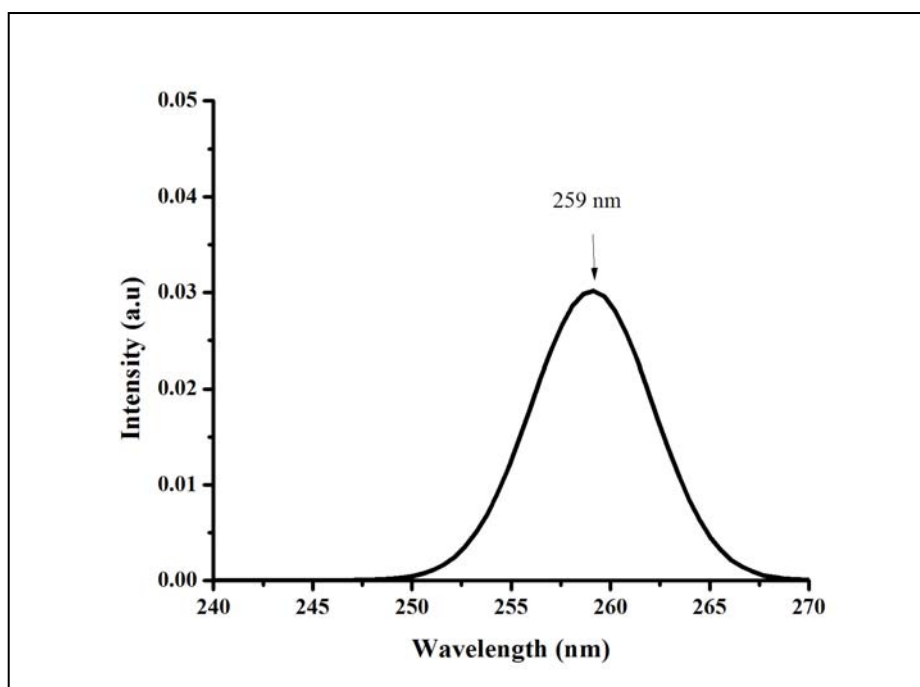


Figure 2.6 The UV-Vis spectrum of thymine calculated using density functional theory.

Thymine molecules have a deviation from the plane, and the average of deviation is approximately 0.320 Å. All atoms in thymine, except the hydrogen atoms, are coplanar. Figure 2.5 (b) indicates the molecular orbital energy level in thymine molecules (HOMO and LUMO levels). HOMO is represented as  $\pi$ , and LUMO as  $\pi^*$ . The arrows indicate the main electronic transitions. UV-Vis spectrum of thymine calculated using density functional theory is shown in Figure 2.6. As depicted in this figure, the maximum wavelength absorption occurs near 260 nm.

### 2.2.2 Cytosine

Cytosine is another base found in DNA. This molecule is the smallest of the four bases. Cytosine is a pyrimidine that contains 13 atoms, and a cytosine can have a hydrogen bond to a guanine molecule.

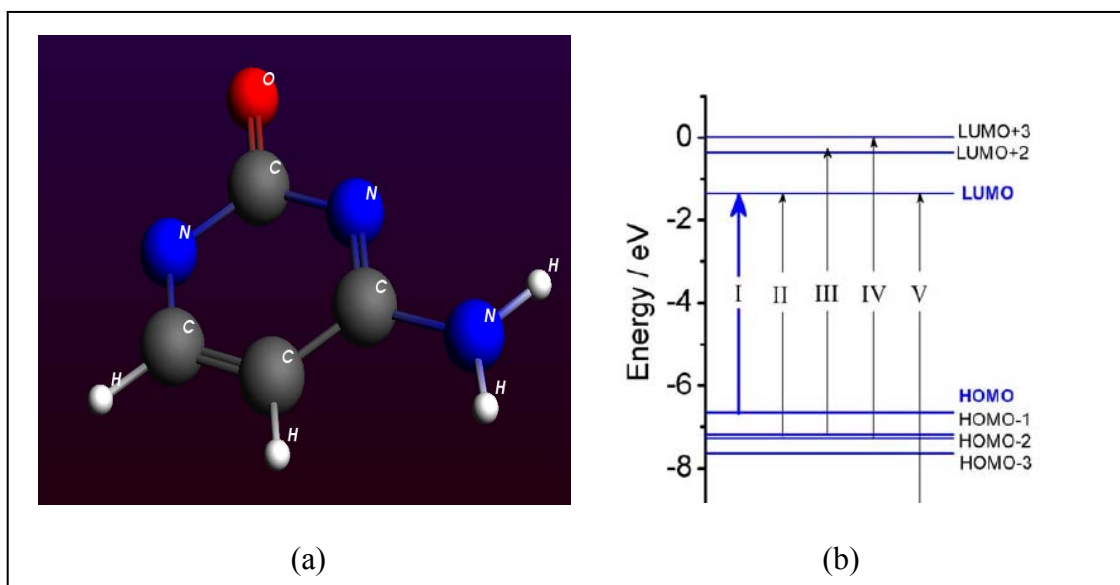


Figure 2.7 (a) Geometry and positions of atoms in cytosine. (b) The molecular orbital energy levels in cytosine molecules (HOMO and LUMO levels) (Silaghi, 2005).

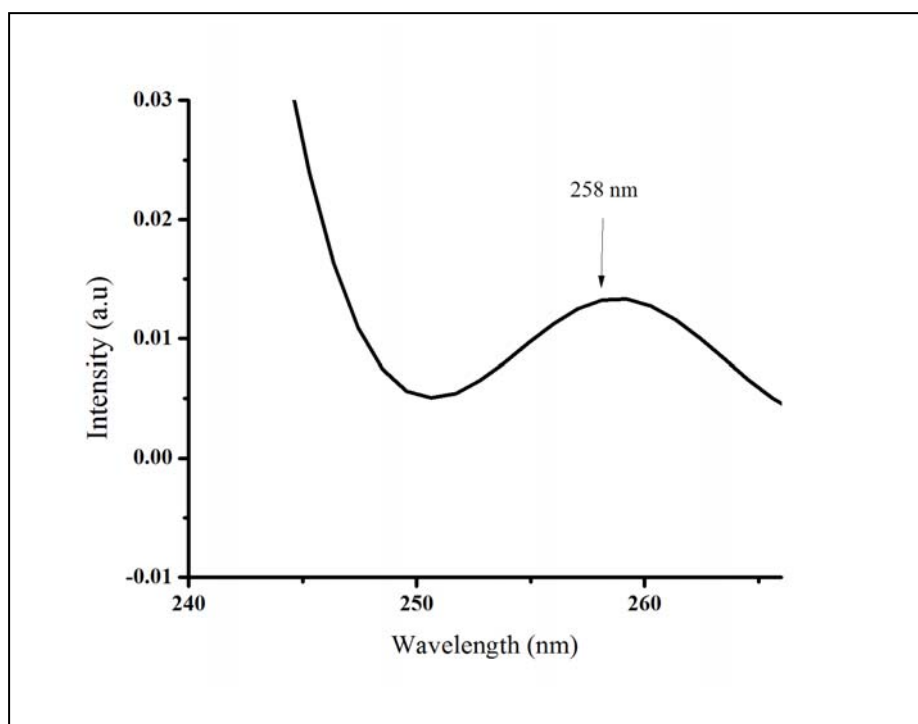


Figure 2.8 The UV-Vis spectrum of cytosine calculated using density functional theory.

Figure 2.7 (a) shows the atomic geometry and positions of cytosine. The blue spheres indicate nitrogen atoms, the grey ones represent carbon and the red is for oxygen. Deviation from planarity in cytosine is approximately 0.007 Å. Figure 2.7 (b) illustrates the molecular orbital energy levels in cytosine molecules (HOMO and LUMO levels). The UV-Vis spectrum of cytosine calculated using density functional theory is shown in Figure 2.8. As depicted in this figure, the maximum absorption occurs at approximately 260 nm.

### 2.2.3 Adenine

Adenine meanwhile is a purine. Adenine and thymine form a hydrogen bonds. The largest component, with 15 atoms, in a DNA helix is adenine. Figure 2.9 (a) shows the molecular structure of adenine.

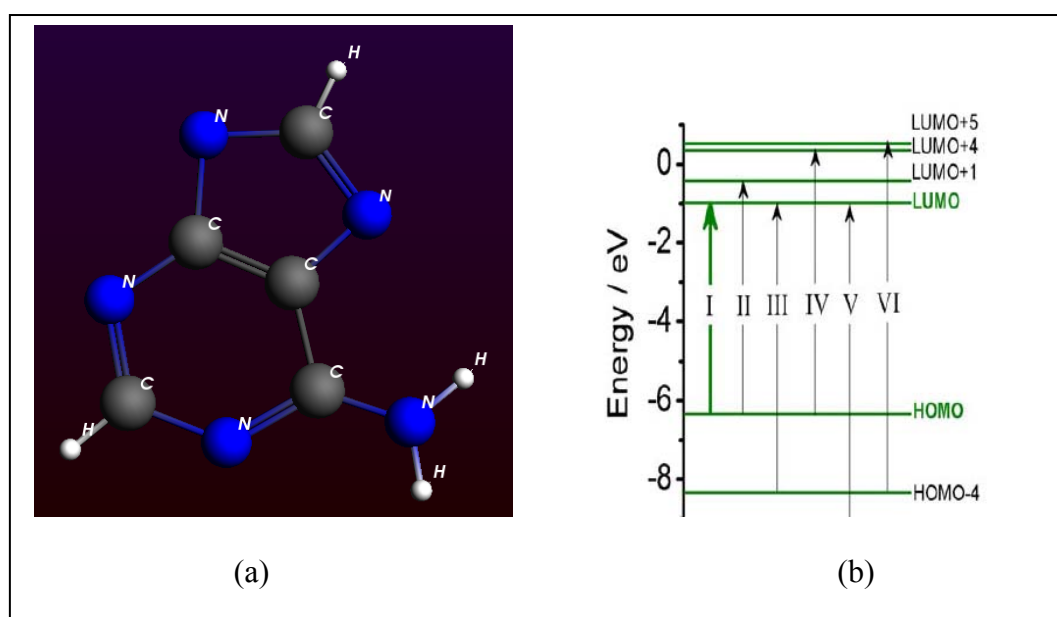


Figure 2.9 (a) Geometry and positions of atoms in adenine. (b) The molecular orbital energy levels in adenine molecules (HOMO and LUMO levels) (Silaghi, 2005).

In this base, there is no oxygen atom. The blue spheres indicate nitrogen atoms and the grey ones represent carbon. Figure 2.9 (b) indicates the molecular orbital energy levels in adenine (HOMO and LUMO levels). The UV-Vis

spectrum of adenine calculated using density functional theory is shown in Figure 2.10. As depicted in this figure, the maximum absorption is at approximately 252 nm.

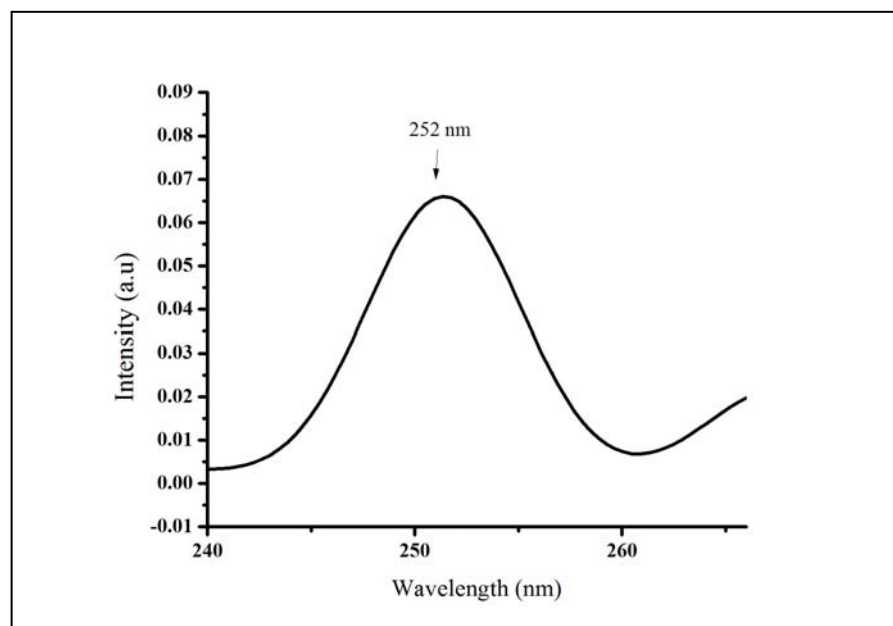


Figure 2.10 The UV-Vis spectrum of adenine calculated using density functional theory.

#### 2.2.4 Guanine

Guanine, with 16 atoms in its molecular structure, is also a purine. Guanine is the counterpart to cytosine, with which it forms hydrogen bonds. The molecular structure of guanine is depicted in Figure 2.11 (a), in which the blue spheres indicate nitrogen atoms and the grey ones represent carbon. Figure 2.11 (b) indicates the molecular orbital energy levels in guanine. The UV-Vis spectrum of guanine according to density functional theory is shown in Figure 2.12. As depicted in this figure, the maximum absorption is approximately 257 nm. A Cartesian depiction of the geometry of guanine shows a deviation from the plane of the molecule of approximately 0.09 Å (APPENDIX E).

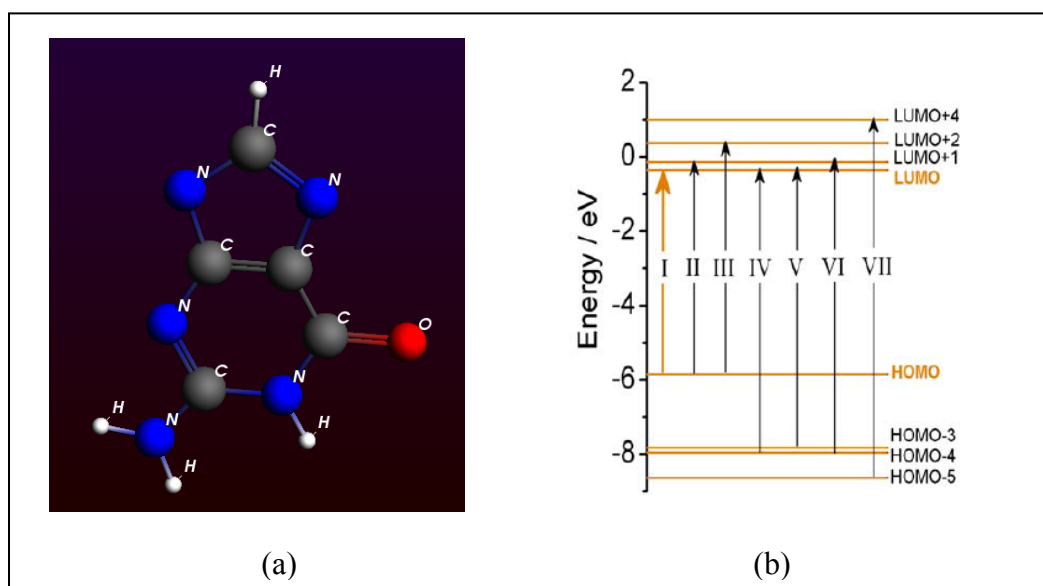


Figure 2.11 (a) Geometry and positions of atoms in guanine. (b) The molecular orbital energy levels in guanine molecules (HOMO and LUMO levels) (Silaghi, 2005).

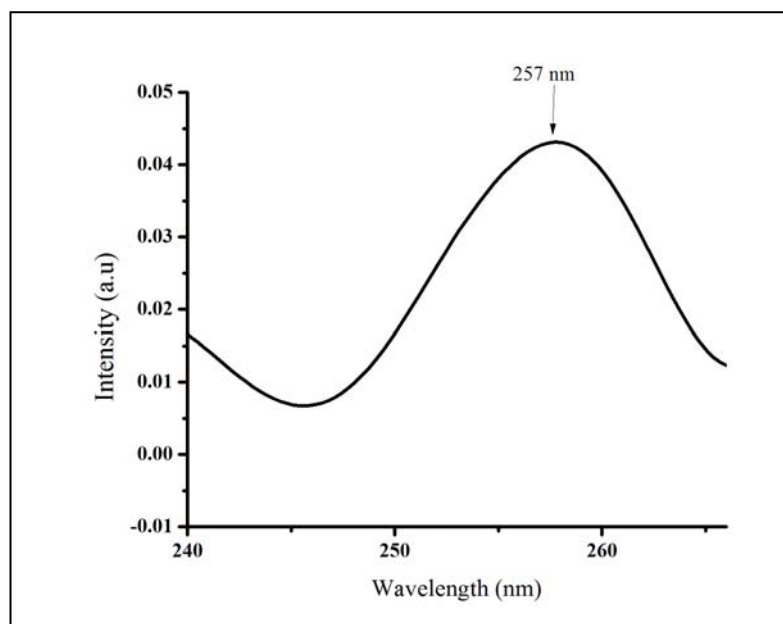


Figure 2.12 The UV-Vis spectrum of guanine calculated using density functional theory.

## 2.3 Types of DNA cleavage

DNA cleavage is an important process in all living cells. There are three categories of DNA cleavage: DNA hydrolysis, photochemical cleavage and oxidative cleavage. The last two types of cleavage are closely related.

### 2.3.1 DNA hydrolysis

The general mechanism of the DNA hydrolysis process is a type of nucleophilic attack on the phosphate side of the DNA helix. Cleavage results in the scission of either the 3'-PO or the 5'-PO.

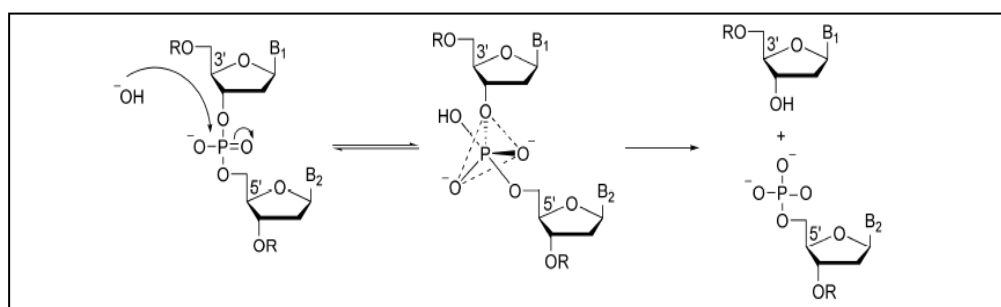


Figure 2.13 DNA and nucleophile hydroxide interaction. A hydroxide or activating water promotes the phosphate group by attaching to and splitting the DNA strand (viewing the picture from left to right shows a schematic of the cleavage mechanism).

Figure 2.13 indicates the mechanism of hydrolysis in the DNA helix. A hydroxide or activating water acts as a nucleophile or activates the phosphate group in a nucleophilic attack (left). Otherwise, the leaving group can depart. In Double strand DNA(dsDNA), the overlap of the molecular orbitals in the base pairs leads to a decrease and minimisation of the light intensity in UV region. Indeed, the cleavage decreases the overlap and then increases the UV absorbance.

### 2.3.2 Photochemical cleavage of DNA

DNA cleavage is a production of reactive species such as oxygen by photochemical process. In photochemical and oxidative DNA cleavage, the reduced oxygen species generate reactive intermediates (Dunn, Lin, Kochevar, 1992; Nielsen, Jeppesen, Egholm et al., 1988).

The DNA cleavage is because of the oxidation interaction in guanine bases (Figure 2.14). Guanine has a low energy of ionization as compared to rest of the bases. Ionization energy for adenine, cytosine, guanine and thymine are 8.24, 8.87, 7.75 and 9.14, respectively (Slavicek, Winter, Faubel et al., 2009; Yang, Wang, Vorpapel et al., 2004).

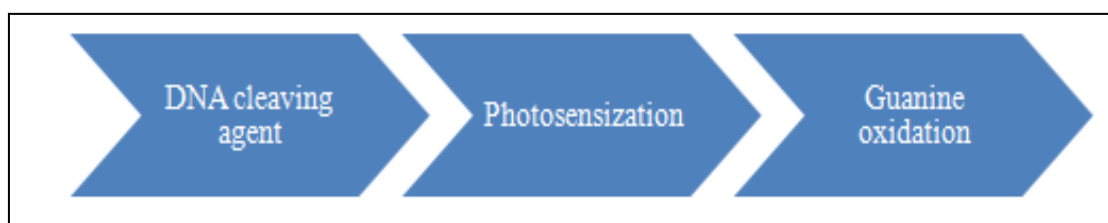


Figure 2.14 The cleavage of DNA by oxidation in the guanine site.

The excited site in DNA generates oxygen, which modifies guanine base, in contrast to superoxide. Damage of DNA observed via this pathway forms guanine radical cations which can then be utilized as a label or tag for detection or attaching other materials.

### 2.4 UV-Vis spectroscopy

UV-Vis spectroscopy is the fundamental scheme of molecular orbitals. Molecular orbitals can define all molecules by subtracting or adding atomic orbitals made from bonding and antibonding levels. Highest Occupied Molecular Orbital or HOMO is the bonding orbital that contains the valence electrons. The Lowest Occupied Molecular Orbital (LOMO) is known as bonding orbital that is normally devoid of electrons. This description is valid



for single molecules. In bulk materials that include many atoms, the addition of individual atomic orbitals form closely spaced orbitals, known as bands.

#### 2.4.1 Biological perspective

Interaction between electromagnetic wave and molecules cause the atoms to undergo vibration; the higher the energy, the shorter the wavelength. The energy of radiation in the UV (200-400 nm) and visible (400-700 nm) range causes transitions between electronic levels in organic materials. Molecular orbital in organic materials consists of one bonding molecular level known as  $\sigma$  MO, and a antibonding level with higher energy called  $\sigma^*$  MO. When the molecule is in the lower-energy (ground state), both electrons are paired. The antibonding level is known by  $\sigma^*$  or the Lowest Unoccupied Molecular Orbital or LUMO.

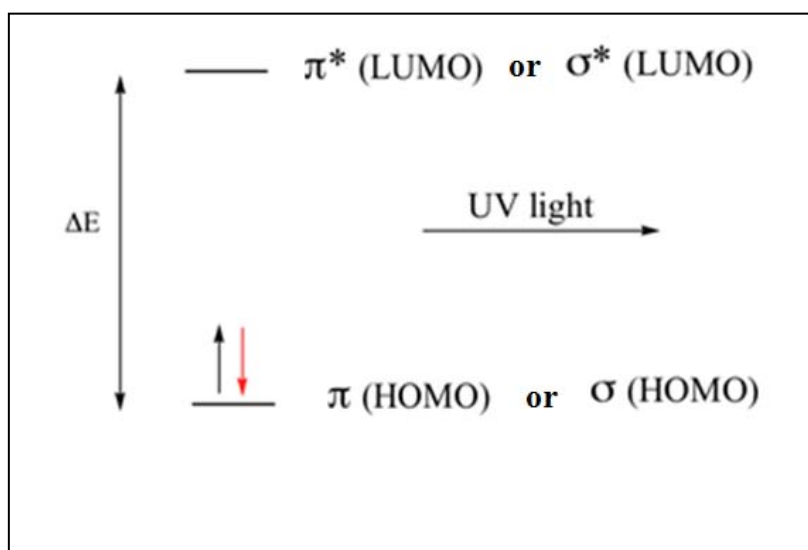


Figure 2.15 The molecule with energy equal to  $\Delta E$ , differences between the HOMO-LUMO levels (energy gap).

If influenced by electromagnetic wave with energy equal to  $\Delta E$ , differences between the HOMO-LUMO levels is the energy gap. This energy is used to move one of the electrons from the HOMO to the LUMO level

resulting in the absorbance of light. This is a form of transition between the  $\sigma$  to the  $\sigma^*$  orbitals ( $\sigma$ - $\sigma^*$  transition). In such condition that a double-bonded molecule is influenced by light and absorbs the exact light, it undergoes transition between  $\pi$  and  $\pi^*$  level ( $\pi$ - $\pi^*$  transition). The  $\pi$ - $\pi^*$  energy gaps are smaller than the  $\sigma$ - $\sigma^*$  energy gap (Figure 2.15).

UV-Vis spectroscopy is useful to biological and organic chemists in the analysis and study of conjugated pi systems. The energy gap in  $\pi$ - $\pi^*$  transition is narrower than isolated double bonds, and then the absorbed wavelength will be longer. This is referred to as an  $n$ - $\pi^*$  transition. The nonbonding molecular level ( $n$ ) MO's have higher energy rather than the highest bonding of p orbitals, and thus, the energy gap for a  $n$ - $\pi^*$  transition is narrower than of a  $\pi$ - $\pi^*$  transition. Indeed, the  $n$ - $\pi^*$  absorption is at a longer wavelength.

Materials or parts of molecules that absorb light in the UV-Vis spectrum are known as chromophores. DNA, which absorbs light between 250-300 nm is a chromophore due to the aromatic pyrimidine and purine bases. In general, there are two things that one expect to record in UV-Vis spectrums. The first is the wavelength at maximal light absorbance ( $\lambda_{\max}$ ). The second is the intensity of absorbed light at maximum wavelength ( $I$ ). Intensity is a unitless quantity called absorbance ( $A$ ). To calculate absorbance at a specified wavelength, the spectrophotometer simply calculate the intensity of light before light passes through the sample ( $I_0$ ), divides the intensity of the same wavelength after light passes through the sample ( $I$ ), then:

$$\text{Eq 2.1} \quad A = \log \left( \frac{I_0}{I} \right)$$

According to the Beer-Lambert principle, the concentration of materials in diluted form has a direct relationship to the absorbance. The extinction coefficient ( $\epsilon$ ), molar absorption, which is a characteristic value for a compound in solution can be measured based on the UV-Vis spectroscopy and Eq 2.1.

If the distance that the beam of light travels through the sample (the path length) is equal to 1 cm, the molar Extinction coefficient is equal by  $\epsilon = \frac{A}{C}$ , then the unit for molar absorptivity is  $\text{mol} \cdot \text{L}^{-1} \text{cm}^{-1}$ .

Molecular biologists and biochemists determine the concentration of samples such as DNA using the value of  $\epsilon = 0.020 \text{ ng}^{-1} \text{mL}$ . Double-stranded DNA have specific extinction coefficient at  $\lambda_{\text{max}}$  of 260 nm. In this application, the concentration is expressed by mass/volume rather than molarities; for instance ng/mL used is a common and convenient unit for DNA concentration.

#### 2.4.2 Physics perspective

UV light, as an electromagnetic wave (EM-wave), is built up of oscillating electric and magnetic fields. The interaction between UV light and materials, based on the Fermi golden rule, is used to calculate the band edge absorption in direct gap material (APPENDIX A). In particular, the discrete bands that form are known as the valence and conduction bands. In the valence band, electrons are tightly coupled with nuclei, while electrons in this band are somewhat separated from their respective nuclei, consequently allowing free motion within the solid.

#### 2.4.2.1 Band gap

Band gap of a material is defined as the energy between the valence and conduction bands. The band gap measured using UV-Vis spectroscopy can be derived using mathematical tools. According to Eq 2.2, there is no absorption below the cut-off edge  $E_g$  (band gap energy), and absorption occurs for light with energy greater than the  $E_g$ .  $\hbar\omega$  is the incident light energy.

$$\begin{aligned} E &= 0 & \text{for } \hbar\omega < E_g, \\ E &\propto (\hbar\omega - E_g)^{\frac{1}{2}} & \text{for } \hbar\omega \geq E_g. \end{aligned}$$

Eq 2.2

Valance and conductance energy levels will change after influenced by magnetic field. The differences between the valance and conduction bands are related to the energy gap and will change after magnetic field exposure. This change is based on the Zeeman Effect.

#### 2.4.2.2 Refractive indices

Refractive indices describe the ratio of the velocity  $c$  of an electromagnetic wave to its velocity in vacuum,  $c_0$  (Eq 2.4). This index describes the optical response of the material to the incident EM wave and is a property of the medium.

$$n = \frac{c}{c_0}$$

Eq 2.3

The refractive index can be written in the following general form:

$$n = n_r + n_i$$

Eq 2.4

$n_r$  ,  $n_i$  are real and imaginary part of refractive index. The amplitude of complex reflection to normal incident light can be derived from the Kramers-Kronig relationship that is defined below:

$$\text{Eq 2.5} \quad R^{1/2} = \frac{(n-1) + ik}{(n+1) + ik} = R^{1/2} e^{i\varphi}$$

where R is the magnitude of the reflectance at the frequency  $\omega$ . The phase  $\varphi$  is related to the reflectance by the dispersion equation, defined in the Kramers-Kronig analysis as follows:

$$\text{Eq 2.6} \quad \varphi(\omega) = 1 - \frac{\omega}{\pi} P \int_0^{\infty} \frac{\ln R(\omega')}{\omega'^2 - \omega^2} d\omega'$$

where P stands for the Cauchy principal value. The real and imaginary parts of the complex optical refractive index, n and k are related to the reflectance amplitude and phase, respectively, by the following equations:

$$\text{Eq 2.7} \quad n(\omega) = \frac{1-R}{1+R+2R^{1/2} \cos \varphi}$$

$$k(\omega) = \frac{-2R^{1/2} \sin \varphi}{1+R+2R^{1/2} \cos \varphi}$$

Consequently, the real,  $\varepsilon'$  and imaginary,  $\varepsilon''$  parts of the complex dielectric function can be obtained using the following:

$$\text{Eq 2.8} \quad \varepsilon(\omega) = \varepsilon'(\omega) + i\varepsilon''(\omega)$$

$$\text{Eq 2.9} \quad \varepsilon' = n^2(\omega) - k^2(\omega)$$

$$\text{Eq 2.10} \quad \varepsilon'' = 2n(\omega)k(\omega)$$

The Kramers-Kronig relationship is a good mathematical tool for extracting the real and imaginary parts of the refractive index (APPENDIX C).

#### 2.4.2.3 Loss function

The imaginary part, also known as the extinction coefficient, is related to the damping of the oscillation amplitude of the incident field. A non-metallic material (dielectric) has low absorption, and the imaginary part is small and often neglected. If the material is conductive, the imaginary part is larger and must be taken into account. The energy-loss spectrum is closely related to a quantity referred to as the energy-loss function,  $\text{Im}[-1/(\varepsilon)]$  (Imaginary part of  $-1/(\varepsilon)$ ) via this relationship (Batson and Silcox, 1983; Ghasemifard, Zavar, Ghasemifard et al., 2010).

$$\text{Eq 2.11} \quad \text{Im}\left(-\frac{1}{\varepsilon}\right) = \frac{2n(\omega)k(\omega)}{(n^2(\omega) + k^2(\omega))^2}$$

### 2.5 Magnetic field effect on materials

To understand the effects of magnetic fields on material, both quantum and classic mechanics are required. Some phenomena can be described using classical mechanics and some should be explained using quantum effects.

#### 2.5.1 Classical mechanics

There are two types of forces that operate on electric charges and ions,  $q$  that are placed inside magnetic and electric fields. Electric fields,  $E$ , apply a force  $F=qE$  proportional to the intensity of the electric field and the magnitude

of the charge. This force is exerted regardless of the motion of the charge or ion. Magnetic field,  $B$ , can only interact with moving ions and charged objects. The magnetic force  $F=q\mathbf{v}\times\mathbf{B}$  is restricted by the rule that only a charge,  $q$ , moving in a non-parallel direction to  $B$  can experience a magnetic force. This limitation is an important feature of the Lorentz force.

The equation of motion for a particle of charge  $q$  and mass  $m$  under the Lorentz force is given by the following:

$$\text{Eq 2.12} \quad m \frac{d\mathbf{v}}{dt} = q(\mathbf{E} + \mathbf{v} \wedge \mathbf{B})$$

This equation requires the particle to accelerate and reach a velocity . Here  $\mathbf{v}$  is the particle's velocity and  $\wedge$  denotes the cross product. The electric field in a real system does not extend to infinity, implying that collisions do slow down the particle. When  $E=0$ ,  $B=B_0Z$ , the charge accelerates and velocity can be derived as shown below:

$$\begin{aligned} \text{Eq 2.13} \quad \frac{dv_x}{dt} &= \frac{q}{m} v_y B_0 \\ \frac{dv_y}{dt} &= -\frac{q}{m} v_x B_0 \\ \frac{dv_z}{dt} &= 0 \end{aligned}$$

The contraction induced by the Lorentz force power and the liquid environment is largely based on dipole-dipole interactions and the free charge interactions that could cause significant differences between their magnitudes. Another mechanism that is important in the interaction between biological samples and a static magnetic field is bound ion dynamics. The oscillation of a bound ion about its binding portion in a signalling molecule can affect its ionic transport. These equations are easily solved as

Eq 2.14. The x,y and z index indicate the direction of velocity and show perpendicular direction.  $\omega_c$  is and  $f$  is .

$$\begin{aligned} \text{Eq 2.14} \quad v_x &= v_{x0} e^{\pm i\omega_c t} & v_x &= v_{\perp 0} \cos(\omega_c t + \varphi) \\ v_y &= v_{y0} e^{\pm i\omega_c t} & \text{where } \omega_c &= \frac{q}{m} B_0 & v_y &= -v_{\perp 0} \sin(\omega_c t + \varphi) \\ v_z &= v_{z0} & v_z &= v_{z0} \end{aligned}$$

This magnetisation causes the cell to experience a rotational torque caused by the static magnetic field. Effect of magnetic field on the orientation of molecules and moving charged objects is the most important when exposed to biomaterials, such as large organised structures (e.g., DNA and proteins). The ionic side of DNA move faster and faster due to the Lorentz force, according to Eq 2.16.

$$\begin{aligned} \text{Eq2.15} \quad \mathbf{F} &= (\mathbf{F}_M + \mathbf{F}_D) = \frac{d}{dt}(m\mathbf{V}), \\ K &= \frac{1}{2} m(v_x^2 + v_y^2) = \frac{1}{2} mV^2 = K_b T \end{aligned}$$

K indicates the kinetic energy, m and v are mass and velocity of ions, respectively, and  $K_b$  and T are the Boltzmann constant and the temperature, respectively.

### 2.5.2 Quantum mechanics of the magnetic field effects on materials

An electron can spin around a nucleus and also has an intrinsic spin around its own axis. Angular momentum follows the right hand rule. The angular momentum and the magnetic moment are in the same direction (Figure 2.16) as that caused by the spin of the nucleus.



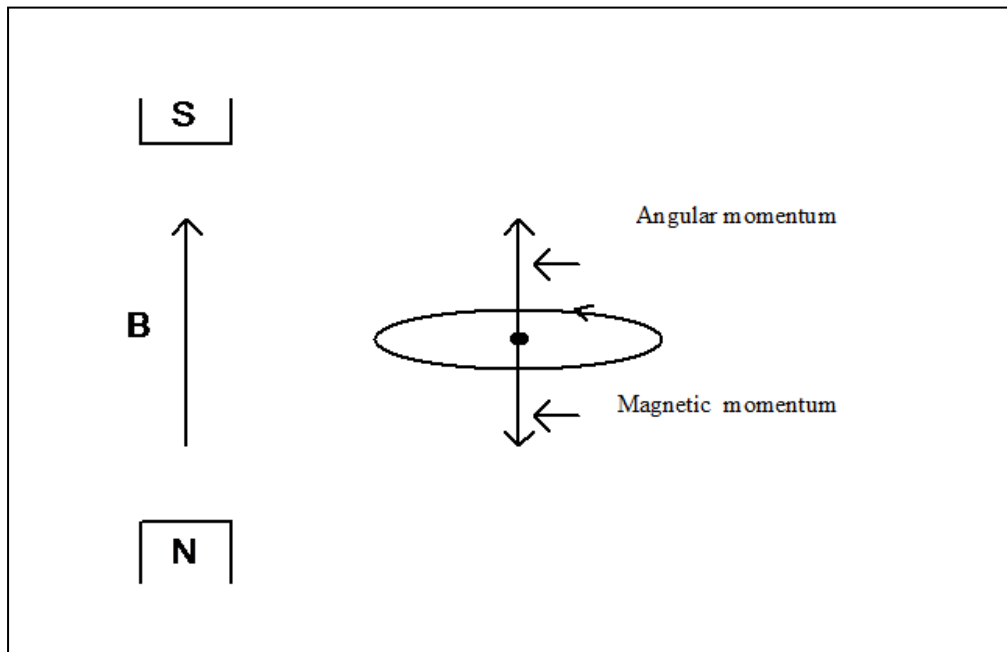


Figure 2.16 The angular momentum vector,  $L$ , can lie along specific orientations with respect to the external magnetic field.

The magnetic momentum vector,  $m$ , can lie along specific orientations with respect to the same direction or opposite direction of external magnetic field (Figure 2.17).

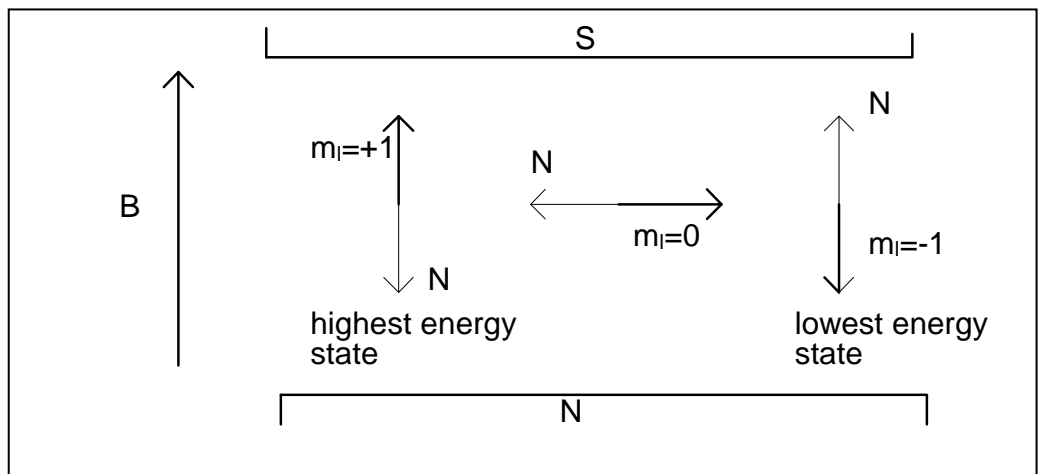


Figure 2.17 An atom is placed in a magnetic field with the convention that the South Pole is at the top and the North Pole is at the bottom.

### 2.5.2.1 The Zeeman Effect

When an atom with  $J > 0$  is placed in a magnetic field, spectral lines split into components. Therefore, by applying a magnetic field  $B$ , the energy levels of an atom change by an amount  $-\mu_B B$ . Indeed, the energies of the absorbed and emitted photons will change. This effect was observed for the first time in 1896 by Zeeman before the development of quantum mechanics and is called the Zeeman effect (Atkins and Friedman, 1997). The energy difference between adjacent levels is described below:

Eq 2.16 
$$E_{MJ} = \mu_B B M_J$$

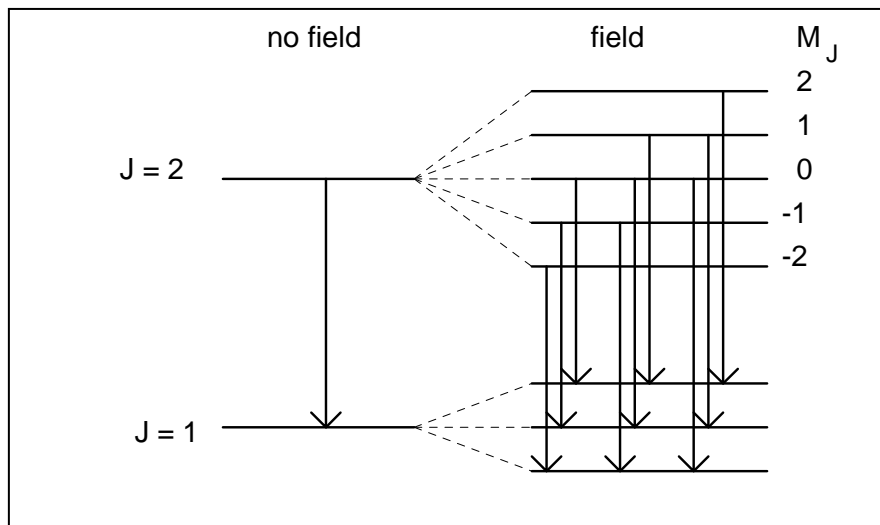


Figure 2.18 The difference in energy between adjacent levels

As shown in Figure 2.18, when the splitting of the energy levels after applying a magnetic field is the same for the lower and upper levels, only three lines result from the 9 transitions. The splitting for  $S = 0$  is the same and is known as the normal Zeeman Effect. Energy equation for the normal Zeeman Effect is as follows:

Eq 2.17 
$$E_{MJ} = E_0 + M_J \cdot \mu_B \cdot B$$

The magnitude of the energy shift,  $\Delta E$ , after applying a magnetic field is given by Eq 2.17 and Eq 2.18 as follows:

Eq 2.18 
$$\Delta E = -\boldsymbol{\mu} \cdot \mathbf{B}$$

Eq 2.19 
$$= \left( \frac{e}{2m_e} \right) \mathbf{L} \cdot \mathbf{B}.$$

If the z axis is selected to be in the same direction as the magnetic field B, then Eq 2.20 simplifies to:

Eq 2.20 
$$\Delta E = \left( \frac{e}{2m_e} \right) L_z B,$$

in which the values of  $L_z$  are  $m\hbar$ ,

Eq 2.21 
$$\Delta E = \left( \frac{e\hbar}{2m_e} \right) mB.$$

and must have the same dimensions as the magnetic moment. This quantity is called the Bohr magneton  $\mu_B$ , in Atomic Physics with the value:

Eq 2.22 
$$\mu_B = 5.79 \times 10^{-5} eV/T$$

Eq 2.23 
$$\mu_B = \frac{e\hbar}{2m_e} = 9.27 \times 10^{-24} A.m^2$$

Eq 2.22 can be rewritten in terms of  $\mu_B$  as follows:

$$\text{Eq 2.24} \quad \Delta E = m\mu_B B.$$

where there are  $2l + 1$  states of  $m$ :  $1, 1 - 1, \dots, -1$ .

### 2.5.2.2 The anomalous Zeeman Effect

Splitting for  $S > 0$  is different for the upper and lower levels and is known as the anomalous Zeeman Effect. The anomalous Zeeman Effect requires a factor of  $g_J$ :

$$\text{Eq 2.25} \quad E_{MJ} = E_0 + M_J \cdot g_J \cdot \mu_B \cdot B$$

Anomalous Zeeman splitting is complicated and depends on the orbital and spin moments. The simple case is a S state and  $l = 0$ . In this situation, the atom would not have a magnetic moment and would be unaffected by a magnetic field. In fact, the electron has spin, and there is a magnetic moment.

$$\text{Eq 2.26} \quad \mu = \mu_{spin} - \frac{e}{m_e} S.$$

$$\text{Eq 2.27} \quad \Delta E = -\boldsymbol{\mu} \cdot \mathbf{B} = \frac{e}{m_e} S_z B.$$

When a magnetic field  $B$  is applied in the  $z$  direction, the energy changes in the following manner when  $S_z$  has the following values:

$$\text{Eq 2.28} \quad S_z = \pm \frac{1}{2} \hbar,$$

Eq 2.29

$$\Delta E = \pm \frac{e\hbar}{2m_e} B = \pm \mu_B B$$

The separation should be twice that of the normal Zeeman Effect. Thus, the separation of levels =  $2\mu_B$ .

### 2.5.2.3 The Paschen-Back Effect

The Paschen-Back regime (PBR) was described by Hill in 1929 and described as the splitting of molecular doublet levels.

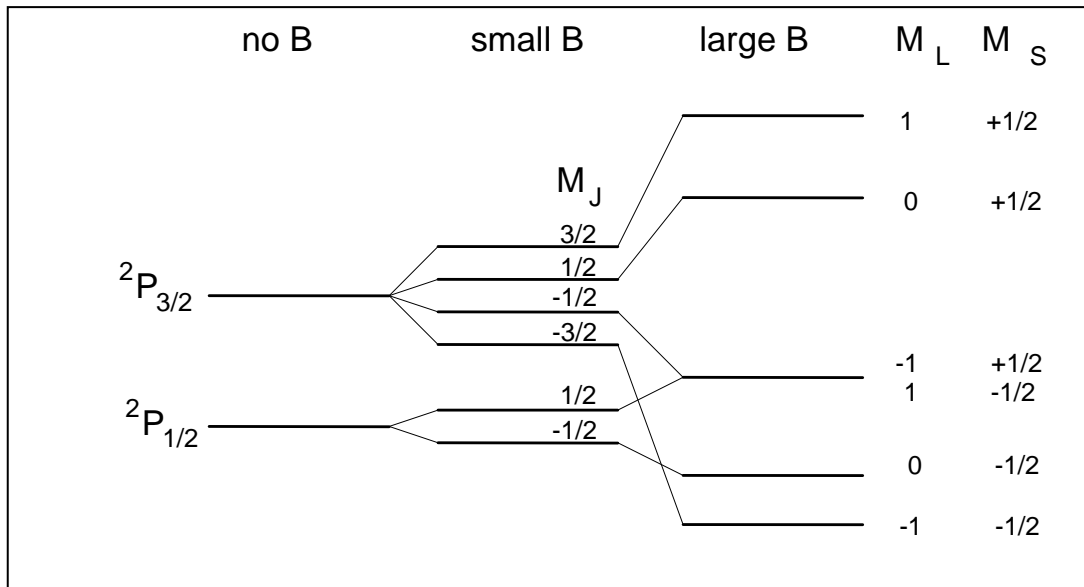


Figure 2.19 The splitting of the sodium D line when the amplitude of the magnetic fields increase from low to high shows this effect.

For sufficiently large magnetic fields, the orbital angular momentum  $L$  and the spin angular momentum  $S$  couple to the magnetic field separately. Figure 2.19 shows the splitting of the sodium D line at the amplitude of the magnetic fields. In this condition, the levels are characterised by  $M_L$  and  $M_S$  values rather than  $M_J$  (Minaichev, Myasishcheva, Obukhov et al., 1970).

In an external magnetic field, the expected Hamiltonian can be calculated using the equations below:

$$\text{Eq 2.30} \quad H = H_{cf} + V_{so} + V_{lB} + V_{sB}$$

$$\text{Eq 2.31}$$

$$H = H_{cf} + \frac{g_s}{(2\mu c)^2} \frac{1}{r} \frac{dV(r)}{dr} \vec{S} \cdot \vec{L} - \frac{qg_l}{(2\mu c)} \vec{L} \cdot \vec{B} - \frac{qg_s}{(2\mu c)} \vec{S} \cdot \vec{B}$$

$$\vec{S} \cdot \vec{L} = 0$$

$$\text{Eq 2.32} \quad H = H_{cf} + \frac{e}{(2\mu c)} \vec{L} \cdot \vec{B} + \frac{e}{(\mu c)} \vec{S} \cdot \vec{B}$$

In a strong magnetic field B,  $\vec{S} \cdot \vec{L} = 0$ , which is known as the Paschen-Back Effect.

#### 2.5.2.4 Raman spectroscopy

Raman spectroscopy is a spectroscopic method based on the scattering of monochromatic light by a molecule. The usefulness of Raman scattering for studying molecular vibrations was discovered in 1928 by C.V. Raman (Lin-Vien, 1991).

The mechanisms by which electromagnetic radiation interacts with molecular systems differ. Electromagnetic waves can interact with a vibrating molecule if the electric field vector of the electromagnetic wave oscillates along the dipole moment  $\mu$  of the molecule. If the dipole moment of the molecule and the normal vibration change, the molecule has an infrared-active vibration.

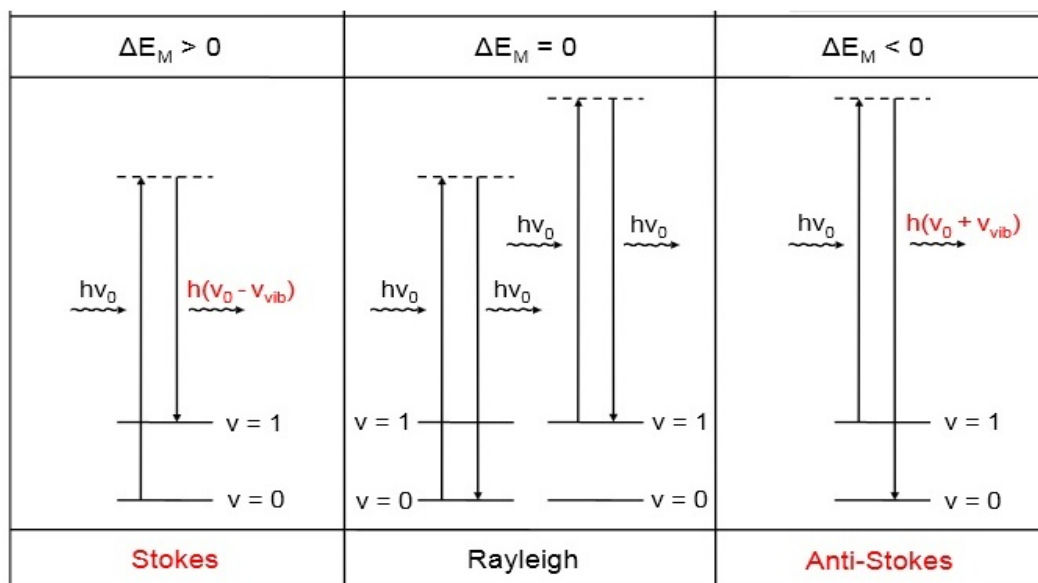


Figure 2.20 Raman scattering mechanism, including Stokes, anti-Stokes and Rayleigh scattering.

Raman spectroscopy is based on scattering. Electromagnetic radiation is scattered by crystal or molecule. As a result of scattering, one photon from the incident light is annihilated and one photon in the scattered radiation is created.

The scattering light can be classified by the difference between the frequency of the incident and scattered light. In Rayleigh scattering, the frequency of the incident light is equal to that of the scattered light. In Raman scattering, the energy of the incident light is not equal to that of the scattered light. The change in frequency leads to the Stokes and anti-Stokes scattering effects. Figure 2.20 shows a schematic of Rayleigh, Stokes and anti-Stokes scattering. As shown in this figure, for Rayleigh scattering, the incident light and the scattered light have the same energy. For Stokes and anti-Stokes scattering, the scattered energy is smaller and larger, respectively, than the incident energy. All electromagnetic waves have an electric field. The electric field interacts with the charge distribution of a molecule (dipole moment) and the resultant perturbation is proportional to the strength of the electric field.

Perturbed electron moves to another state, an excited state. Dipole moment changes in the molecule according to Eq 2.33.  $\alpha$ ,  $E$ ,  $\mu$  and  $\mu_0$  are the polarizability, the electric field, the dipole momentum and the dipole momentum in zero fields, respectively.

Eq 2.33 
$$\mu = \mu_0 + \alpha E$$

The excited electron returns to the initial state in Rayleigh scattering and can move to a higher-energy state in Stokes scattering or a lower-energy state in anti-Stokes scattering. All of these transitions should follow selection rules (APPENDIX D).

Vibration modes in Raman spectroscopy obey the selection rule that  $\Delta v = \pm 1$  for a harmonic oscillator and  $\Delta v = \pm 1, \pm 2, \pm 3, \pm 4, \pm 5, \dots$  for an anharmonic oscillator. Not all vibrations can participate in Raman scattering. Vibrations that change the molecule polarisability during the interaction will have a Raman response.



## CHAPTER III: DESIGN, METHODS AND PROCEDURE

### 3.1 Introduction

This chapter deals with the experimental part of the thesis, including the materials, chip fabrication, set up and measuring instruments. The best methods for extraction, measurements, fabrication and analysis were selected using the following criteria; the available facility, the best accuracy, high quality and safety. Each part of this chapter includes a brief explanation on the possible regular methods for comparison with the presented method. Due to the highly sensitive DNA samples and the microchip fabrication process, the extraction and fabrication techniques were conducted in a controlled condition of a 10K clean room.

### 3.2 Materials

A p-type Si wafer (orientation <100>) with a resistivity of 1 to 10–20  $\Omega$ -cm (MEMC Electronic Materials) was used as the substrate. The gold wire (Kurt J. Lesker Company) that was used in the evaporation and magnetron sputtering technique had a purity of 99.999%. Other necessary chemicals ( $C_2H_5OH$ , deionized water and acetone) and MicroChem's SU-8 photoresist and developer were supplied by Sigma Aldrich and were used without further purification. Borosilicate or Pyrex glass was used as a substrate material with an electrical resistivity of approximately  $10^{13}$   $\Omega$ .m (William Jr, 2007). DNA from *Mimosa pudica* (the sensitive plant) was extracted using the extraction kit Gene All kit (Plant SV mini). The sample preparation in this work was divided into two sections consisting of DNA extraction and oligonucleotide

preparation. Two types of DNA were used in this research, DNA extracted from plant and oligonucleotide DNA.

### 3.2.1 DNA extraction

The DNA was extracted from a common local Malaysian plant, *Mimosa pudica*, also known as sensitive plant depicted in Figure 3.1.



Figure 3.1 An image of *Mimosa pudica* commonly known as the sensitive plant.

Extraction process was performed according to the standard protocol for plant extraction using a Gene All kit (Plant SV mini). GENE-ALL™ Plant SV Kits provide a simple method for the purification of small amounts of DNA from plant tissues. Pure genomic DNA (P-DNA) resulting from this method is suitable for various applications without manipulation. Up to 100 mg of plant tissue can be processed using this method. The fast and safe extraction due to elimination of organic solvents was the main reason for selecting this method. Materials used in the extraction process include various types of buffer (PL, PD, BD, CW, AE and RNaseA). After washing, cleaning and proper grinding, the extraction process was started systematically. In the first step, 100 mg of ground tissue was placed into a 1.5 or 2 ml tube, which was then inverted

(lysis) several times. Next, 400  $\mu$ l of buffer PL and 4  $\mu$ l of RNase were added to the solution and vortexed, followed by incubation for 10 to 15 min at 65°C. The solution was then filtered, centrifuged and transferred by pass-through to a new tube. In the next step, 1.5 ml of buffer BD was added and mixed immediately for optimal binding. In washing and elution steps, 700  $\mu$ l of mixture was placed in a filter tube, followed by centrifugation (30 seconds). The supernatant was then discarded through the pass-through. Next, 300  $\mu$ l of buffer CW was added and centrifuged for 2 min. In the last step, 100  $\mu$ l of buffer AE was added and incubated for 5 min at room temperature, followed by centrifugation for an additional 1 min ( The protocol shown in Figure 3.2 step by step).

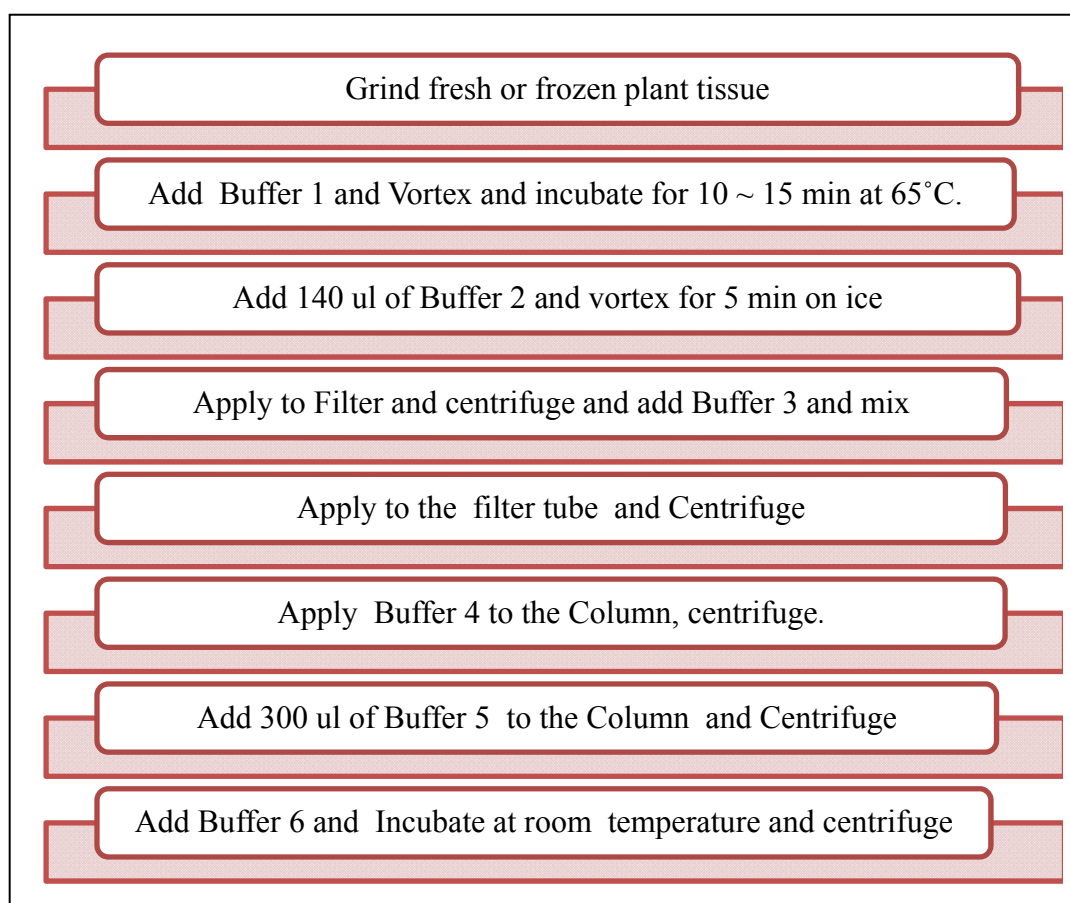


Figure 3.2 DNA extraction protocol

### 3.2.2 Oligonucleotide

Oligonucleotides are short lengths of nucleic acid polymers, typically with 200 or fewer bases. Two types of oligonucleotide DNA were used in this research; either adenine (A) - thymine (T) pairs or cytosine (C) - guanine (G) pairs. The properties of the used oligos such as molecular weight and melting temperature are respectively 30817.6 and 59.48 for 100 mer AT and for 100 mer CG are 30777.5 and 101.25.

Table 3-1 Oligonucleotide DNA feature used in this work

Oligonucleotide	Molecular Weight	Melting temperature	Number (mer)
AT-100	30817.6	59.48	100
CG-100	30777.5	101.25	100

### 3.3 Fabrication of chip

The fabrication consists of several basic steps. A brief overview of the fabrication process, including the cleaning, mask design, lithography and deposition is presented.

#### 3.3.1 Cleaning

There are regular processes involving liquid solvents to clean common samples and substrates, such as silicon, glass and wafers (Banks, 2006). The materials and equipment for these processes are available in a clean room environment as part of the common facilities. After cutting the silicon or substrate manually or using a regular cutter, the cleaning process should be performed using standard RCA method. Simple cleaning process for removing contamination: 1. Rinse the wafer in acetone , 2. Scrub the wafer properly using a swab, 3. Wash the wafer with DI water, 4. Dry the wafer using nitrogen gas

### 3.3.1.1 Standard RCA cleaning process

The RCA method involves major steps to sequentially remove ionic and heavy metals, photoresist, organic and oxide contaminations (Ohmi, 1996).

1. Organic cleaning: Removal of insoluble organic contaminants with a 5:1:1 H<sub>2</sub>O:H<sub>2</sub>O<sub>2</sub>:NH<sub>4</sub>OH<sup>1</sup> solution.

2. Oxide stripping: Removal of a thin silicon dioxide layer where metallic contaminants may be accumulated as a result of step 1, using a diluted 20:1 H<sub>2</sub>O:HF<sup>2</sup> solution.

3. Ionic cleaning: Removal of ionic and heavy metal atomic contaminants using a solution of 6:1:1 H<sub>2</sub>O:H<sub>2</sub>O<sub>2</sub><sup>3</sup>: HCl<sup>4</sup>

4. Mix 98% H<sub>2</sub>SO<sub>4</sub><sup>5</sup> (sulphuric acid) and 30% H<sub>2</sub>O<sub>2</sub> (hydrogen peroxide) in volume ratios of 2-4:1

### 3.3.2 Mask

Mask design is an important stage in chip fabrication that depends on the sample size, minimum feature size, photoresist and irradiation source. Two different masks should be designed, those for positive and negative photoresists. The photo masks are regularly printed on a transparent layer. Figure 3.2 shows the positive and negative masks designed in this experimental section for the fabrication of the biochip. To design high accuracy masks that have good feature sizes, such as 10-90 µm in spacing and lines, the mask

---

1 Irritating to skin and mucous membranes. Emits highly toxic vapors when heated.

2 Liquid and vapors cause burns that may not be immediately painful or visible. HF attacks glass. HF looks like water, can be fatal in small amounts, and is found in the buffered oxide etch (BOE).

3 Highly corrosive to skin and mucous membranes. Repeated exposure causes erosion of teeth.

4 Strong oxidizing agent. Irritating to skin and mucous membranes. Reacts violently with acids and organic solvents.

5 Liquid and vapors are extremely corrosive to skin and mucous membranes. Generates heat upon contact with water. Reacts with acetic acid ([http://www.cleanroom.byu.edu/acid\\_safety.phtml](http://www.cleanroom.byu.edu/acid_safety.phtml)).

should be designed and fabricated precisely. Laser writers or high-resolution printers are common tools in the mask fabrication process. Quartz and transparent films are common mask materials; they have advantages and disadvantages. Quartz masks have a very long lifetime but are very costly. Transparent films have a low cost but the low quality in the contact mode decreases their lifetime. High resolution printing methods can offer up to 5000 dpi; therefore, small feature sizes of approximately 5 microns are achievable. However, the minimum size is in the range of 10 microns in terms of practicality. Masks are regularly designed using AutoCAD 14 and CorelDraw softwares. Figure 3.3 shows the mask designed using AutoCAD 14 software for both the positive and negative levels.

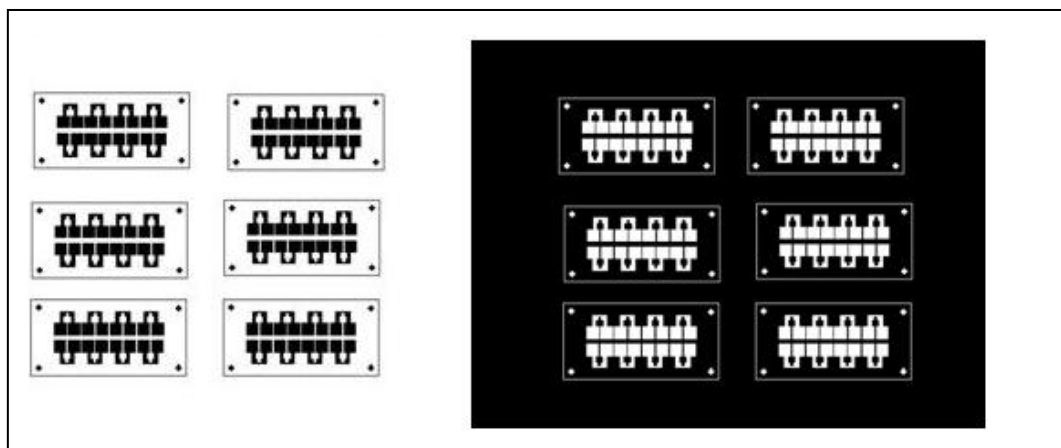


Figure 3.3 Mask designed using AutoCAD 14 software. The left one is for the negative photoresist while the right one is for the positive photoresist.

### 3.3.3 Lithography

Lithography is printmaking technique used in several industrial processes. Lithography consists of the transfer of a pattern onto a substrate by light exposure through a transparent mask on the substrate that is covered by photoresist. Irradiation sources include UV or X-ray light. For micron-sized patterning, UV irradiation is commonly selected.

### 3.3.3.1 Photo resist

A photoresist is a material that responds to the specific light used in the lithography process. Two types of photoresist are offered; negative and positive. For positive photoresists, the portions that absorb the light irradiation are removed after completing the process and vice versa. The unexposed portions will be polymerised and are difficult to dissolve, thus remaining on the surface and appearing as negative photoresist. Figure 3.4 schematically shows the patterns fabricated using positive and negative photoresists. Coating, baking, exposure, developing and all other processes should be performed in clean room conditions with yellow ambient light to obtain high quality patterns. Table 3-2 shows categorises of several popular photoresist (negative and positive) materials used in lithography (Banks, 2006).

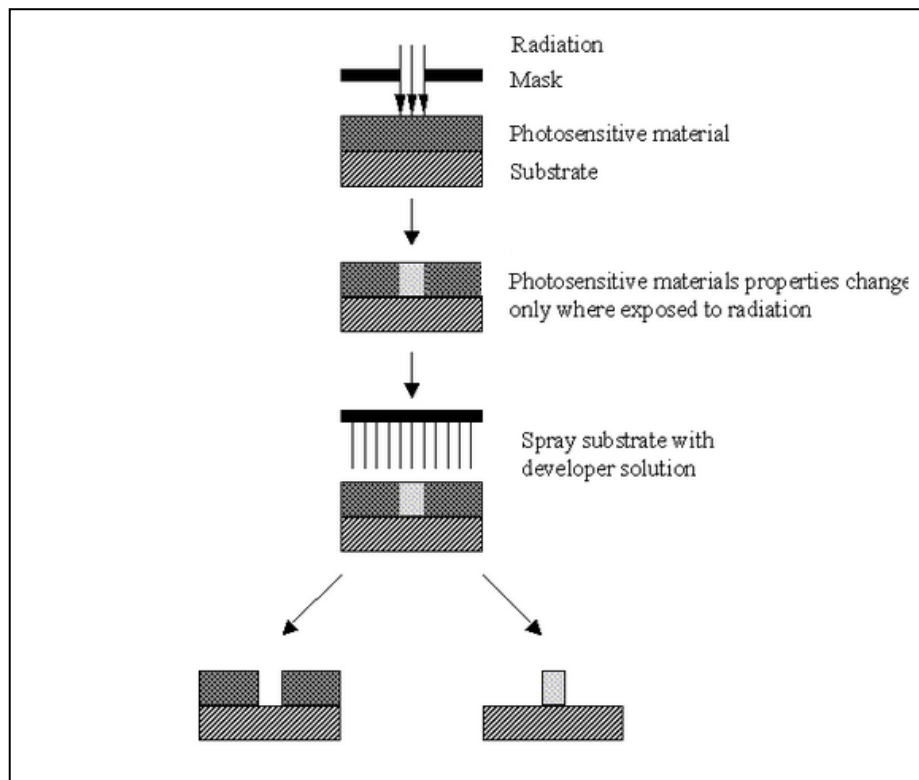


Figure 3.4 Patterns fabricated using positive and negative photoresists, positive (left) and negative (right)

AZ, Shipley, Nlof and SU-8 series are some common photoresists utilised in micro- and nanoengineering. In the present work, SU-8-3000 was selected due to its high sensitivity to the concentration of developer and the high aspect ratio ( $> 10:1$ ) compared with that of other photoresists.

A p-type Si wafer (orientation  $\langle 100 \rangle$ ) possessing a resistivity of 1 to  $10^{-20} \Omega\text{-cm}$  (MEMC Electronic Materials) was used as the substrate. MicroChem's SU8 photoresist and developer were supplied by Sigma Aldrich. SU-8 3000 is an epoxy-based photoresist used for micromachining and microelectronic purposes that provides high contrast and thermally stable images. The standard SU-8 patterning processes is as follows; spin coat, soft bake, expose, PEB and develop. Figure 3.5 shows the sequence of the lithography process. Figure 3.6 depicts the procedure used to create a layer of SU-8 photoresist on prepared substrate.

Table 3-2 Categorisation of popular photoresists used in micro-engineering (Banks, 2006).

<b>Positive Photo resist</b>	<b>Developer</b>	<b>Type</b>
AZ 3312	AZ300MIF	Positive
AZ 3330	AZ300MIF	Positive
Shipley 1.2 L	Shipley MF-26A	Positive
Shipley 1.8 M	Shipley MF-26A	Positive
Nlof 2020	110°C/60s	Negative
SU-8-2000.5	SU-8 Developer, gently agitate	Negative
SU-su8-3000	SU-8 Developer, gently agitate	Negative



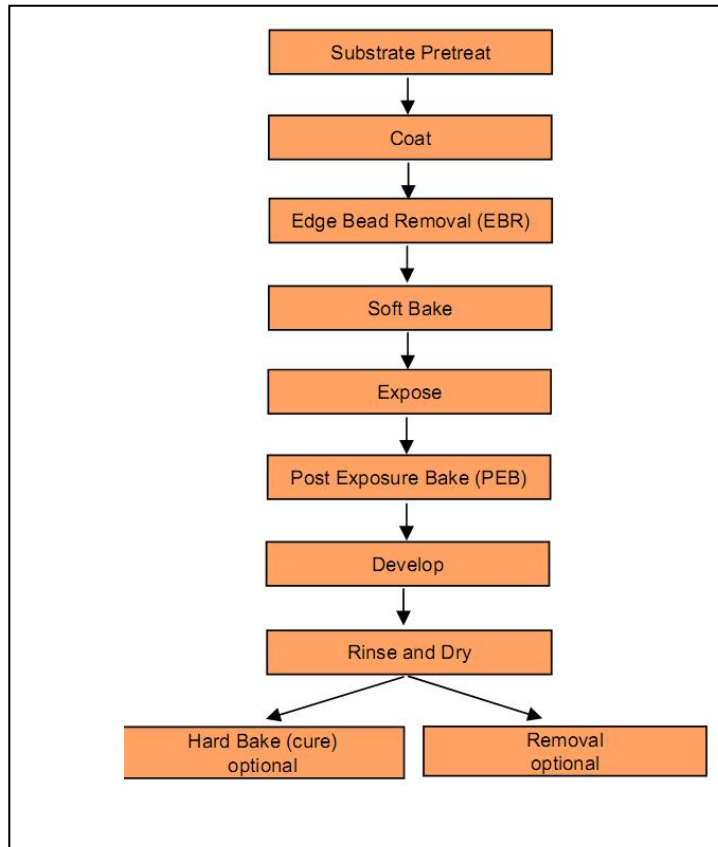


Figure 3.5 Schematic of the patterning mechanism.

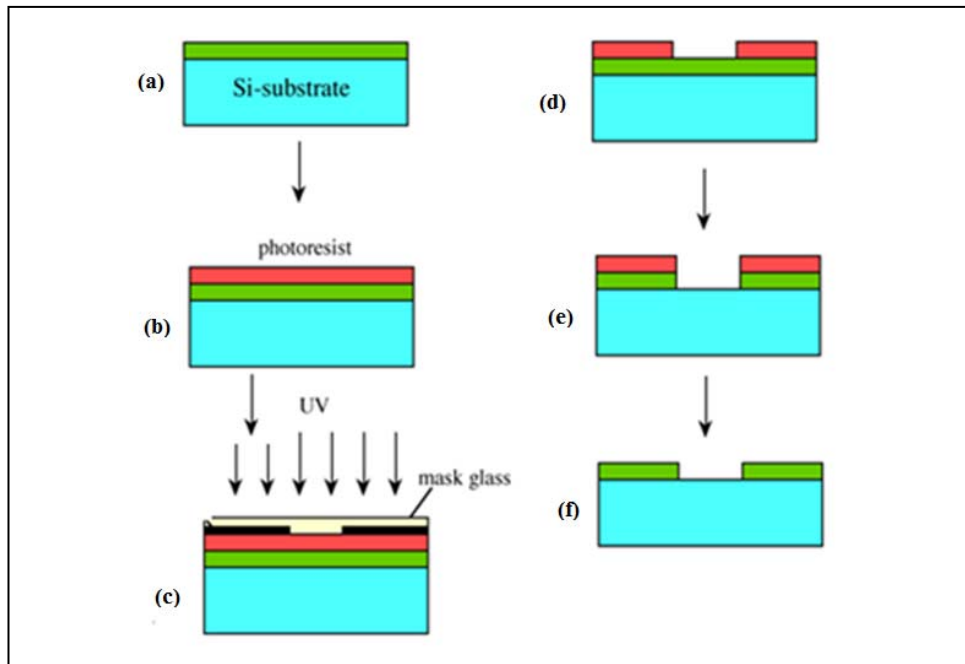


Figure 3.6 Procedure used to make a layer of SU-8 photoresist on a prepared substrate.

According figure 3.6, The SU8-3000 photoresist deposited over cleaned silicon( a and b) wafer by spin coating method for spin parameter about 2000-2500 rpm for 30 sec . After exposed in the UV-light for 40 sec through the designed mask (c) developed the pattern( d) and cleaned by HF (e). The final section shows rinse and dry the sample (f).

### 3.3.3.2 Spin coating

Before spin coating the SU-8 photoresist (used in the present work) on the wafer, the bubbles should be removed. Photoresist can be heated to allow the bubbles to float to the top, and after that, the photoresist should be cooled to room temperature. The current photoresists are available in several viscosities, as shown in Table 3-3.

Table 3-3 Current photoresists in several viscosities.

<b>SU-8</b>	<b>Viscosity (cSt)</b>	<b>Density (g/ml)</b>
3005	65	1.75
3010	340	1.106
3025	4400	1.143
3035	7400	1.147

The table above provides the appropriate parameters for the various viscosities of photoresist and the spin conditions required to achieve the preferred film thickness.

- (1) Dispense 1 ml of resist for each 25 mm diameter of wafer.
- (2) Spin at 2000-2500 rpm for 30 sec.

### 3.3.3.3 Soft bake

In the soft bake stage, the samples should be heated up in uniform thermal conditions to achieve a good aspect ratio and reduce the solvent level. The recommended time and temperature for soft baking is shown in Table 3.4.

Table 3-4 Soft bake times for different thicknesses of SU-8 photoresist.

<b>Thickness (microns)</b>	<b>Soft Bake Time (minutes) at 90°C</b>
4-10	2-3
8-15	5-10
20-50	10-15
30-80	10-30
40-100	15-45

### 3.3.3.4 Exposure

Table 3-5 Exposure dose for different thicknesses of SU-8 photoresist.

<b>Thickness (microns)</b>	<b>Exposure Energy MJ/cm<sup>2</sup></b>
4-10	100-200
8-15	125-200
20-50	150-250
30-80	150-250
40-100	150-250

Table 3-6 Exposure dose for different substrates for SU-8 photoresist.

<b>Material</b>	<b>Relative Dose (x/times)</b>
Silicon	1x
Glass	1.5x
Pyrex	1.5x
Indium Tin Oxide	1.5x
Silicon Nitride	1.5-2x
Gold	1.5-2x
Aluminum	1.5-2x
Nickel Iron	1.5-2x
Copper	1.5-2x
Nickel	1.5-2x
Titanium	1.5-2x

The exposure time and dose depend on the thickness of the photoresist. Recommended exposure times and doses are shown in Tables 3-5 and 3-6.

#### 3.3.3.5 Post exposure bake (PEB)

The post-exposure bake should occur directly after exposure at a temperature between 90-95°C for 60 minutes although ramping up the temperature and starting at a lower temperature near 50°C shows better result. Furthermore, slowly ramping the temperature down is recommended after PEB to prevent cracks and stress problems. Table 3-7 indicates the post-exposure bake times for different thickness of SU-8 photoresist. The best parameter for SU-8 that used in this work is 95 C and 1 min (after several test to optimize the pattern).

Table 3-7 Post-exposure bake times for different thickness of SU-8 photoresist.

<b>Thickness (microns)</b>	<b>PEB Time (minute) at 65°c</b>	<b>PEB Time (minutes) at 95°c</b>
4-10	1	1-2
8-15	1	2-4
20-50	1	3-5
30-80	1	3-5
40-100	1	3-5

### 3.3.3.6 Development

The developer for the SU-8 photoresist is based on acetone, which removes material. The largest issue is that when drying the acetone, some thermal-expansion occurs at the film. Recommended times for developing immersion the processes are shown in Table 3-8.

Table 3-8 Development times for different thicknesses of the SU-8 developer

<b>Thickness (microns)</b>	<b>Development Time (minutes)</b>
4-10	1-3
8-15	4-6
20-50	5-8
30-80	6-12
40-100	7-15

### 3.3.3.7 Rinsing

Table 3-9 The lithography parameters for the chip fabrication process.

Process	Parameter	Condition
Spin coat	Spin speed	2500-3000 rpm
	Spin time	60 sec
Pre-bake	Method	hotplate
	Temperature	95°C
	Time	1 minute
Exposure	UV light wave length	360-375 nm
	Intensity	15 mW/cm <sup>2</sup>
	Time	40 sec
Development	Developer time	SU-8-3000 60 Sec
Post-bake	Method	hotplate
	Temperature	95°C
	Time	1 minute

After the development time, whole samples should be rinsed in fresh developer (PGMEA). In the next step, the samples should be blown dry using Nitrogen gas, placed on the spin coater and spun at 2000 rpm for roughly 15 seconds. All the parameters used for chip fabrication are summarised in Table 3-9. These processes include the spin coat, pre-bake, exposure, development and post-bake.

### 3.3.4 Deposition

A thin layer of metal or semiconductor is applied to a surface using thin-film deposition techniques. Deposition techniques fall into two main categories, including chemical and physical process (Figure 3.7).

#### 3.3.4.1 Chemical deposition

For chemical deposition, a chemical change occurs at a solid surface and results in a solid layer. This process includes plating, chemical solution deposition (CSD) or chemical bath deposition (CBD), spin coating, chemical vapour deposition (CVD) and atomic layer deposition (ALD).

#### 3.3.4.2 Physical deposition

Physical deposition uses mechanical and electromechanical methods to create a thin layer of a solid film on a substrate. Physical deposition techniques include electron beam evaporation, molecular beam epitaxial (MBE), sputtering, pulsed laser deposition, cathode arc deposition (arc-PVD) and electro hydrodynamic deposition (Figure 3.7).

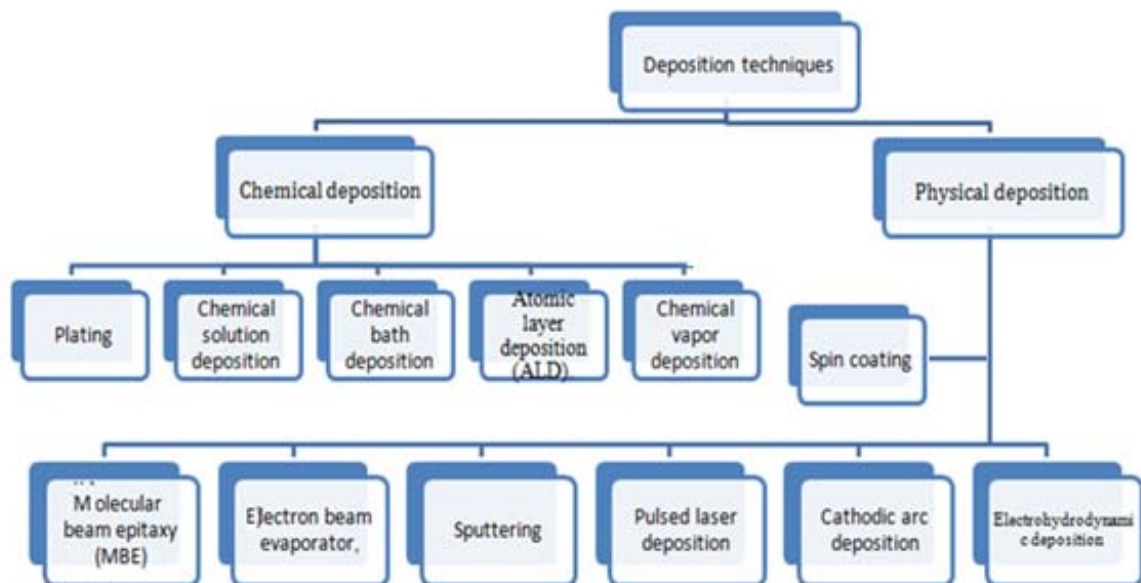


Figure 3.7 Deposition techniques; chemical and physical processes.

The two methods used to fabricate thin metal layers in the present work are described. These processes are often utilised in the semiconductor industry to make thin films of Al and gold. Thermal evaporators are chosen for thicker layers of metal and have poorer control over the rate of the deposition.



Figure 3.8 Thermal evaporation machine, belonging to the Department of Physics, University of Malaya, used in the present study.

Tungsten filaments were used with the vacuum chamber at a pressure of approximately  $2.5 \times 10^{-5}$  mbar. The required current should be applied to heat up and evaporate an aluminium wire placed on a filament (as shown in Figure 3.8). A DC Magnetron Sputtering machine was used to deposit Au and Cr. Deposition rates for different targets in DC Magnetron Sputter system are listed in Table 3-10.

After substrate preparation and cleaning of the silicon wafers, the lithography process of exposing UV light through the designed mask was performed. Subsequently, a layer of gold (100 nm), was deposited using thermal evaporation of the sample.

Table 3-10 Deposition rates for DC Magnetron sputter system.

Target	Current (mA)	Deposition Rate (nm/min)
Cu	45	30
Au	35	42



### 3.4 Set up preparation

As depicted in Figure 3.9, a Helmholtz coil pair system with a cylindrical cap (with a 2500 W DC power supply, 4500D Electromagnet 3472-50)<sup>6</sup> was used to create the magnetic field. Helmholtz coils can provide a very homogeneous magnetic field using a cylindrical cap.

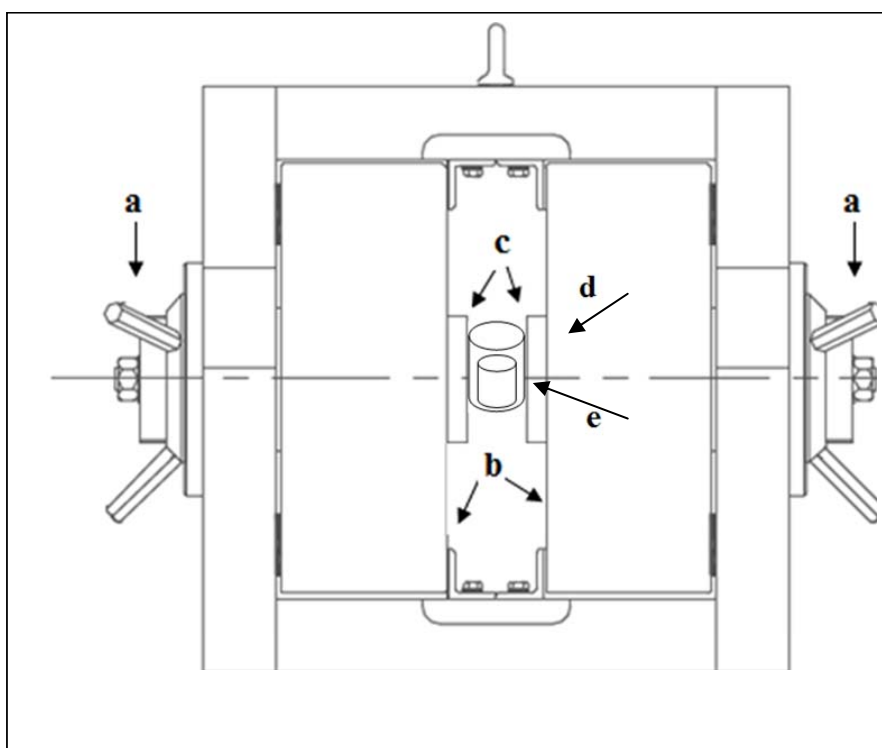


Figure 3.9 A side view of the magnetic field generator used in this work. Two coils are located parallel to each other and separated by a small distance.

Two coils are located parallel to each other and separated by a small distance comparable to the diameter of the microtube that creates a homogeneous magnetic field in the centre between the coils. A side view of magnetic field generator (Helmholtz coil) is shown in Figure 3.10. As shown as figure 3.9, there are two handle to adjust the poles to the desired gap (a), two

---

<sup>6</sup> Personnel Safety: During operation, the magnet fringing field is greater than 0.5 mT (5 G). This field can cause heart pacemakers and other medical implants to malfunction. We recommend that the fringing field should be mapped, and warning signs should be placed outside the 0.5 mT (5 G) contour. Entry to this region should be restricted to qualified personnel.

coil that feeding with high current (b), two pole (c), samle (e) and sample holder (d).

The sample was placed between the two poles, North and South. Magnetic fields generated for various current intensities are shown in Figure 3.10.

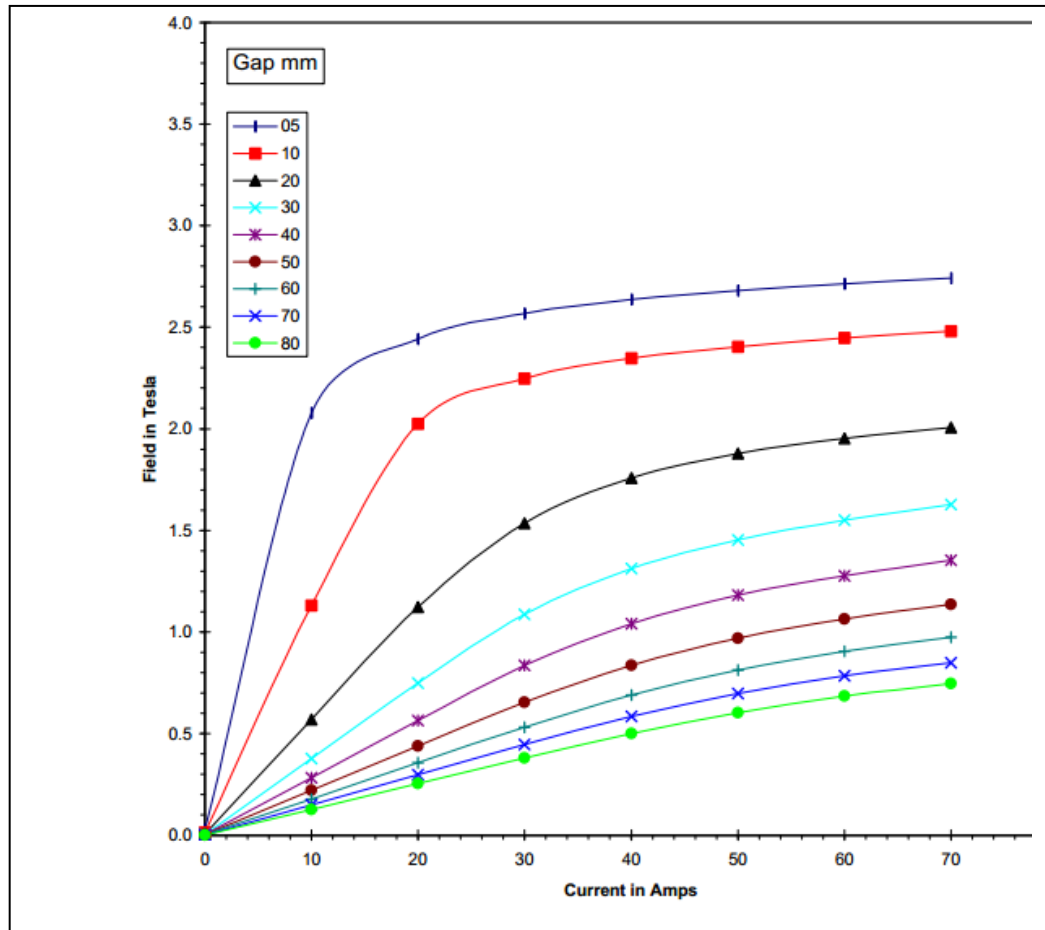


Figure 3.10 Magnetic field generated via current in the magnetic generator in various gap size between two coil pair (Helmholtz coil pair system)

The maximum magnetic field is approximately 3 T in this type of Helmholtz coil. A Teslameter was used to measure the magnitude of the magnetic field, a thermometer (Thermocouple Wires Type K and Temperature controller, Lakeshore 331) measured the variation of temperature during the magnetic field exposure and an electrometer (Keithley 617) was used to

investigate the magnetic field effects on the resistivity before and after the exposure of a DNA solution to the magnetic field. A digital timer was used to control the measurement and exposure times.

### 3.5 Analysis and measuring

DNA strands (5 to 20  $\mu$ l) were diluted and exposed to the magnetic field. Figure 3.11 shows a schematic of the set up elements, instruments and wire connections, and Figure 3.12 displays the overall set up used in this work. The cell containing the DNA is located in the centre of the coil, where the magnetic field is uniform (25°C and 2 to 10 min). UV-Vis spectrum was measured using a Perkin Elmer 750UV-Vis spectrometer. A DI is used as background sample. DI water have no peak in the region 200-350 nm, was utilized to dilution DNA. The micro-Raman spectroscopic analysis was performed after preparing a sample of p-type silicon that was cleaned and coated with 80 nm of gold via the thermal evaporation technique. A Renishaw inVia micro-Raman spectrometer at 514 nm was used to record the spectra. Experiments were repeated after several extractions to eliminate low concentration of samples after extraction; the UV-Vis measurement carried out three times for each sample. The results were analysed using softwares (Microsoft Excel, SPSS and Spectrum Analyzer) statistically.

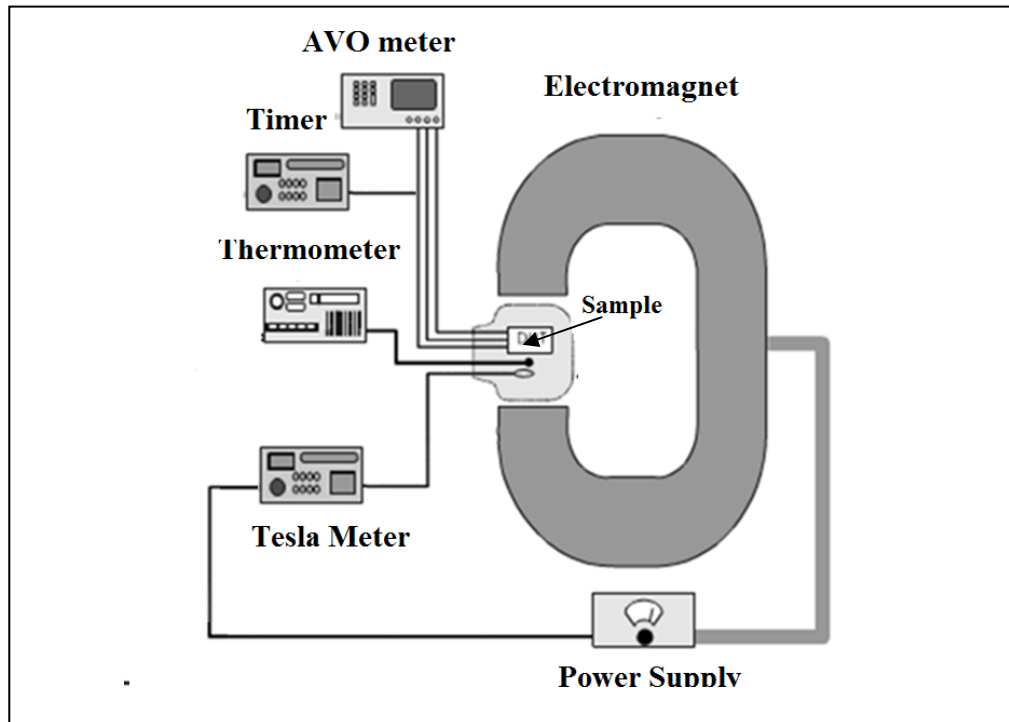


Figure 3.11 Measurement set up, including AVO meter, Tesla meter, timer, thermometer , magnetic generator that included power supply and electromagnet and wire connections .

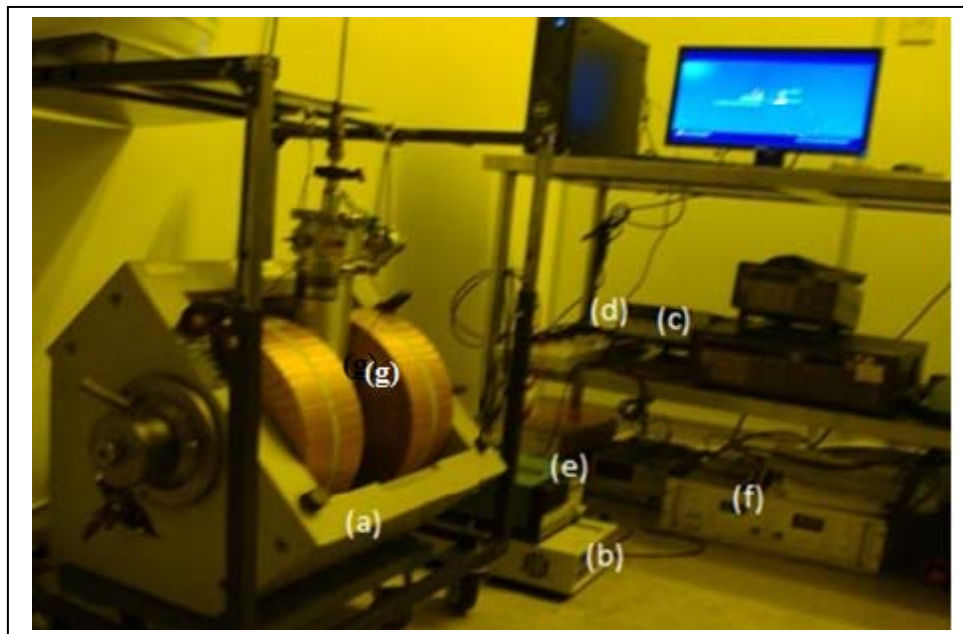


Figure 3.12 Diluted DNA sample placed in the magnetic field region (a) Electromagnet; (b) Thermometer; (c) Multimeter; (d) Timer; (e) Teslameter; (f) Electromagnet power supply and (g) DNA sample.

As depicted in Figure 3.10 thermal controlling device and thermometer used for decrease and increase and monitoring temperature, tesla meter used to measure the strength of magnetic field, AVO measurement units utilized for measuring current via voltage and resistivity and electromagnet, electromagnet power supply and Programmable power supply used to generate and tune magnetic field.

## CHAPTER IV:RESULTS AND DISCUSSIONS: BIOLOGICAL PERSPECTIVE

### 4.1 Introduction

The first part of research findings is presented in this chapter. Analysis carried-out is categorized into two perspectives covering the biological and Physics aspects as shown in the flow chart in Figure 4.1. Two types of DNA samples were analysed namely native DNA extracted from plant and oligonucleotide DNA. Measurements were done before and after exposure to magnetic fields of different strengths. The magnetic field was tuned to the required magnitude prior to each measurement.

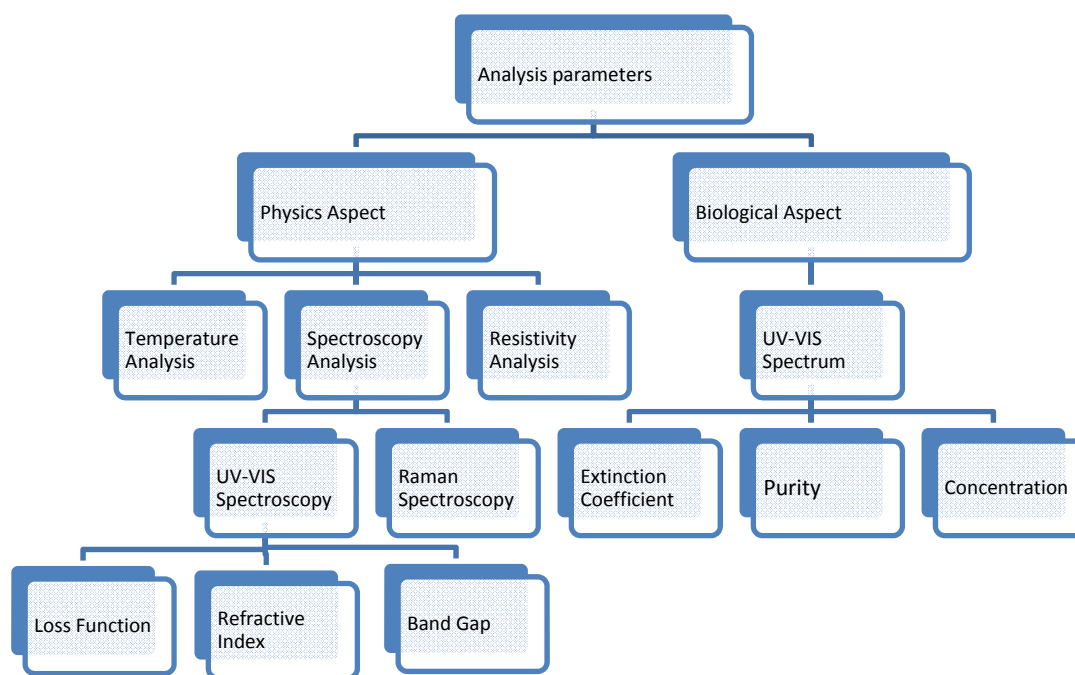


Figure 4.1 Flow-chart showing the two perspectives of analyses done in this work based on the biological and Physics aspects.

UV-Vis and Raman spectroscopy measurements were done on the DNA samples to study the effects of magnetic field exposure on parameters derived

from these measurements. The band gap, refractive index, loss functions and bond vibrations were the parameters analysed from the Physics perspective. Purity and extinction coefficient meanwhile were the parameters investigated from the biological perspective. Resistance and temperature measurements were done in magnetic fields of different strengths to study the influence of the field on these parameters. The results were presented in the next chapter along with the parameters derived from the UV-Vis and Raman results analysed from the Physics perspective. All the fundamental goals defined in the objectives listed in Chapter 1 drove towards the collection of data and the subsequent data analysis.

In  $\mu$ -Raman spectroscopy, the spot size of the scanning laser beam is only a few micrometers in diameter. For DNA deposited on the ultra-thin film of gold, this size provides accurate spatial information on the characteristics of the sample such as the chemical composition of the sample.

UV-Vis spectroscopy is used to investigate the absorbance spectra of DNA molecules in solution. UV-Vis data can provide qualitative as well as quantitative analysis and information. DNA bases absorb light at wavelength of 260 nm, and this value is used to determine DNA properties. Absorption spectroscopy is commonly used on organic materials to investigate the aromatic conjugation within molecules. Usually, organic materials are used in the form of liquid solutions for this measurement. Solvents, such as water and ethanol do not absorb in the UV-Vis spectral region and therefore can be used as the solvent for organic compounds and this includes DNA. The logarithmic ratio between the incident radiation and the radiation transmitted through diluted DNA is measured and can be used in the Beer-Lambert law to determine the optical density, a dimensionless parameter. According to the

Beer-Lambert law (Eq 4.1), the concentration of DNA strands can be calculated.  $I_0$  and  $I$  are the incident and transmitted light intensity, respectively;  $T$  and  $A$  are the transmittance and absorbance, respectively; and  $l$ ,  $\epsilon$  and  $C$  are the cell path length, extinction coefficient and concentration respectively.

$$\text{Eq 4.1} \quad T = \frac{I}{I_0}, A = -\log T = -\log\left(\frac{I}{I_0}\right), A = \epsilon Cl$$

The UV-Vis spectra of AT DNA (100 mer), CG DNA (100 mer) and P-DNA were measured before and after exposure to magnetic field. Figures 4.2, 4.3 and 4.4 show the UV-Vis spectra of three samples exposed to magnetic fields of strengths 250, 500, 750 and 1000 mT. In order to investigate the effects of the magnetic field on DNA samples, the physical and biological parameters were measured before and after magnetic field exposure. Concentration of the samples was determined using Eq 4.1. The first step involved diluting the DNA samples to a suitable concentration in a non-reactive liquid, such as water and later stored in a 1.5 ml cuvette. Before any measurement was carried-out, the DNA must be homogeneously spread within the solution, which was done with proper pipetting. If the solution requires additional mixing of DNA, it should be incubated at 37°C for several 10 minutes of cycle periods. Concentration  $C$  may be given in mol/l or ng/ml. The two types of DNA samples used in this work included natural DNA (extracted from *Mimosa pudica*) and oligonucleotide DNA (AT (100 mer) and CG (100 mer) oligomers).

The setup for exposing the DNA samples to magnetic field included a magnetic field generator, a thermometer to control and monitor the temperature. AVO meter was used to calculate the resistance (Figure 4.5). All



samples were placed at the centre of a uniform magnetic field for 10 minutes. After the spectrophotometer was turned on, the absorbance and transmittance of the samples were measured.

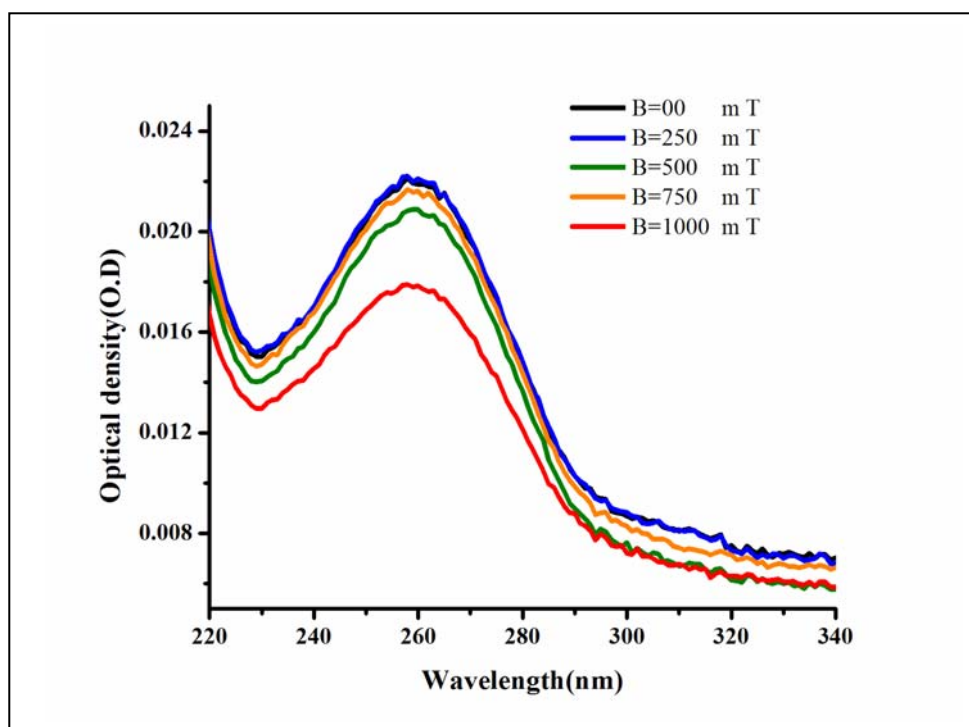


Figure 4.2 UV-Vis spectra of diluted AT-100 DNA sample after exposure to magnetic fields of various strengths (250, 500, 750 and 1000 mT).

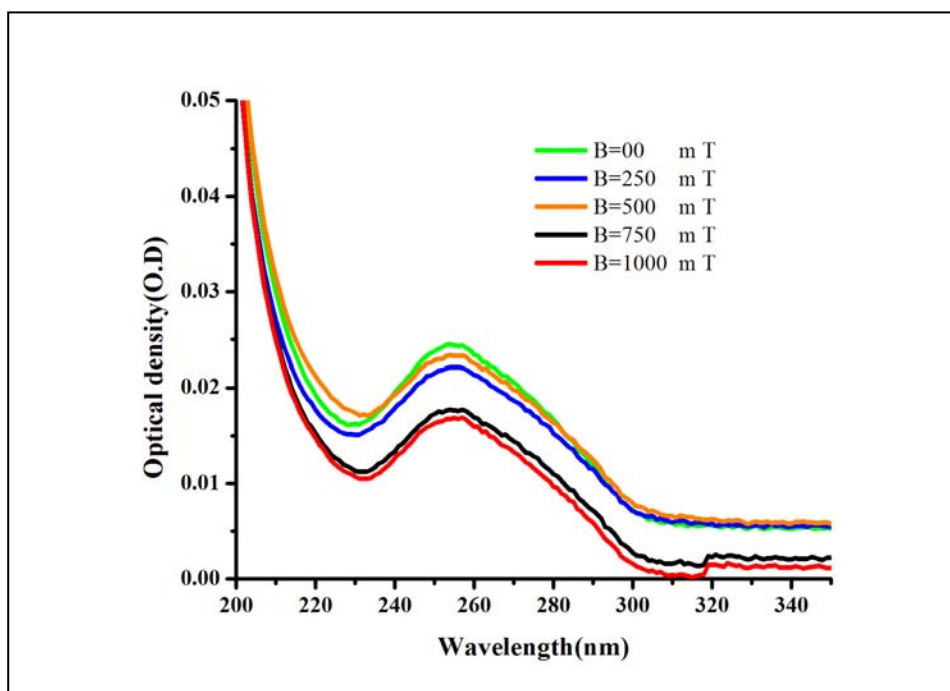


Figure 4.3 UV-Vis spectrum of diluted CG-100 DNA sample after exposure to magnetic fields of various strengths (250, 500, 750 and 1000 mT).

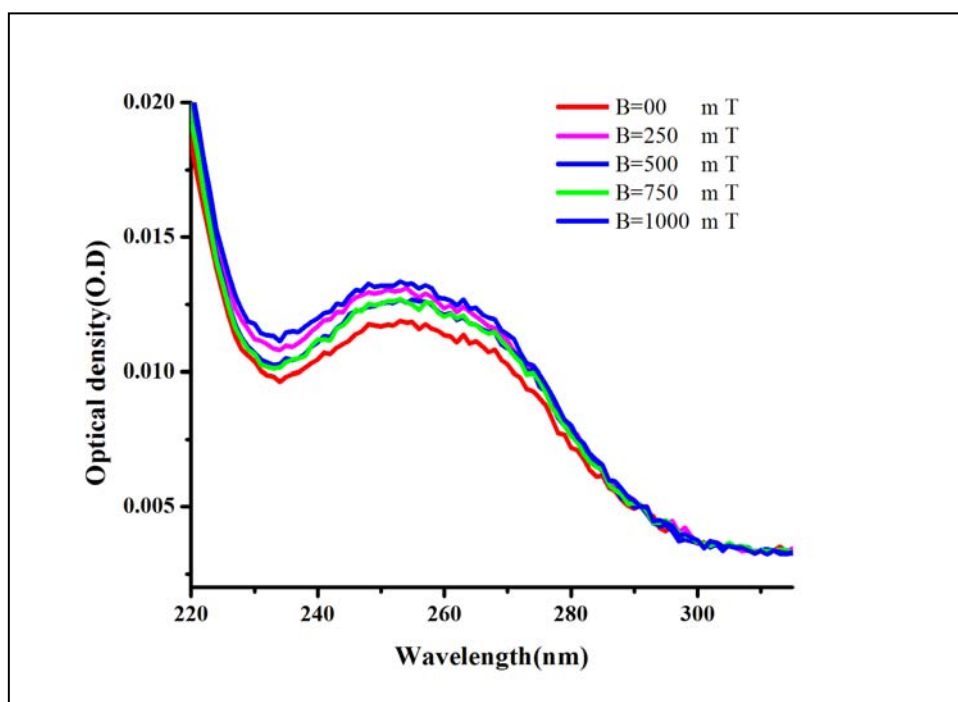


Figure 4.4 UV-Vis spectrum of diluted P-DNA sample after exposure to magnetic fields of various strengths (250, 500, 750 and 1000 mT)

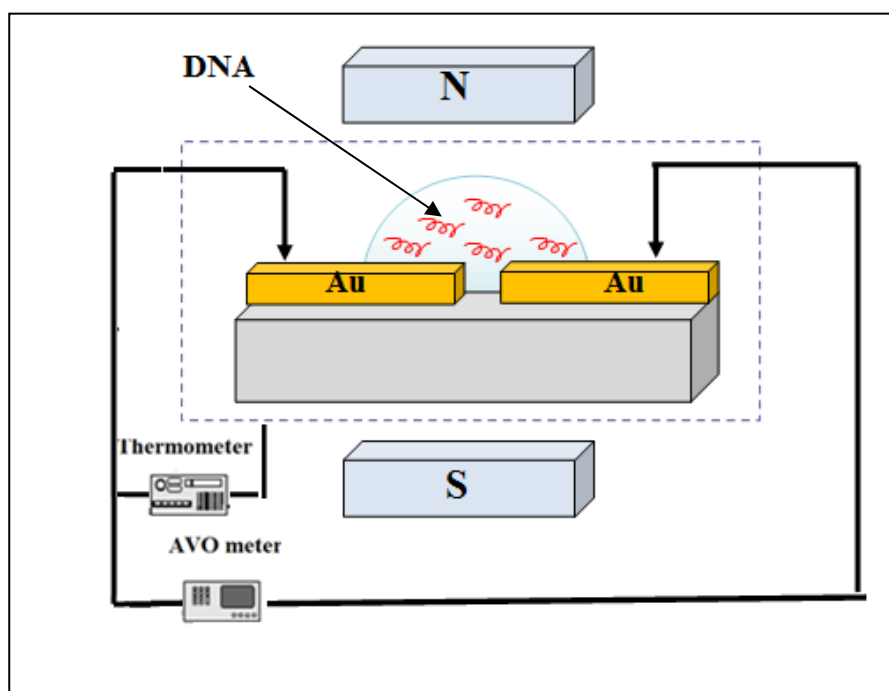


Figure 4.5 The measurement setup included a magnetic field generator for applying a uniform magnetic field, a thermometer to control and monitor the temperature and an AVO meter to calculate the resistance. A drop of diluted DNA placed between two metal electrode.

All measurements were performed before and after magnetic field exposure by tuning the strength of the magnetic field. The biological analysis included analysis of the purity, optical density, maximum wavelength and extinction coefficient.

#### 4.2 Purity calculation

Proteins, which can contaminate extracted DNA, can absorb light in the ultraviolet region. The ratio of absorbance at 260 and 280 nm can be used to assess the purity of DNA samples since DNA and proteins absorb light most strongly at 260 nm and 280 nm respectively. This ratio is used to investigate the purity of DNA before and after exposure to a magnetic field. If the ratio of the absorbance of DNA sample at 260 nm is above 1.75, the DNA should be pure enough to proceed for further measurements. The variation in the purity of the measured diluted p-DNA samples with the magnitude of the magnetic field strength exposure is shown in Figure 4.6.

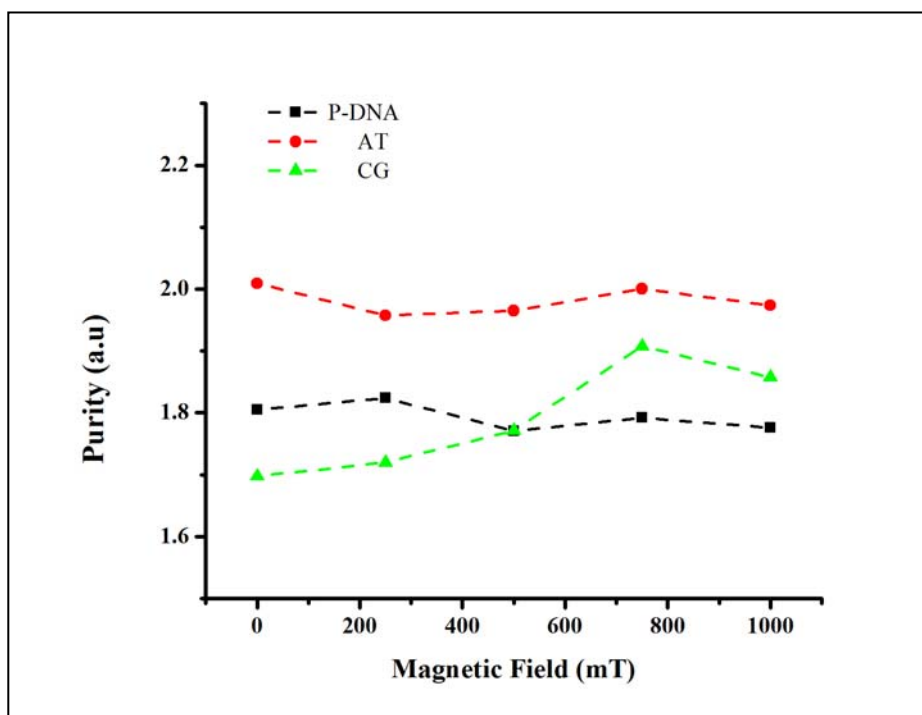


Figure 4.6 The variation in the purity of diluted DNA samples (P-DNA, AT-100 and CG-100) against the magnitude of magnetic field strengths.

As depicted in Figure 4.6, the purity of DNA samples ( ratio of Optical density in 260 to 280) exposed to magnetic field did not decrease. The ratio of the absorbance at 260 nm to that at 280 nm did not change significantly. In spite of the change in the optical density after exposure to the magnetic field, as shown in Figures 4.3, 4.4 and 4.5, the purity remained constant for AT-100 and P-DNA and slightly increased for CG-100. This result occurred because of the decreased amount of contamination in the CG-100 solution. Indeed, the contamination in CG-100 was already greater than that in the other two samples because of the synthesis process (Because of low potential energy of the G base make synthesis difficult). The magnetic field did not decrease the amount of contamination; however, the contaminants were deposited in the solution because of the Lorentz force. Due to the difference in the magnetic response of the DNA and the contamination in the water, the contamination in the water drifted in a specific direction and precipitated (Iwasaka and Ueno, 1998). The magnetic field acted as a filter to separate the contaminant because of its different susceptibility and weight.

Table 4-1 The statistical regression analysis for the purity curve of AT-100, CG-100 and P-DNA exposed to the magnetic field.

	<b>Purity</b>	<b>Coefficients</b>	<b>p-Value</b>
<b>AT</b>	Intercept	1.99±0.02	2.16×10 <sup>-6</sup>
	X Variable 1	-1.12×10 <sup>-5</sup>	0.57
<b>CG</b>	Intercept	1.69±0.03	2.11×10 <sup>-6</sup>
	X Variable 1	2.03×10 <sup>-4</sup>	0.40
<b>P-DNA</b>	Intercept	1.81±0.01	1.16×10 <sup>-6</sup>
	X Variable 1	-3.60×10 <sup>-5</sup>	0.23

Table 4-1 shows the statistical regression analysis from the purity curve measured with a magnetic field, which is also shown in Figure 4.6. According to the p-value shown in Table 4-1, there is a meaningful relationship between the purity and the magnetic field strength based on the p-value. The intercept and X p-values for AT-100, CG-100 and P-DNA are 0.57;  $2.16 \times 10^{-6}$ , 0.40;  $2.11 \times 10^{-6}$  and 0.23;  $1.16 \times 10^{-6}$ , respectively, and their standard errors are 0.02, 0.03 and 0.01, respectively.

### 4.3 Extinction coefficient

Extinction coefficient can be used to evaluate the absorption of light in a material. In Biochemistry and Molecular Biology, the molar extinction coefficient emphasises how strongly a medium absorbs light at a specific wavelength. From the Physics point of view, the extinction coefficient refers to the refractive index, which is a complex parameter and is also related to light absorption. The molar extinction coefficient  $\epsilon$  has units of  $\text{L} \cdot \text{mol}^{-1} \cdot \text{cm}^{-1}$ . To determine how strongly AT-100 and CG-100 DNA oligonucleotides absorb light at a given wavelength. According to the Beer -Lambert law (Eq.4.1), the molar extinction coefficient for a DNA oligonucleotide can be calculated using UV-Vis spectroscopy.

$$\text{Eq 4.2} \quad A(\lambda_i) = l \sum_{j=1}^N \epsilon_j(\lambda_i) C_j$$

Eq 4.2 shows the equation, where  $C_i, \lambda_i, A(\lambda_i), l$  and  $\epsilon_j(\lambda_i)$  being concentration, wavelength, absorbance, path length and molar extinction, respectively. The molar extinction coefficients for single-stranded AT-100 and CG-100 oligonucleotides that are calculated using this method are  $930000 \pm 5000$  and  $90000 \pm 4000 \text{ mol}^{-1} \text{cm}^{-1}$ , respectively. Extinction coefficient of a DNA

oligonucleotide can be predicted from the sequence of the oligonucleotide and depends on the number of bases. The molar extinction coefficient  $\epsilon$  for an oligonucleotide with a different sequence would have to be ascertained theoretically using nearest-neighbour and base composition methods (Cantor, Warshaw, Shapiro et.al., 1970; Richards and Fasman, 1975). In the nearest-neighbour method, the extinction coefficient of an oligonucleotide of length N can be given by the following expression:

$$\text{Eq 4.3} \quad \epsilon = 2 \times \sum_{i=1}^{n-1} \epsilon_{N_{i,i+1}} - \sum_{i=1}^n \epsilon_I - \sum_{i=2}^{n-1} \epsilon_M$$

$\epsilon_N$  is the neighbour extinction coefficient of neighbouring nucleotides i and i+1, and  $\epsilon_I$  and  $\epsilon_M$  the individual and modified extinction coefficients, respectively (Cavaluzzi and Borer, 2004). In the base composition method, the molar extinction coefficients are the sum of molar extinction coefficients. In this method, the isolated nucleosides (A, C, G and T) are multiplied (Eq 4.4) by a factor of 0.9 to account for base stacking. A, C, G and T are related by  $N_i$ , and  $\epsilon_{N_i}$  is the extinction coefficient for an individual base pair.

$$\text{Eq 4.4} \quad \epsilon = 0.9 * \sum_{N_i=A,C,T,G} N_i \epsilon_{N_i}$$

Experimental and theoretical calculations of  $\epsilon$  are shown in Table 4-2. The results for AT-100 and CG-100 contrasted with each other; the experimental result was less than the theoretical calculation because of the solvent effect in the experimental results.

Table 4-2 Theoretical and experimental results of  $\epsilon$  for AT 100 mer and CG 100 mer oligonucleotides (E-BC; Base composition method, E-NN; Nearest neighbour method, E-EX; Experimental result).

DNA Sample	E-BC ( <i>l/mol.cm</i> )	E-NN ( <i>l/mol.cm</i> )	E-EX ( <i>l/mol.cm</i> )
AT (100 mer)	1141000±6000	1083000±5000	930000±5000
CG (100 mer)	842000±4000	846000±4000	890000±4000

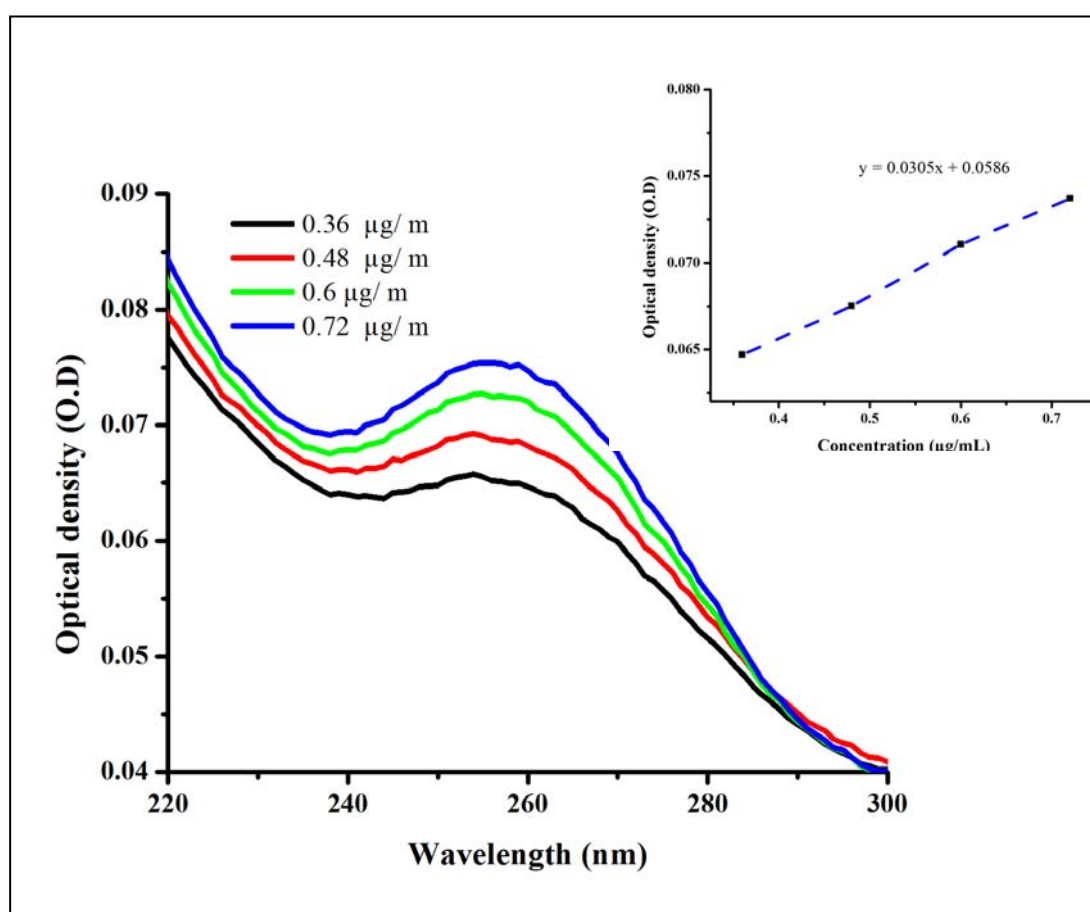


Figure 4.7 UV-Vis Spectrum for four different concentrations. Subfigure shows the optical density versus concentration for the AT-100 oligonucleotide DNA.

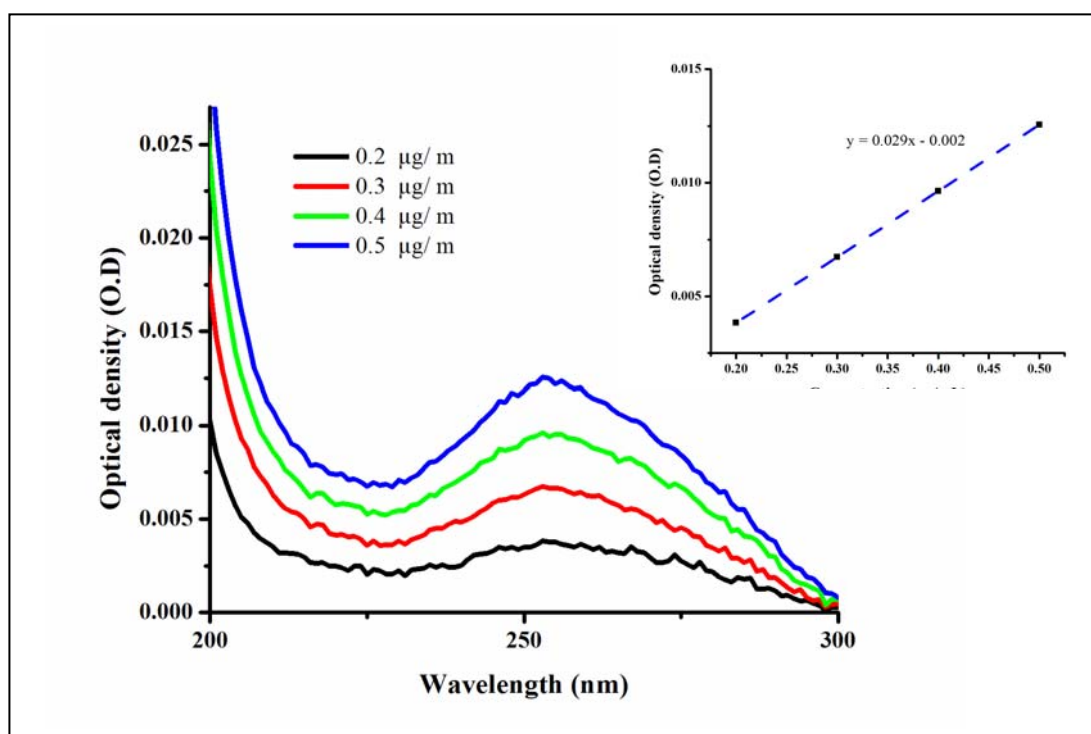


Figure 4.8 UV-Vis Spectrum for four different concentrations. The subfigure shows the optical density versus concentration for CG-100 oligonucleotide DNA.

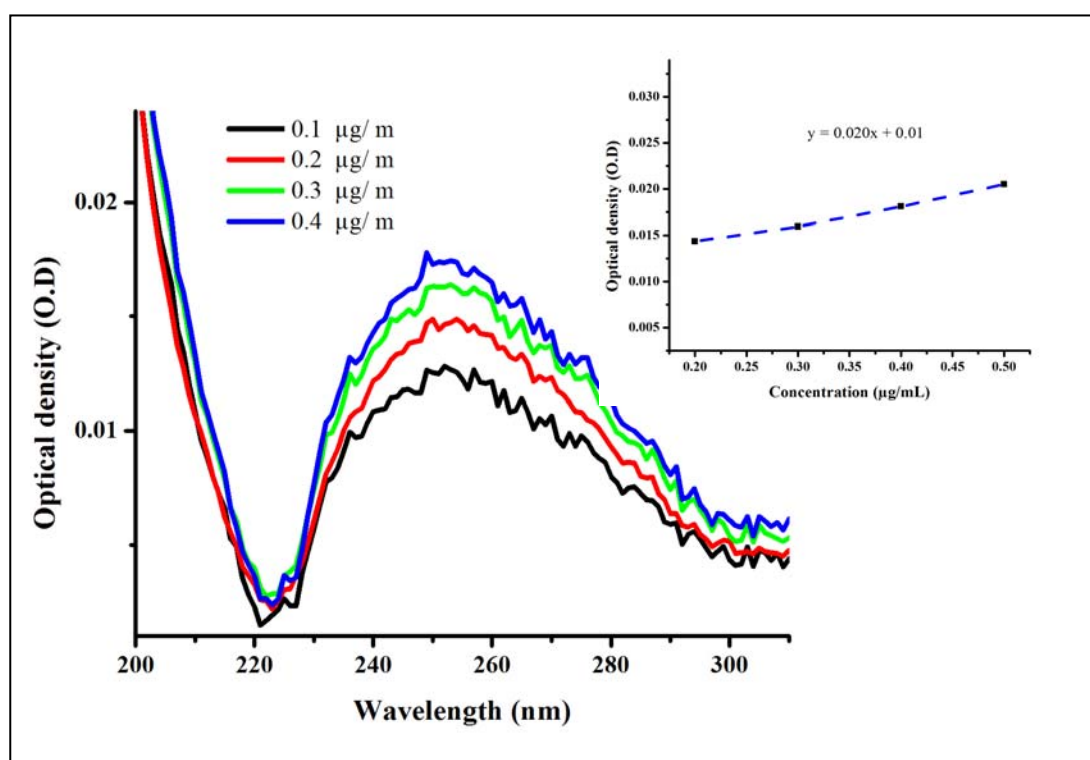


Figure 4.9 UV-Vis absorption at various wavelengths and four different concentrations. The subfigure shows the optical density versus concentration for the P-DNA.



The extinction coefficients of the samples of DNA was measured after obtaining the UV-Vis spectra for different concentrations (the slope is important) of DNA that are and applying the extrapolation method. Figures 4.7, 4.8 and 4.9 indicate the UV-Vis spectra for several concentrations of DNA. The subfigures of those figures indicate the molar extinction coefficient calculated using the optical density and the concentration.

Based on the extrapolation method, as shown in Figures 4.7, 4.8 and 4.9, the extinction coefficient measured for the AT-100, CG-100 and P-DNA DNA samples were  $0.030 \pm 0.001$ ,  $0.029 \pm 0.001$  and  $0.020 \pm 0.001$   $\text{ml}/\mu\text{g}\cdot\text{cm}^{-1}$ , respectively. The extinction coefficient for the double strands and single strands are approximately 0.02 and 0.03  $\text{ml}/\mu\text{g}\cdot\text{cm}^{-1}$ , respectively, and are consistent with the values found in the literature (Ahmadi, Dehghan, Hosseinpourfeizi et al.; Arbona, Aimé Elezgaray et al., 2012). In addition to experimental measurements of the extinction coefficients of DNA samples, the coefficients AT-100 and CG-100 were determined using another method and their defined sequence. To investigate the magnetic field effects on the extinction coefficient, the extinction coefficient of three DNA samples exposed to a magnetic field were measured using the Beer-Lambert method. Figure 4.10 shows the variation in the extinction coefficients of AT-100, CG-100 and P-DNA exposed to magnetic fields of 250, 500, 750 and 1000 mT. 20 samples are studied for each type of DNA measured in this figure.

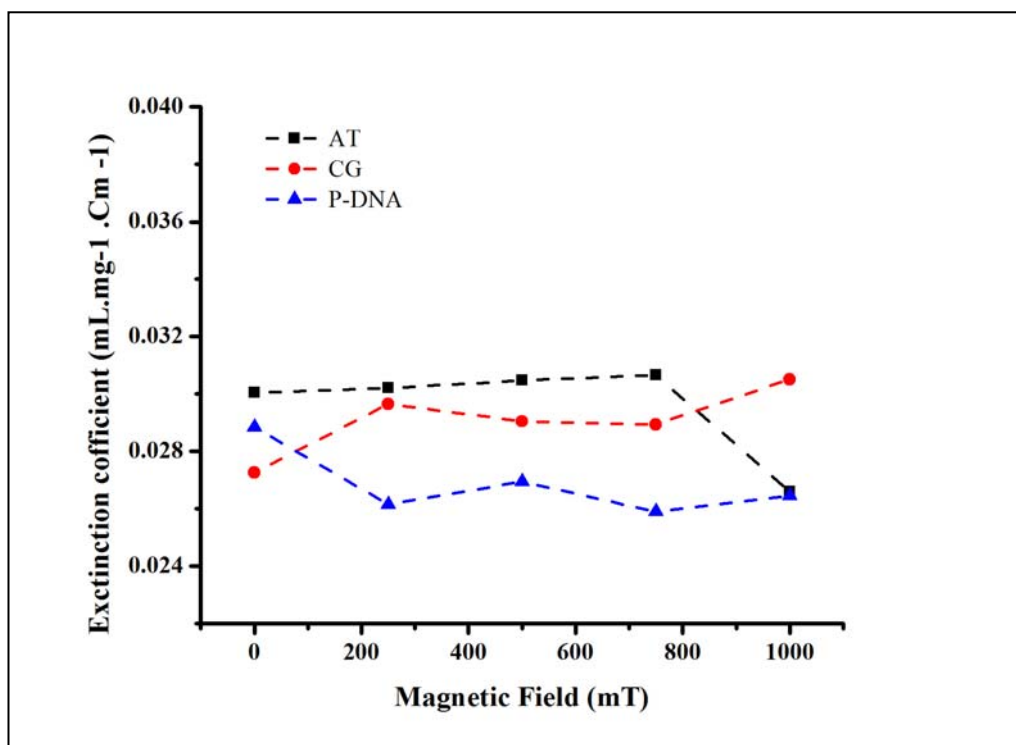


Figure 4.10 The variation in the extinction coefficients of diluted DNA exposed to magnetic fields.

These results show a decrease in the molar extinction coefficients after exposure to the magnetic field for AT-100 and CG-100 and a slow increase in the molar extinction coefficient for P-DNA.

The extinction coefficients of AT-100 and CG-100 decreased because of the magnetic field and a decrease in the number of base pairs that formed the basic structure of the DNA. AT-100 and CG-100 oligonucleotides are single strands, and after exposure to the magnetic field, the magnetic field and Columbic force affected the ionic area of the backbone side, separating opposite charges. Then, the portions of the single-stranded DNA segments with different charges were subjected to magnetic forces of opposite directions, causing the DNA to divide into two or more parts with shorter lengths than that of the original sample. DNA with shorter lengths has a smaller extinction

coefficient, which decreased upon exposure to the magnetic field due to the resultant short strands.

Application of magnetic field to the double-stranded DNA (P-DNA) changed the DNA to single strands, and the DNA strands were cleaved (Miyakoshi J, 2000). DNA cleavage is an important process in all living cells. The general mechanism of DNA hydrolysis involves a type of nucleophilic attack on the phosphate side of the DNA helix. Cleavage results from scission of either the 3'-PO or the 5'-PO. In the presence of a magnetic field, an activated hydroxide (Hydroxide ion will be accelerated by the magnetic field and will act as activated hydrogen ) attacks the phosphate group, as shown in the right side of Figure 4.11, and the leaving group will promote the continuation of this process. The mechanism for cleavage is based on the promoted 3'-PO scission. Increasing the extinction coefficient is considered a hypochromic effect (biological perspective) that could increase the UV absorbance of DNA as a result of the separation of two strands.

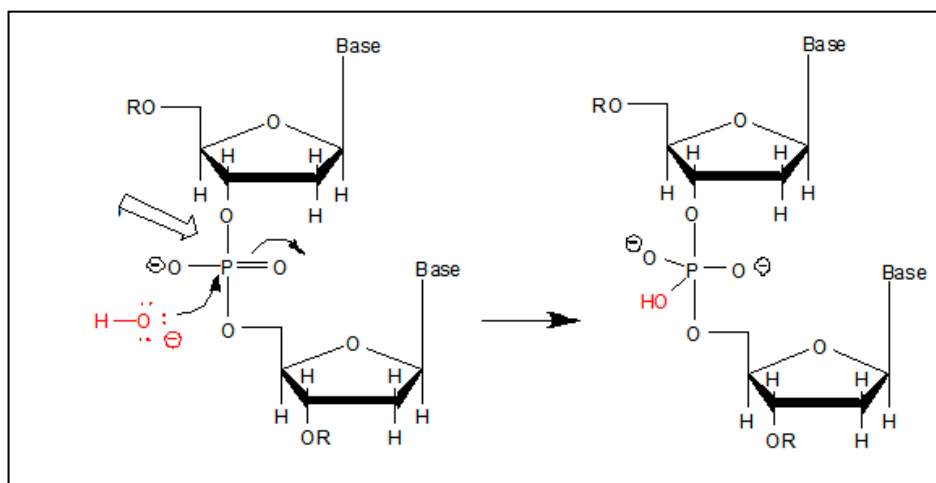


Figure 4.11 Mechanism of the hydrolysis interaction in the DNA helix.

Table 4-3 Statistical regression analysis for the extinction coefficient curve for various magnetic fields.

	<b>Extinction</b>	<b>Coefficients</b>	<b>p-Value</b>
<b>AT</b>	Intercept	$(2.25 \pm 0.08) \times 10^{-2}$	$1.31 \times 10^{-4}$
	X Variable 1	$-1.88 \times 10^{-6}$	0.28
<b>CG</b>	Intercept	$(2.35 \pm 0.07) \times 10^{-2}$	$0.72 \times 10^{-4}$
	X Variable 1	$-2.01 \times 10^{-6}$	0.20
<b>P-DNA</b>	Intercept	$(2.33 \pm 0.05) \times 10^{-2}$	$3.27 \times 10^{-5}$
	X Variable 1	$1.93 \times 10^{-6}$	0.13

Table 4-3 shows the statistical regression analysis of the extinction coefficient curve for various magnetic fields depicted in Figure 4.10. The p-values shown in the table indicate a significant relationship between the purity and the magnetic field strength. The intercept and X p-values for AT-100, CG-100 and P-DNA are 0.28;  $1.31 \times 10^{-4}$ , 0.20;  $0.72 \times 10^{-4}$  and 0.13;  $3.27 \times 10^{-5}$ , respectively, and their acceptable standard errors are 0.08, 0.07 and 0.05, respectively. The intercept p-value less than 0.05 show data that is more reliable data.

#### 4.4 Wavelength at maximum optical density (WMOP)

The peak position is another parameter than is important for monitoring the environmental effect on DNA strands. Changes in the peak position are related to changes in chemical bonds. To investigate the magnetic field effects on the peak position of DNA, the UV-Vis spectra was measured for four magnetic field intensities (250, 500, 750 and 1000 mT). As depicted in Figure 4.12, there is no significant change in the peak position for the AT-100 and P-DNA samples. The effect of the magnetic field is monotonous. CG-100 shows

a slight increase from 254 to 257 nm. Guanine base pairs have a positive susceptibility and less ionisation potential compared to those of the other bases. In CG-100, 50% of the bases are G. The smallest ionisation potential of the DNA bases is for guanine (Kawanishi, HirakuOikawa, 2001). The peak position was related to the magnetic field effect on the HOMO and LUMO states that changed by change in overlapping orbital's.

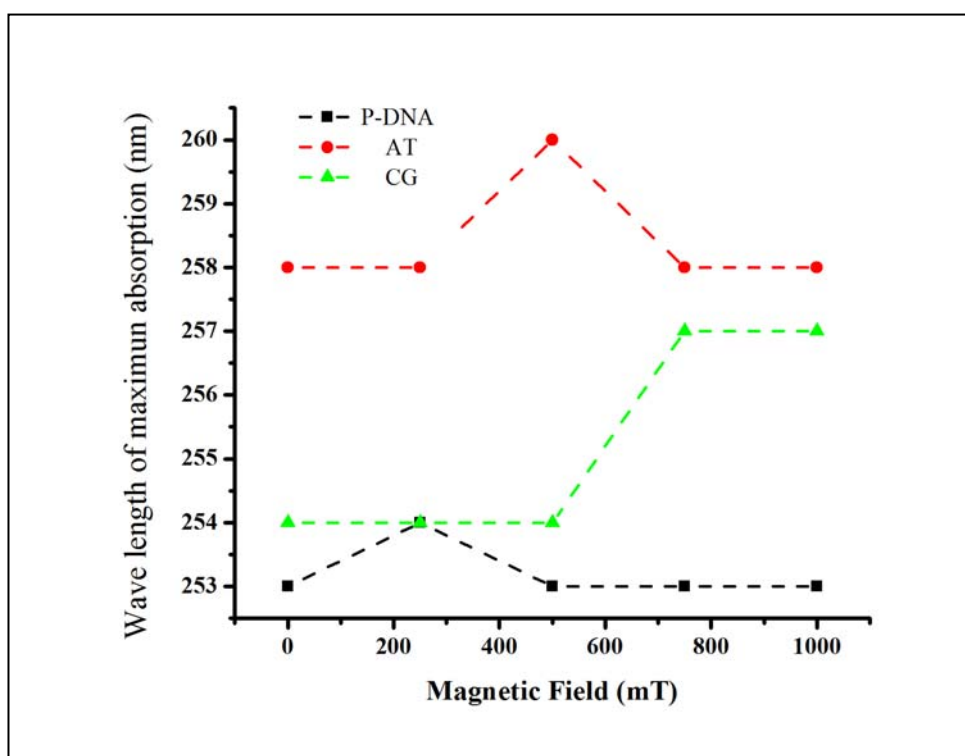


Figure 4.12 Variation of the maximum wavelength in the absorption spectra of diluted DNA influenced by magnetic field exposure.

Table 4-4 shows the statistical regression analysis of the maximum wavelength for various magnetic field strengths, which is also depicted in Figure 4.12. The p-values shown in the table indicate a significant relationship between the purity and the magnetic field strength. Intercepts and X p-values for AT-100, CG-100 and P-DNA are  $7.1 \times 10^{-9}$ ; 0.157,  $6.54 \times 10^{-8}$ ; 1.00 and  $5.38 \times 10^{-8}$ ; 0.58 with acceptable accuracy.

Table 4-4 Statistical regression analysis of the maximum wavelength in the absorption spectra of dilute DNA at various magnetic field strengths.

	Wavelength - max	Coefficients	p-Value
<b>AT</b>	Intercept	$(2.53 \pm 0.03) \times 10^2$	$7.1 \times 10^{-9}$
	X Variable 1	$-4.00 \times 10^{-4}$	0.57
<b>CG</b>	Intercept	$(2.58 \pm 0.08) \times 10^2$	$6.54 \times 10^{-8}$
	X Variable 1	0	1.00
<b>P-DNA</b>	Intercept	$(2.53 \pm 0.07) \times 10^2$	$5.38 \times 10^{-8}$
	X Variable 1	$3.60 \times 10^{-3}$	0.58

#### 4.5 Optical density

To investigate the effect of the magnetic field on the optical density of an absorption spectrum, the optical density (O.D.) of diluted samples exposed to different strengths of magnetic field was measured, as depicted in Figure 4.13.

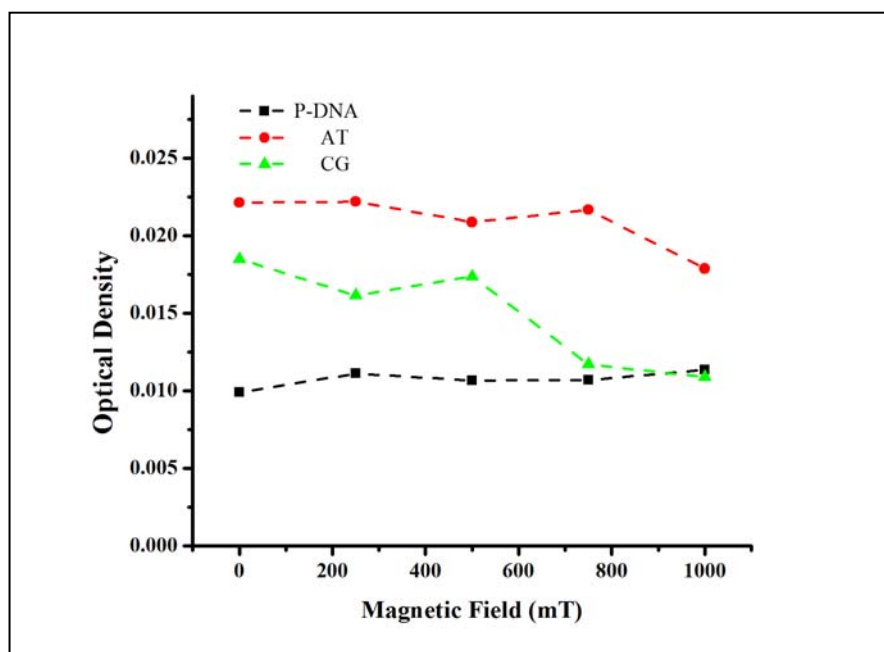


Figure 4.13 Variation in the optical density of dilute DNA that was exposed to magnetic fields.

Figure shows that the O.D. of DNA, which is related to the concentration, slightly decreased when exposed to high magnetic field of 750 mT.

Table 4-5 Statistical regression analysis of the optical density at various magnetic field strengths.

	<b>O.D<sub>max</sub></b>	<b>Coefficients</b>	<b>p-Value</b>
<b>AT</b>	Intercept	$(2.28 \pm 0.1) \times 10^{-2}$	$1.73 \times 10^{-4}$
	X Variable 1	$3.61 \times 10^{-6}$	0.19
<b>CG</b>	Intercept	$(1.89 \pm 0.01) \times 10^{-2}$	$6.83 \times 10^{-4}$
	X Variable 1	$-7.87 \times 10^{-6}$	0.33
<b>P-DNA</b>	Intercept	$(1.02 \pm 0.04) \times 10^{-2}$	$8.88 \times 10^{-5}$
	X Variable 1	$1.00 \times 10^{-6}$	0.18

Optical density of AT-100 and CG-100 decreased after exposure to magnetic field, and that of P-DNA increased. The explanation for the extinction coefficient also applies for the optical density; the P-DNA was cleaved after exposure to the magnetic field. Cleavage increased the absorption of light and the optical density.

Table 4-5 show the statistical regression analysis for optical density at various magnetic field strengths, which is also depicted in Figure 4.13. The p-values in the table indicate a significant relationship between the purity and magnetic field strength. Intercepts and X p-values for AT-100, CG-100 and P-DNA are  $1.73 \times 10^{-4}$ ; 0.19,  $6.83 \times 10^{-4}$ ; 0.33 and  $8.88 \times 10^{-5}$ ; 0.18 with acceptable accuracy.

## **CHAPTER V: RESULTS AND DISCUSSIONS:**

### **PHYSICS PERSPECTIVE**

#### 5.1 Introduction

In this section, the physical properties of DNA samples exposed to different magnetic fields were studied using techniques such as UV-Vis analysis, Raman spectroscopy, temperature analysis and resistance monitoring. Typically, the spectral absorbance measurements can be used in conjunction with Beer-Lambert's law, Kramers-Kronig rules and the Lorentz force to calculate band gap, refractive index, loss function, chemical bond shifting, temperature and resistivity.

##### 5.1.1 Optical parameter

Numerous optical studies have been performed using deoxyribonucleic acid at a variety of wavelengths. Optical properties, such as the band gap, refractive index ( $n$  and  $k$ ) and loss function are known. The band gap calculations use direct band gap analysis, and the loss function and the imaginary and real parts of the refractive index are derived using the Kramers-Kronig method.

##### 5.1.1.1 Band gap

Optical absorption of semiconductors is smallest for light with energies less than the band gap and strong for larger energies. Therefore, there is a sharp increase in absorption at wavelengths close to the band gap. Aqueous suspensions of DNA were utilised to investigate the band gap using UV absorption spectra. Absorption spectra were fitted by the equations for direct



band gap transitions. The equation to measure the direct band gap was explained in Chapter 3 and its proof shown in APPENDIX A.

For a direction transition,  $(\alpha E\text{-photo})^2$  versus  $E\text{-photo}$  is used, where the absorption coefficient and photon energy are  $\alpha$  and  $E\text{-photo}$ , respectively. The  $E\text{-photo}$  value extrapolated in the curve corresponds to a band gap  $E_g$ . Figures 5.1, 5.2 and 5.3 show the  $(\alpha E\text{-photo})^2$  versus  $E\text{-photo}$  profiles that were used to calculate the cut-off wavelengths. Cut-off wavelengths can be estimated by obtaining the intersection of the tangent line with the wavelength axis based on Eq 5.1 and 5.2. This wavelength is usually used to determine the value of the band gap value.

$$\text{Eq 5.1} \quad T = I / I_0, A = -\log T = -\log (I / I_0)$$

$$\begin{aligned} \text{Eq 5.2} \quad & \hbar\omega < E_g, \quad \alpha(\hbar\omega) = 0. \\ & \hbar\omega > E_g, \quad \alpha(\hbar\omega) \propto (\hbar\omega - E_g)^{\frac{1}{2}}. \end{aligned}$$

Interaction with higher light energy, in the UV and visible range of the electromagnetic spectrum, causes DNA molecules and many other organic materials to undergo transitions and electronic jumps between energy levels. Upon absorption of the energy of UV or visible irradiation by an atom or a molecule, electrons travel from lower to higher energy level of the molecular orbitals.

Figures 5.1, 5.2 and 5.3 show the UV-Vis spectra of three samples exposed to different magnetic fields. The peak shape of the three samples clearly shows that the absorption spectra exhibit a tail that is beyond the band-gap region; this tail indicates that the cut-off is not a sharp transition. This tail

can be explained by an exponential decay in the absorption coefficient analysis. The band-gap/ Kubelka-Munk model can be used to describe the band-gap value using this feature. Band gaps of the three samples can be calculated using the K-M relationships explained in Chapter III and APPENDIX C. Figures 5.4, 5.5 and 5.6 depict the band gaps derived using the latter method. Extrapolation of the straight line in the figures reveals the intercept and the band gap values can be extracted.

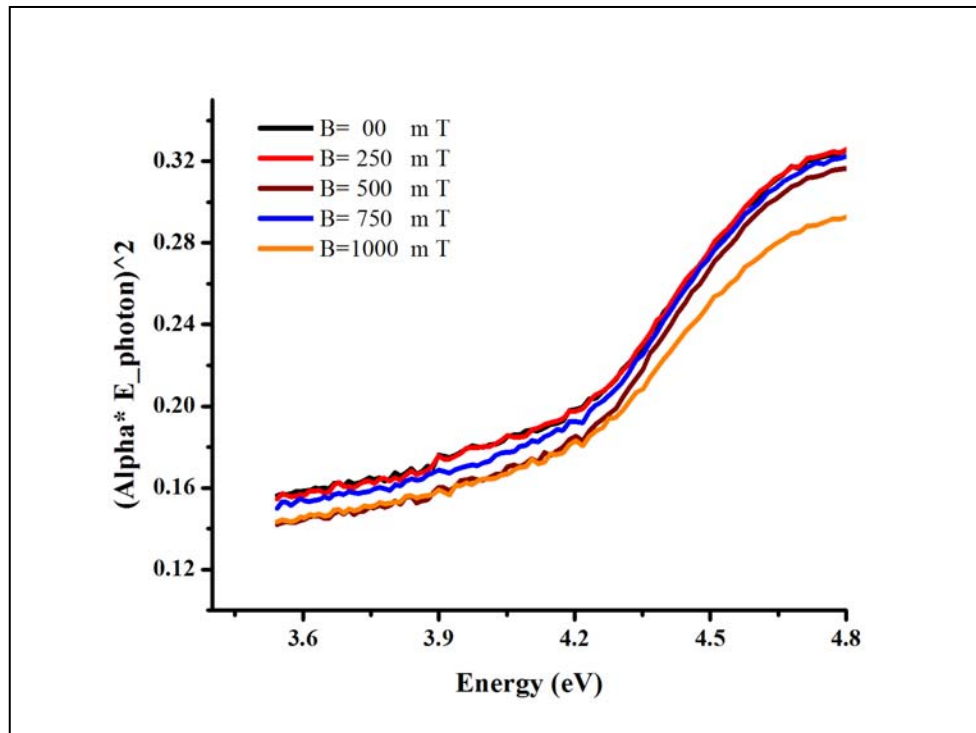


Figure 5.1 The absorption spectra of diluted AT-DNA exposed to magnetic field fitted by the equations for direct band gap transitions.

Figures 5.7, 5.8 and 5.9 depict the band gap derived using Beer-Lambert method. Extrapolation of the straight line of the figures reveals the intercept and the band gap values can be extracted.

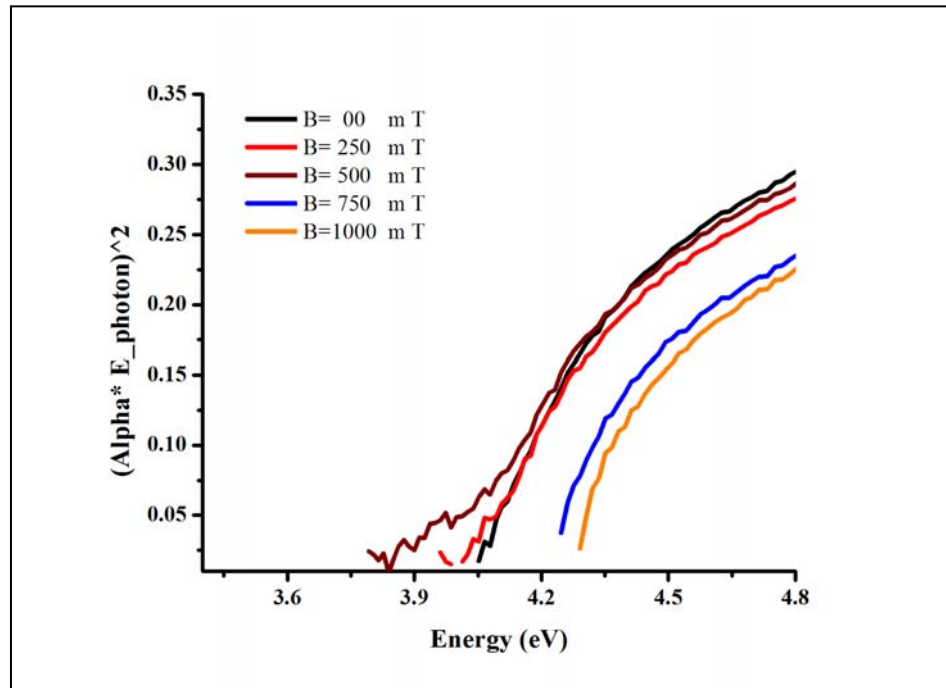


Figure 5.2 The absorption spectra of diluted CG-DNA exposed to magnetic field fitted by the equations for direct band gap transitions.

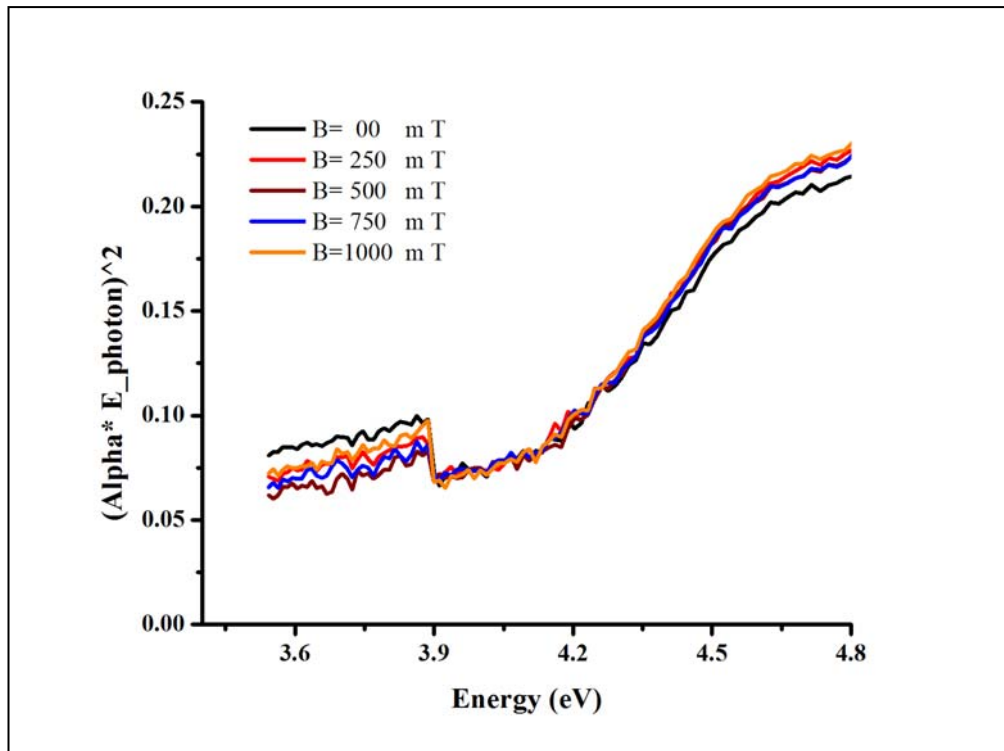


Figure 5.3 The absorption spectra of diluted P-DNA exposed to a magnetic field were fitted by the equations for direct band gap transitions.

Table 5-1 compares the  $E_g$  values extracted from two methods; Beer-Lambert and Kubelka-Munk methods. The Kubelka-Munk method involves shorter wavelengths than the band gap energy that is directly obtained from the absorption spectrum using the direct band gap method. Additionally, the two methods show similar results. Band gaps were found to generally increase in the samples. The contraction caused by the Lorentz force and the liquid environment is largely based on dipole-dipole and free charge interactions that could cause significant differences between their magnitudes. Interactions between biological samples and static magnetic field occur via bounded ion dynamics.

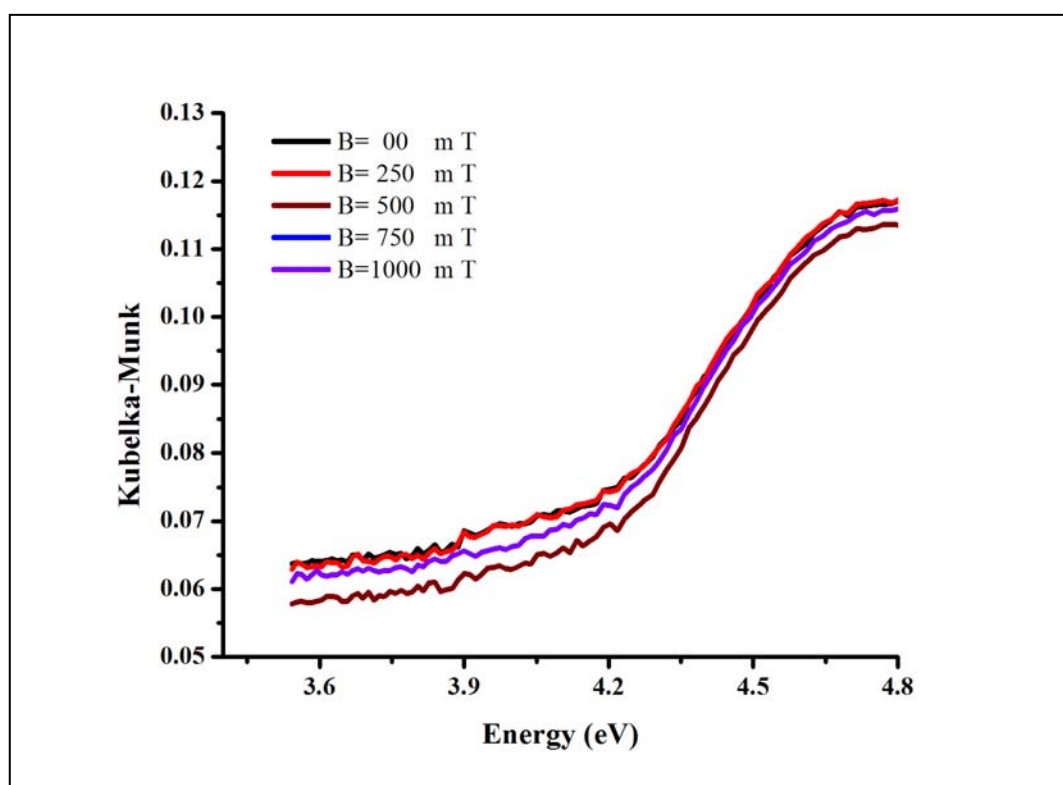


Figure 5.4 Kubelka-Munk coefficients of the absorption spectra of AT-DNA exposed to various magnetic fields.

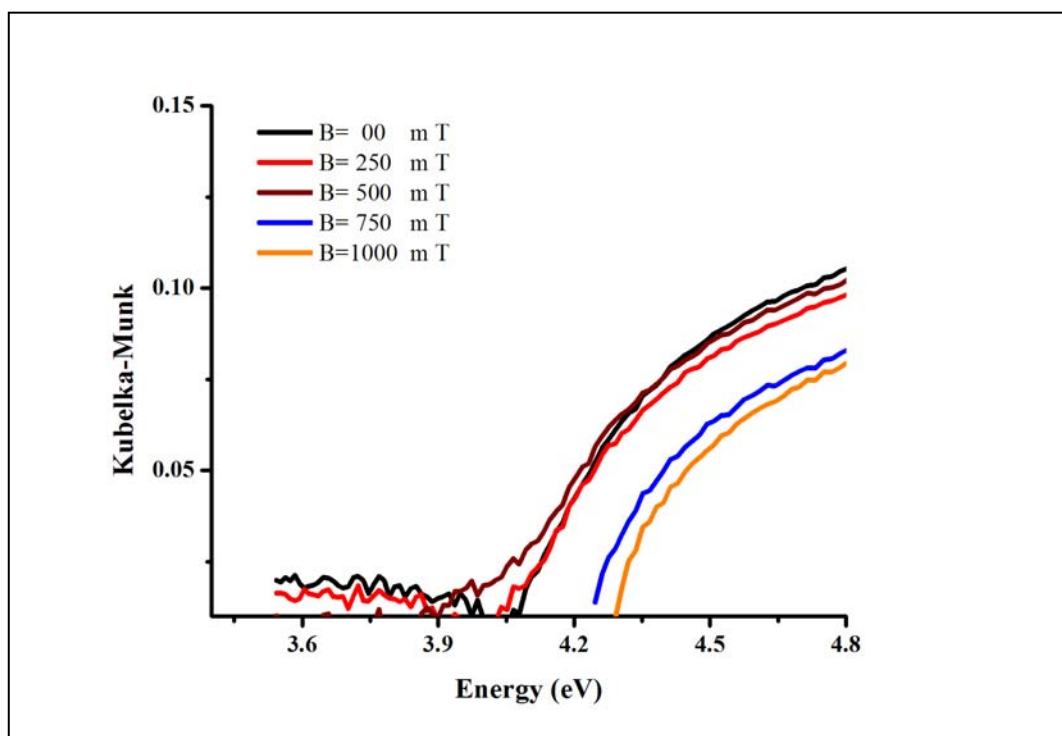


Figure 5.5 Kubelka-Munk coefficients of the absorption spectra of CG-DNA exposed to various magnetic fields.

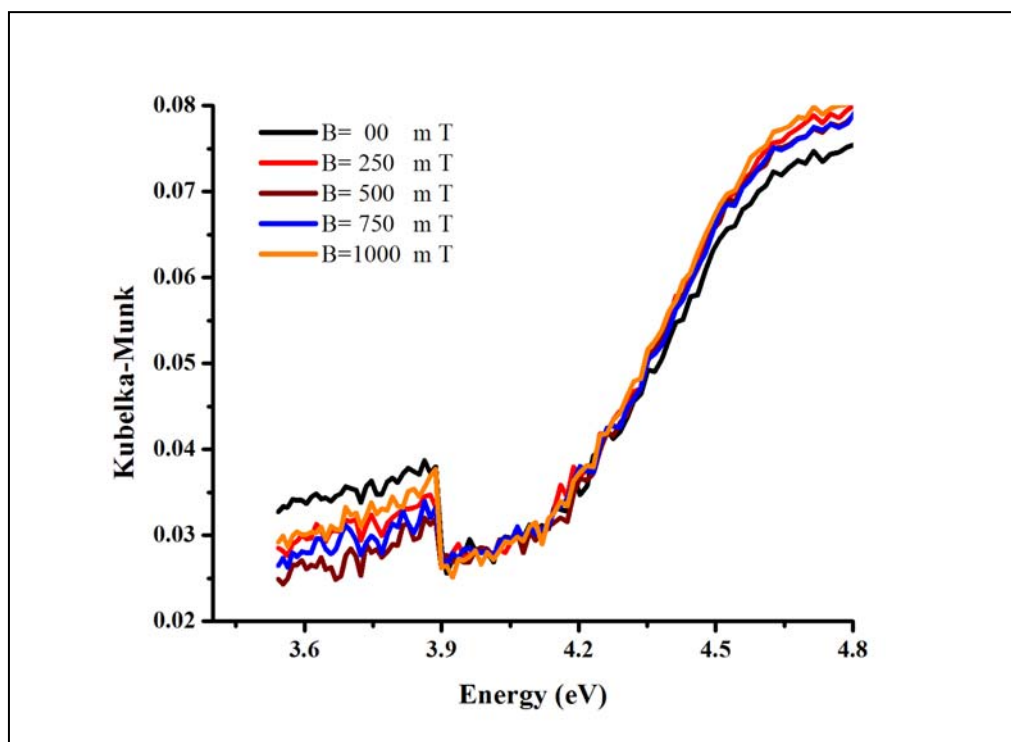


Figure 5.6 Kubelka-Munk coefficients of the absorption spectra of P-DNA exposed to various magnetic fields.

The oscillation of a bound ion about its binding portion in a signalling molecule can affect ionic transport. Overlap of the base molecular orbitals lead to a decrease in the absorbance of UV light. Indeed, cleavage decreased the overlap of the orbitals and the liberated dsDNA molecules are no longer stacked as they were in dsDNA. Thus the orbital overlap is minimised and the UV absorbance increases.

Table 5-1 Comparison of the  $E_g$  values determined using two methods; Beer-Lambert and Kubelka-Munk.

		<b>B=0 mT</b>	<b>B=250 mT</b>	<b>B=500 mT</b>	<b>B= 50 mT</b>	<b>B=1000 mT</b>
<b>Beer-Lambert</b>	AT	3.665±0.003	3.635±0.003	3.726±0.003	3.665±0.002	3.694±0.003
	CG	3.850±0.07	3.859±0.004	3.747±0.005	4.124±0.005	4.211±0.007
	P- DNA	3.860±0.007	3.944±0.008	3.929±0.005	3.918±0.006	3.917±0.006
<b>Kubelka -Munk</b>	AT	3.625±0.007	3.602±0.003	3.702±0.003	3.636±0.003	3.636±0.003
	CG	3.835±0.005	3.843±0.004	3.720±0.005	4.120±0.005	4.209±0.008
	P- DNA	3.839±0.008	3.931±0.008	3.915±0.006	3.903±0.007	3.902±0.006

#### 5.1.1.2 Real and imaginary part of refractive index

The refractive index of tissues/biomaterials is a fundamental parameter used in optical diagnosis tests and laser treatments. In basic biomaterials, such

as DNA, blood plasma and protein, studies using optical methods indirectly rather than directly attract a lot of attention. This attention was not only because of its wide application in biomedicine and bioscience but the combination of sensors and optical devices increased its potential applications further. Kramers-Kronig method is a crucial tool for studying the imaginary and real parts of the refractive index. This tool is broadly used in the optics of liquids and solutions to derive the real and imaginary parts of the refractive index (Houssier and Kuball, 1971; Pinchuk, 2004).

In damped simple harmonic oscillator model,  $n$  and  $k$  are the real and imaginary parts of the complex refractive index respectively. The Kramers-Kronig transformation has been commonly used to determine the dielectric constant from normal-incidence absorption spectra. Eq 5.3 and 5.4 derived from the Kramers-Kronig relationship show the real and imaginary parts of the refractive index, which can be used to derive the dielectric constants ( $\varepsilon_1(\omega)$  and  $\varepsilon_2(\omega)$ ).

$$\text{Eq 5.3} \quad n_i = \left\{ \frac{1}{2} [(\varepsilon_1^2 + \varepsilon_2^2)^{1/2} - \varepsilon_1] \right\}^{1/2} / \varepsilon_0$$

$$\text{Eq 5.4} \quad n_r = \left\{ \frac{1}{2} [(\varepsilon_1^2 + \varepsilon_2^2)^{1/2} + \varepsilon_1] \right\}^{1/2} / \varepsilon_0$$

Figures 5.7, 5.8 and 5.9 show the real part ( $n_i$ ), and Figures 5.10, 5.11 and 5.12 indicate the imaginary part of the refractive index ( $n_r$ ); these values are derived from Eq 5.4 and 5.5. Figure 5.7 shows the real part of the refractive index of AT-100 DNA. The real part of the refractive index of AT-DNA (as shown in Figure 5.7) did not change significantly when exposed to magnetic fields below 750 mT but clearly increased at energies above 4.14 eV.

Figures 5.7, 5.8 and 5.9 show the dispersion curve of the real part of the refractive index of AT-100 DNA, CG-100 DNA and P-DNA after exposure to different magnetic field strengths. The real part of the refractive index of CG-DNA showed no significant change when exposed to magnetic fields below 750 mT. Similarly for AT-100, the refractive index decreased when exposed to magnetic fields of 750 mT at energies less than 4.14 eV (indicated by the arrow in Figure 5.7) following an increase in the energy region above. Density of liquid corresponds to the real part of the refractive index. As shown in Figures 5.7 and 5.8, for both single strand AT and CG samples, the density of DNA liquid samples in high energy region increased. In low energy region meanwhile, it decreased when exposed to magnetic field above 750 mT. However, the number of short length DNA oligo suspended in the liquid increased. This result indicates cleavage of the DNA oligonucleotide.

The real part of the refractive index of P-DNA (as shown in Figure 5.9) decreased after exposure to magnetic fields, indicating decrease in liquid density. It can be due to cleavage of DNA, as a result of exposure to increasing strength of magnetic field and this can result in increase of distribution of ions in the liquid.



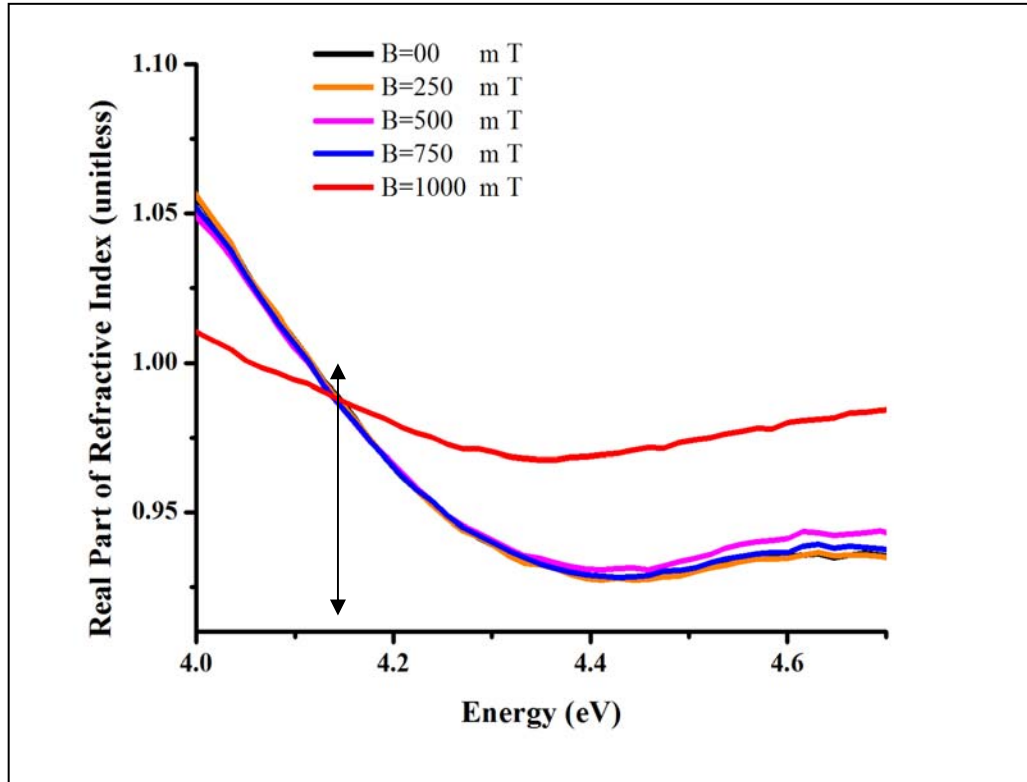


Figure 5.7 Dispersion curves of real part of the refractive index of AT-100 DNA after exposure to different strengths of magnetic fields.

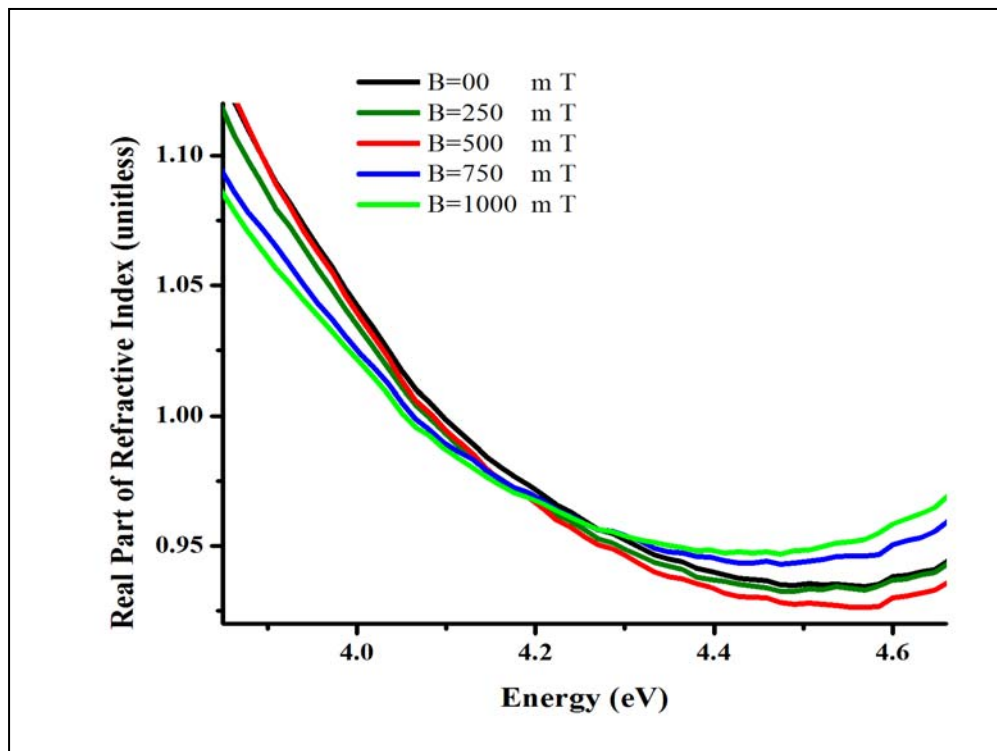


Figure 5.8 Dispersion curves of real part of the refractive index of CG-100 DNA after exposure to different strengths of magnetic fields.

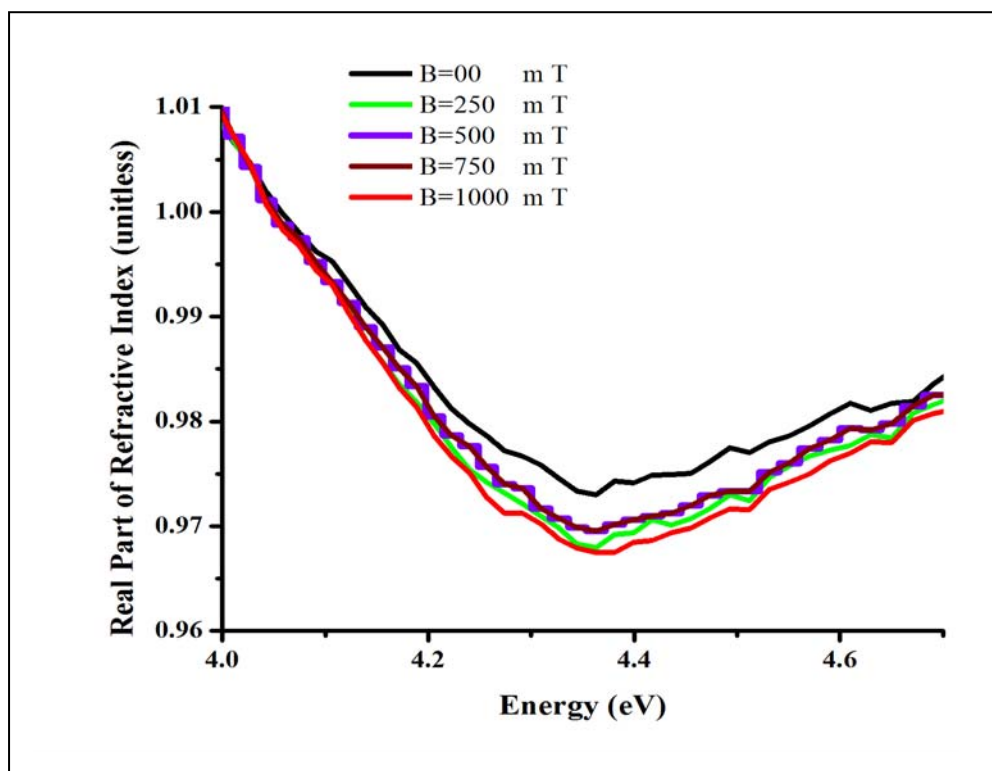


Figure 5.9 Dispersion curves of real part of the refractive index of P-DNA after exposure to different strengths of magnetic fields.

Imaginary part of the refractive index of the AT-100 DNA and CG-100 DNA (as shown in Figures 5.10 and 5.11, respectively) meanwhile decreased when exposed to a magnetic field of 750 mT. The imaginary part of refractive index is related to the extinction coefficient. Molar extinction coefficient and imaginary part of refractive index decreased in AT-100 and CG-100. Shorter length of oligo DNA has the smaller extinction coefficient. The result proved that the imaginary part of refractive index and molar extinction coefficient decreased upon exposure to magnetic field due to cleavage of DNA, creating small lengths of oligomers.

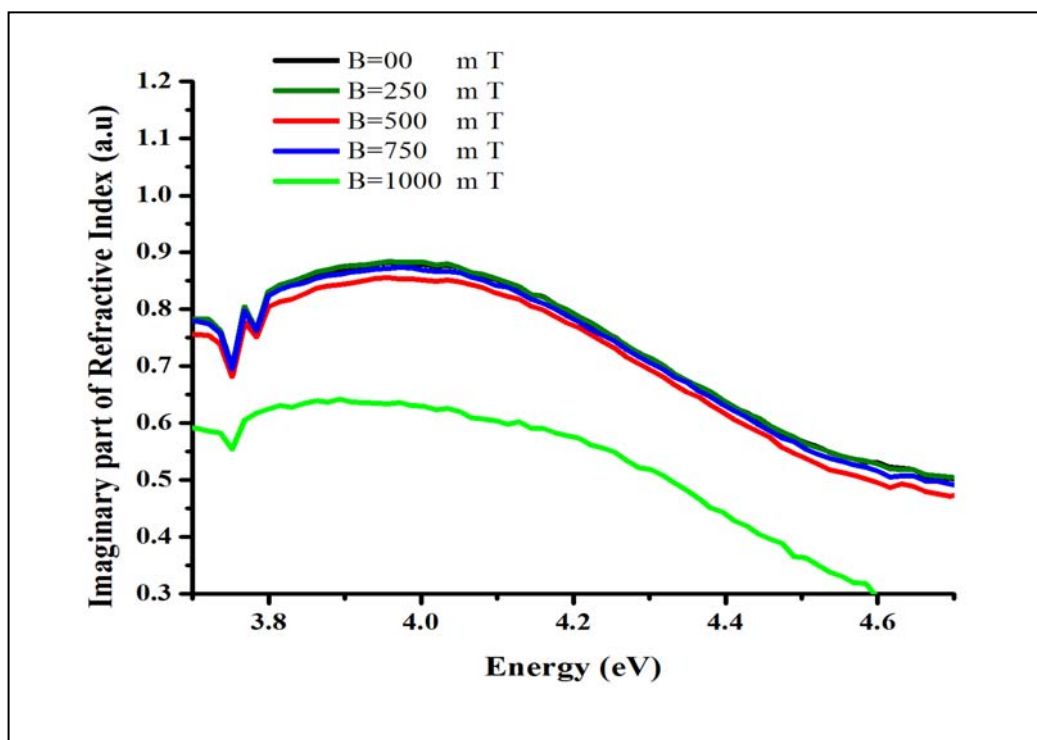


Figure 5.10 Imaginary part of the refractive index of AT-100 DNA exposed to magnetic fields.

Figure 5.12 shows the gradual increase of the imaginary part of the refractive index of P-DNA when exposed to magnetic fields. The imaginary part of refractive index corresponding to the molar extinction coefficient was observed to increase because of cleavage of DNA strands to two single strands. As a result of this cleavage, number of suspended chain in liquid environment increased and therefore density of DNA increased.

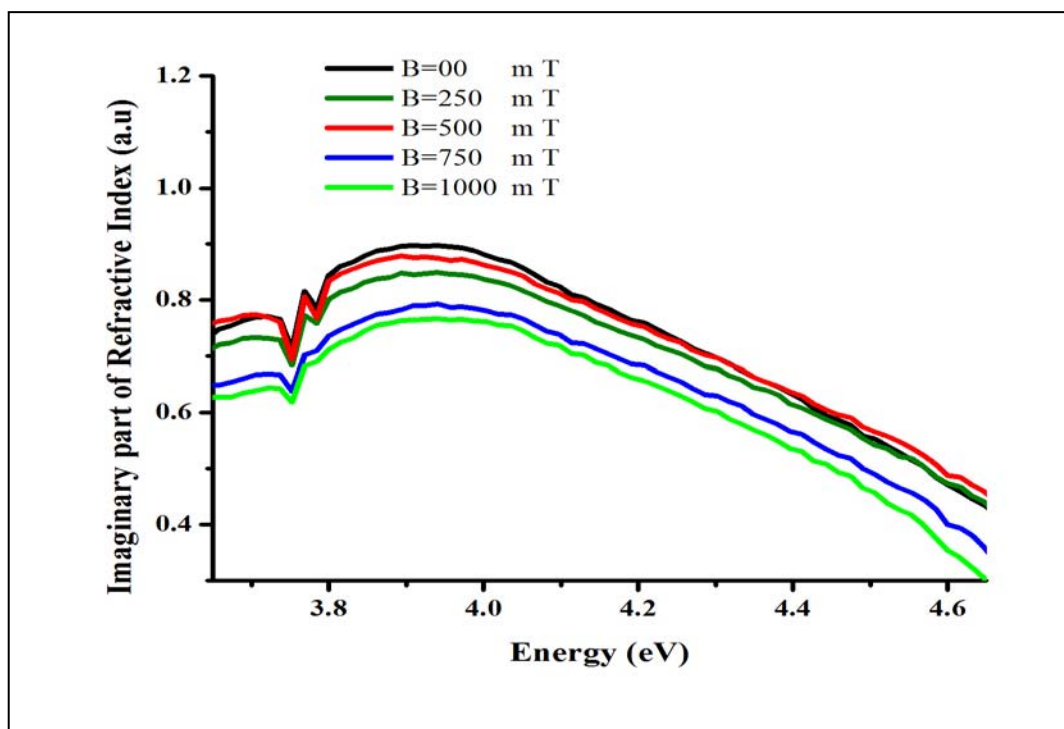


Figure 5.11 Imaginary part of the refractive index of CG-100 DNA exposed to magnetic fields.

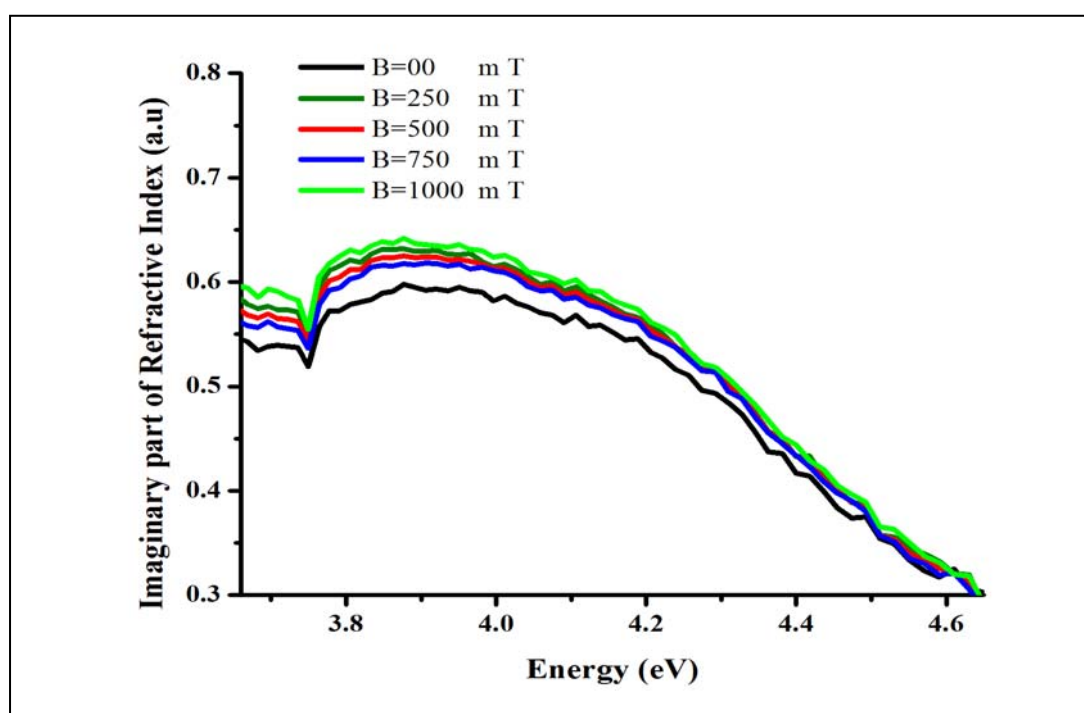


Figure 5.12 Imaginary part of the refractive index of P-DNA exposed to magnetic fields.

### 5.1.1.3 Loss function

Cells can repair some parts of DNA helix damaged by the environment. Interaction between the environment and molecules depend upon the range of the interaction. Energy required for this interaction includes two types of forces. The forces, Coulombic and van der Waals affect the partial charge in a DNA double helix in the opposite directions of nucleotide arrangement. The van der Waals interactions depend on the dielectric function and the imaginary frequency in the liquid conditions of the cellular environment. Loss function is dependent on the imaginary part of the dielectric constant according to the relationship in Eq 5.5.

$$\text{Eq 5.5} \quad \text{Loss}(\omega) = -\left(\frac{1}{\epsilon''(\omega)}\right) = \frac{2n(\omega).k(\omega)}{(n(\omega)^2+k(\omega)^2)^2}$$

The loss function was modelled using Lorentz fitting according to Eq 5.6. Parameters in this equation are  $y_0$ ,  $w$ ,  $x_c$  and  $A$  representing the offset, the width of peak, the centre point of peak position on the x-axis and the area under the peak curve, respectively. Two more parameters  $w$  and  $x_c$  are significant for the analysis using this fitting as in the equation below:

$$\text{Eq 5.6} \quad y = y_0 + \frac{2A}{\pi} \frac{w}{w^2 + 4(x-x_c)^2}$$

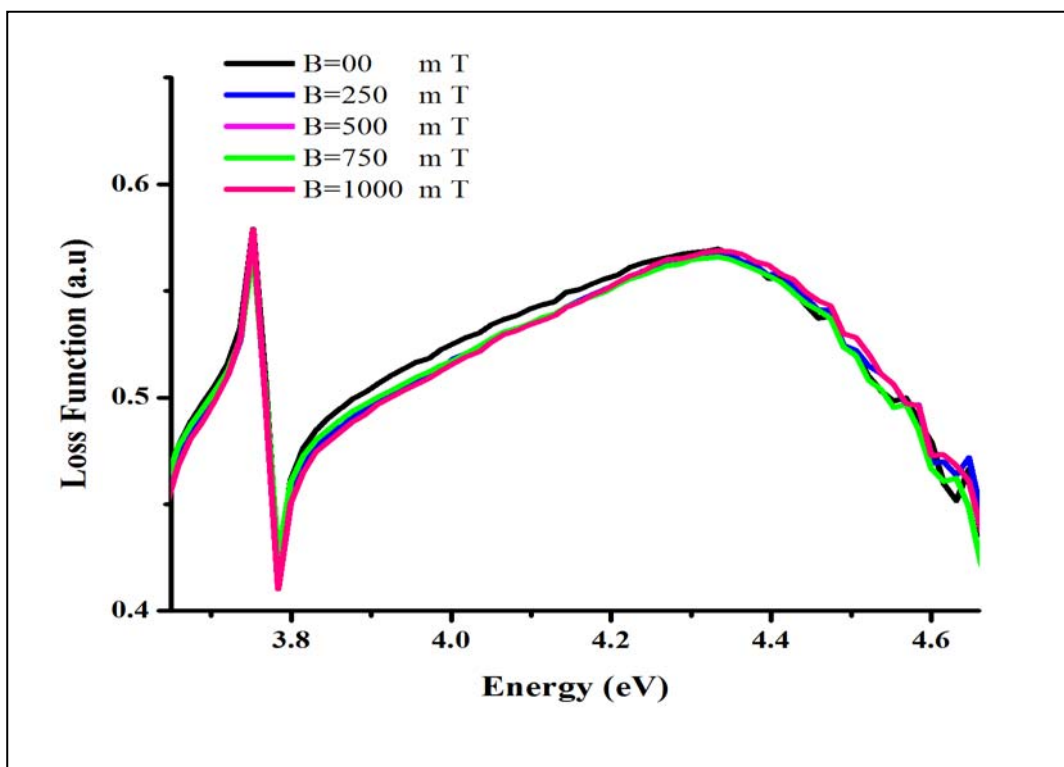


Figure 5.13 Loss function of AT-100 DNA exposed to different magnetic field strengths.

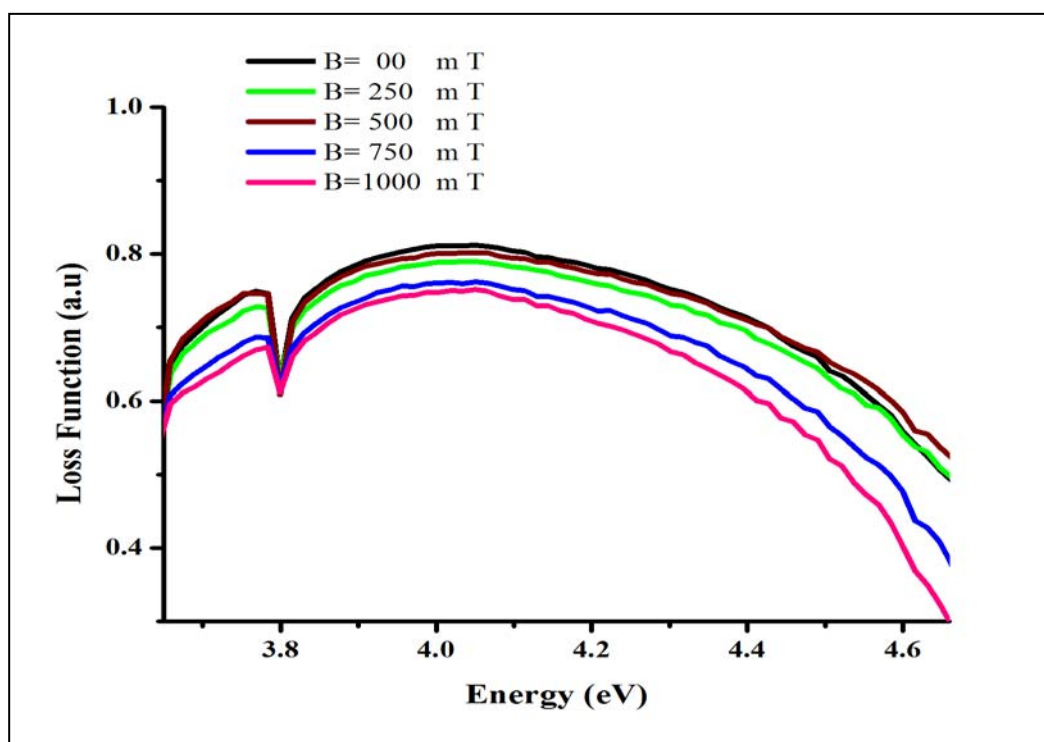


Figure 5.14 Loss function of CG-100 DNA exposed to different magnetic field strengths.

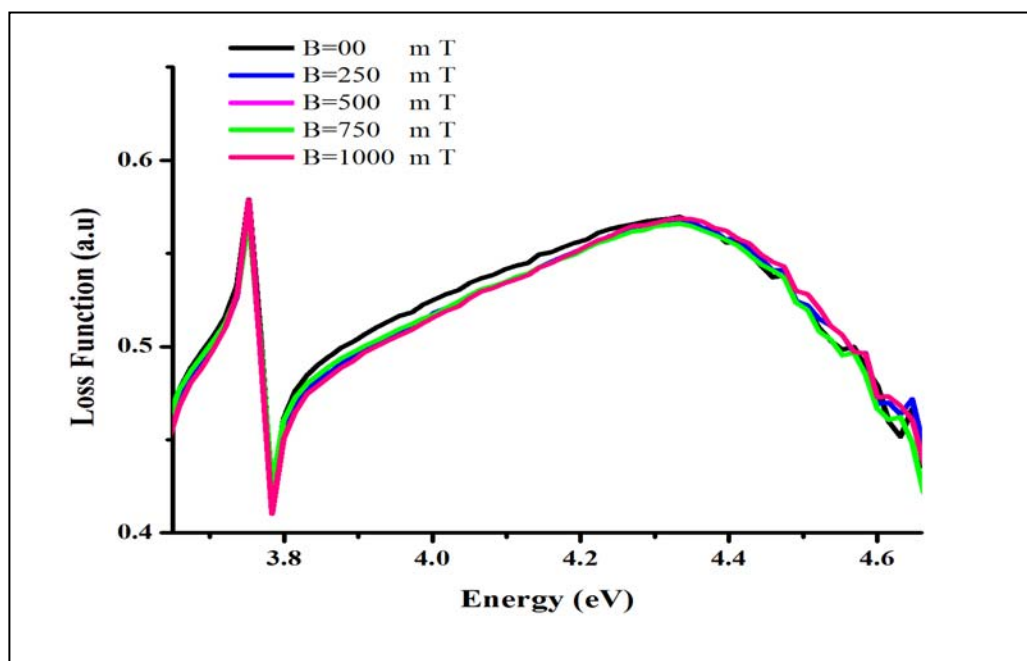


Figure 5.15 Loss function of P-DNA exposed to different magnetic field strengths.

Loss functions of the three samples (AT-100, CG-100 and P-DNA) are depicted in Figures 5.13, 5.14 and 5.15, respectively. The Lorentz fit parameters for the loss functions of three samples (AT-100, CG-100 and P-DNA) are summarised in Table 5-2.

As shown in Table 5-2, the value of  $x_c$  increased slightly with stronger magnetic fields. This change was from  $4.83 \pm 0.01$  to  $4.97 \pm 0.01$  for AT-100 and from  $4.84 \pm 0.01$  to  $4.87 \pm 0.01$  for CG-100. The  $x_c$  value for P-DNA decreased slightly from  $4.62 \pm 0.01$  to  $4.61 \pm 0.01$ . Peak width value,  $w$ , also increased, and the peak was broader after the exposure to high magnetic field of 1000 mT. This change was from  $1.8 \pm 0.3$  to  $1.8 \pm 0.3$  for AT-100 and from  $8.7 \pm 0.3$  to  $10.1 \pm 0.9$  for CG-100. Increase in the  $w$  value for P-DNA ( $2.9 \pm 0.3$  to  $3.4 \pm 0.8$ ), was greater than that for AT and CG.

Table 5-2 Lorentz fit parameters for the loss function of AT-100, CG-100 and P-DNA.

<b>Magnetic Field</b>	<b>Lorentz Parameter</b>	<b>AT-100</b>	<b>CG-100</b>	<b>P-DNA</b>
B=0 mT	$x_c$	$4.83 \pm 0.01$	$4.84 \pm 0.01$	$4.62 \pm 0.01$
	w	$1.8 \pm 0.3$	$8.7 \pm 0.3$	$2.9 \pm 0.3$
B=250 mT	$x_c$	$4.83 \pm 0.01$	$4.84 \pm 0.01$	$4.61 \pm 0.01$
	w	$1.8 \pm 0.3$	$8.5 \pm 0.3$	$3.6 \pm 0.3$
B=500 mT	$x_c$	$4.85 \pm 0.01$	$4.84 \pm 0.01$	$4.62 \pm 0.01$
	w	$2.1 \pm 0.3$	$8.8 \pm 0.3$	$2.0 \pm 0.3$
B=750 mT	$x_c$	$4.84 \pm 0.01$	$4.86 \pm 0.01$	$4.62 \pm 0.01$
	w	$1.9 \pm 0.3$	$9.7 \pm 0.3$	$2.0 \pm 0.3$
B=1000 mT	$x_c$	$4.97 \pm 0.01$	$4.87 \pm 0.01$	$4.61 \pm 0.01$
	w	$4.1 \pm 0.3$	$10.1 \pm 0.8$	$3.4 \pm 0.8$

The peak width increased when the DNA samples were exposed to large magnetic field. The harmonic vibrations between atoms and molecules were disturbed by the large magnetic field creating non equilibrium condition. After switching off the magnetic field, the vibration returned to new equilibrium states due to the changes spring constants of these systems. This increased the width of the peak. These results are explained based on the Lorentz model for increase in band width.



### 5.1.2 Raman spectroscopy

Raman spectroscopy is a powerful technique to observe vibrational modes in a system. A 514 nm Raman analysis was performed to investigate the magnetic field effects on DNA strands. To increase and enhance the Raman signals, a thin layer of gold of approximately 80 nm thickness was deposited on a silicon surface before coating DNA (Yu, Guan, Qin et al., 2008). Figures 5.16, 5.17 and 5.18 compare the Raman spectra of AT-100, CG-100 and P-DNA before and after magnetic field exposure (at approximately 1000 mT).

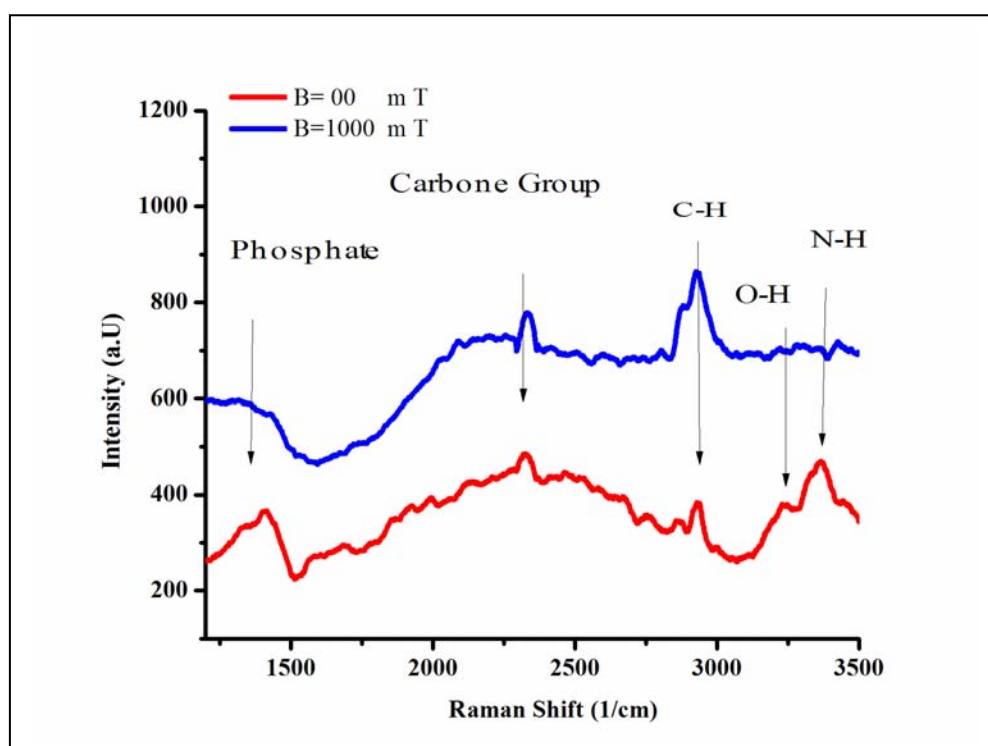


Figure 5.16 Comparison of the Raman spectra of AT-DNA before and after exposure to magnetic field.

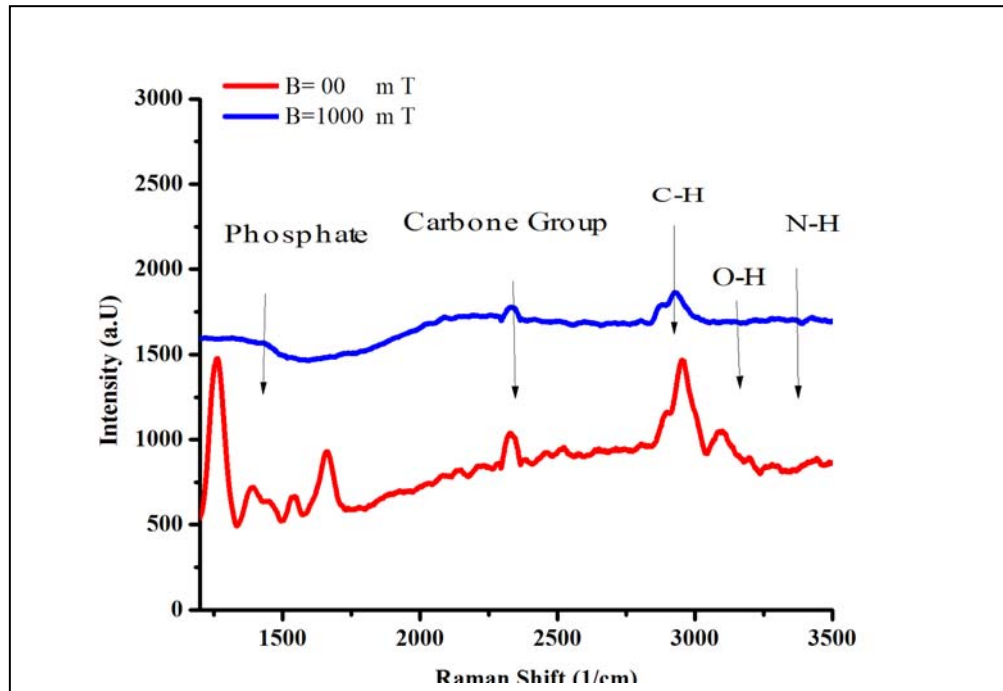


Figure 5.17 Comparison of the Raman spectra of CG-DNA before and after exposure to magnetic field.

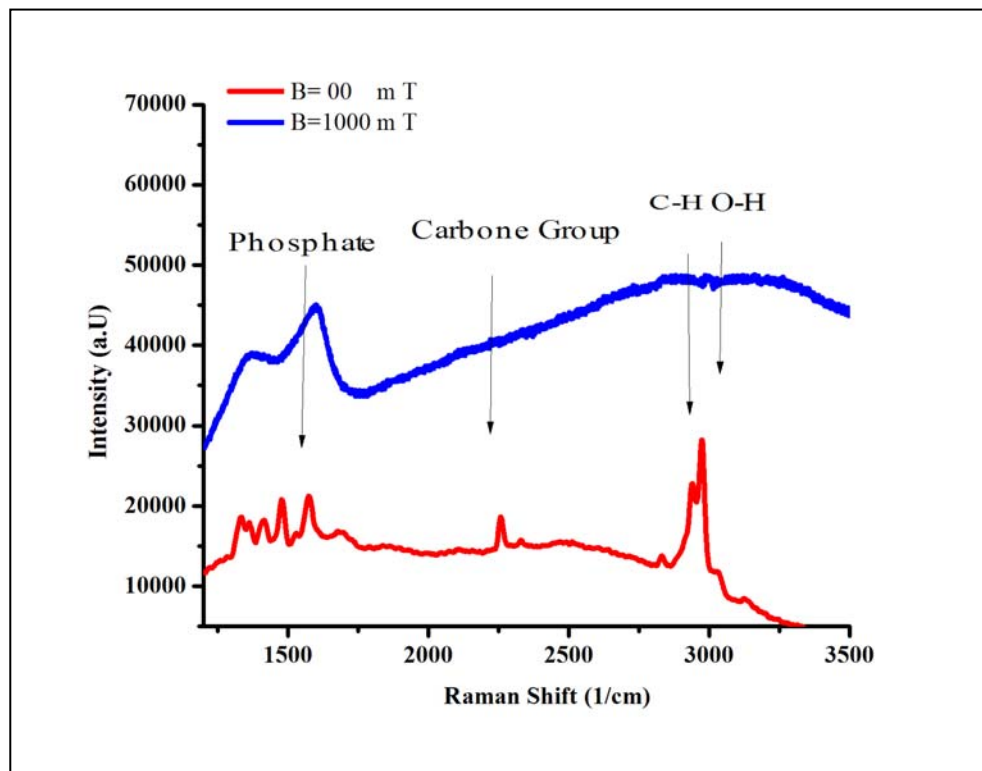


Figure 5.18 Comparison of the Raman spectra of P-DNA before and after exposure to magnetic field.

Figures 5.16, 5.17 and 5.18 show that the intensity of peak in the 3000–3500  $\text{cm}^{-1}$  region representing hydrogen bonds which decreased significantly after exposure to magnetic fields. Indeed, hydrogen bonds are the main feature of the chemical structure of biomolecules measurable by Raman spectroscopy. Hydrogen bond intensity decreased in the three samples but was stronger in P-DNA than in the other two samples.

The hydrogen bonds between two strands decreased in the case of P-DNA. This decrease is related to the breaking of the hydrogen bonding between the two stands (Faulkner and Macrae, 2006). Although AT-100 and CG-100 are single-stranded DNA and P-DNA is double-stranded, the hydrogen bonds decreased because of cleavage as a result of scission in either the 3'-PO or the 5'-PO. The hydroxide that was activated in the magnetic field attacked the phosphate group; continuation of the process being promoted by the removed group.

$\text{PO}_2$  has an asymmetric stretching vibration mode at  $1221\text{cm}^{-1}$ . The  $892\text{cm}^{-1}$  vibration meanwhile belongs to the sugar-phosphate stretch (Alex and Dupuis, 1989). For symmetric phosphate vibrations at  $1221\text{cm}^{-1}$ , there is a shift towards the high frequency direction in P-DNA. The intensity of this peak for AT-100 and CG-100 decreased at approximately  $1230\text{-}1240\text{cm}^{-1}$  (Nafisi, Kahangi, Azizi et al., 2007; Nafisi and Norouzi, 2009). Changes observed in the bands represented a type of scission in either the 3'-PO or the 5'-PO and a conformational change (Neault, Naoui, Manfait et al., 1996; Alex and Dupuis, 1989). Interactions between biological samples and a static magnetic field occur via bound ion dynamics. Magnetic exposure increases the electrostatic charge in hydrogen bonds at base pairs and the polarities of DNA. Increasing the strength of a magnetic field induces charge accumulation and larger

electrostatic polarities. Different charges in the segments impose a Columbic force and increase the strengths of the magnetic field-induced Lorentz force. The oscillation of a bound ion about its binding portion in a signalling molecule can affect the vibrational frequency. In addition, increases in the magnetic field increases the Columbic force and breaks the hydrogen-bond network, thus increasing the number of double helix that split and break.

### 5.1.3 Resistivity

Electrical resistivity is a property of ionic solutions that depends on the charge and ion status in diluted DNA samples. It should be noted that the concentration is the same for all samples. To investigate the variation in resistivity after exposure to magnetic field, the effect of four magnetic field strengths (250, 500, 750 and 1000 mT) on diluted DNA was measured. Figures 5.19, 5.20 and 5.21 show the resistivity of AT-100, CG-100 and P-DNA, respectively, when exposed to magnetic fields. All figures show decrease in the resistivity of DNA when exposed to magnetic fields.

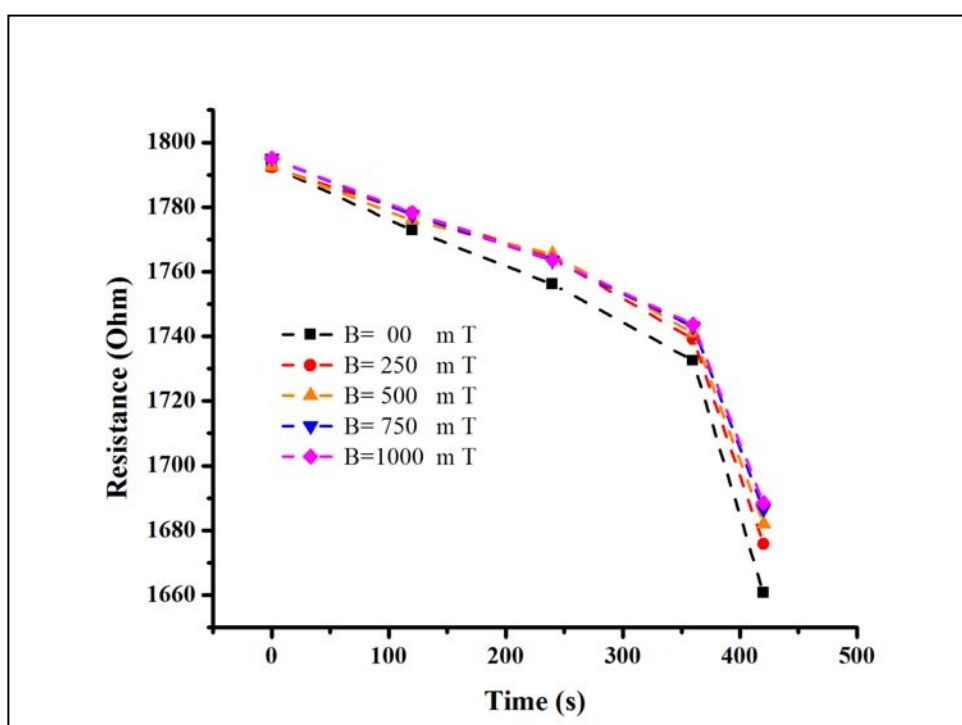


Figure 5.19 Resistivity of AT-DNA exposed to magnetic fields.

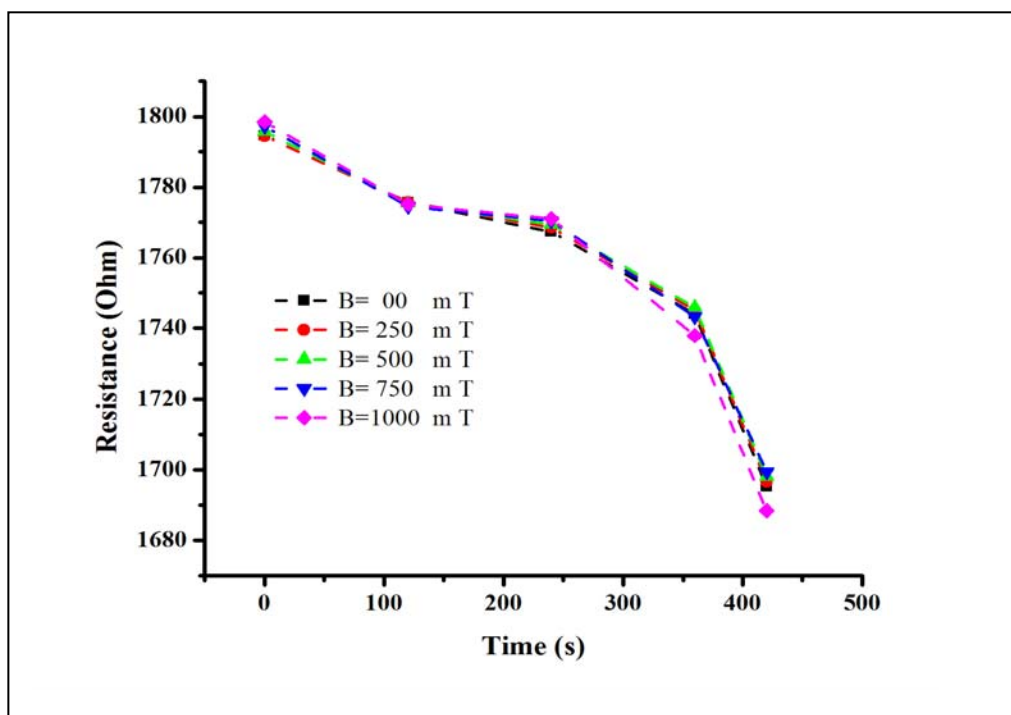


Figure 5.20 Resistivity of CG-DNA exposed to magnetic fields.

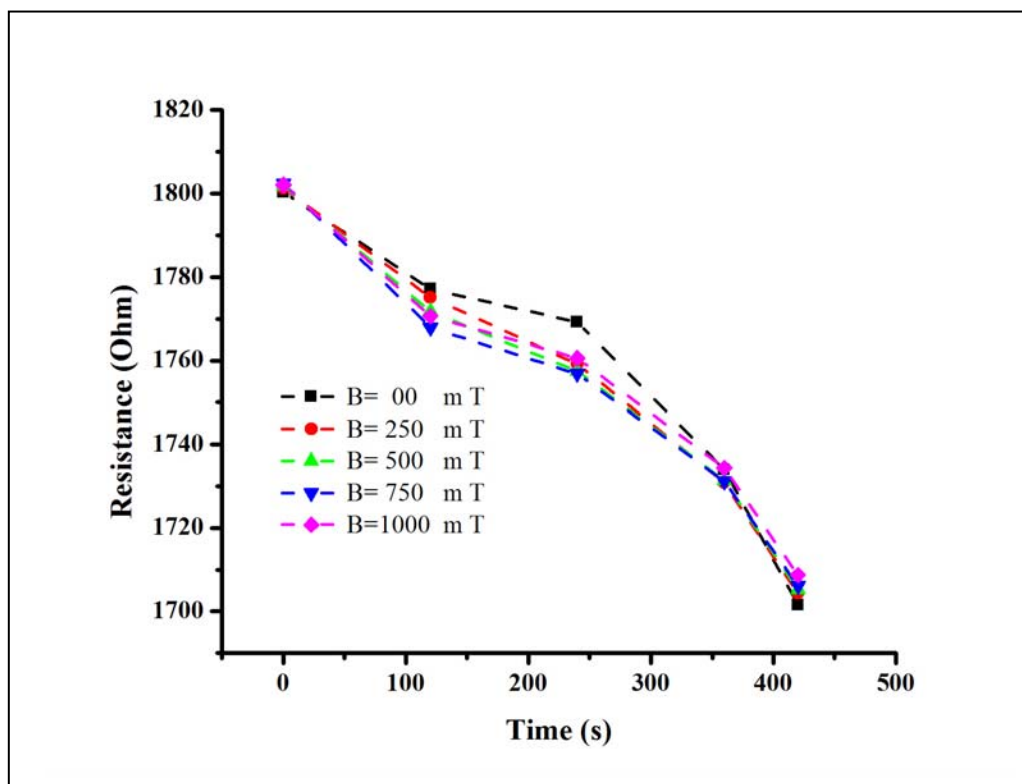


Figure 5.21 Resistivity of P-DNA exposed to magnetic fields.

There is an exponential decrease in resistivity, which is fitted by Eq 5.7. The variation in energy caused by the magnetic field exposure,  $\Delta(B)$ , that results from the Effect is approximately  $1.02 \times 10^{-4} \text{ eV} \cdot k_B T$  (which is the thermal energy or Boltzmann constant times temperature), or approximately 0.0256 eV.

Increasing the magnetic field applied to the three samples allows the resistivity to be determined. The resistivity is not strong because of the low energy of the magnetic field effect.

Eq 5.7 
$$R(B) \propto \exp(\Delta(B)/k_B T)$$

Table 5-3 Statistical regression analysis of the resistivity of AT-100 A exposed to various magnetic fields.

Magnetic Field	Trend Line Parameter	Coefficients	p-Value
B=0 mT	Intercept	$(1.80 \pm 0.02) \times 10^3$	$3.25 \times 10^{-6}$
	X Variable 1	$2.67 \times 10^{-1}$	0.37
B=250 mT	Intercept	$(1.80 \pm 0.02) \times 10^3$	$2.55 \times 10^{-6}$
	X Variable 1	$2.39 \times 10^{-1}$	0.40
B=500 mT	Intercept	$(1.80 \pm 0.07) \times 10^3$	$2.04 \times 10^{-6}$
	X Variable 1	$2.25 \times 10^{-1}$	0.38
B=750 mT	Intercept	$(1.80 \pm 0.01) \times 10^3$	$1.51 \times 10^{-6}$
	X Variable 1	$2.22 \times 10^{-1}$	0.31
B=1000 mT	Intercept	$(1.80 \pm 0.01) \times 10^3$	$1.40 \times 10^{-6}$
	X Variable 1	$2.19 \times 10^{-1}$	0.30

Table 5-4 Statistical regression analysis of the resistivity of CG-100 exposed to various magnetic fields.

Magnetic Field	Trend Line Parameter	Coefficients	p-Value
B=0 mT	Intercept	$(1.80 \pm 0.01) \times 10^3$	$1.07 \times 10^{-6}$
	X Variable 1	$2.03 \times 10^{-1}$	0.29
B=250 mT	Intercept	$(1.80 \pm 0.01) \times 10^3$	$1.11 \times 10^{-6}$
	X Variable 1	$2.00 \times 10^{-1}$	0.31
B=500 mT	Intercept	$(1.80 \pm 0.01) \times 10^3$	$1.06 \times 10^{-6}$
	X Variable 1	$1.98 \times 10^{-1}$	0.30
B=750 mT	Intercept	$(1.80 \pm 0.01) \times 10^3$	$8.74 \times 10^{-7}$
	X Variable 1	$2.02 \times 10^{-1}$	0.25
B=1000 mT	Intercept	$(1.80 \pm 0.01) \times 10^3$	$1.39 \times 10^{-6}$
	X Variable 1	$2.28 \times 10^{-1}$	0.27

Table 5-5 Statistical regression analysis of the resistivity of P-DNA exposed to various magnetic fields.

Magnetic Field	Trend Line Parameter	Coefficients	p-Value
B=0 mT	Intercept	$(1.80 \pm 0.01) \times 10^3$	$3.97 \times 10^{-7}$
	X Variable 1	$2.17 \times 10^{-1}$	0.96
B=250 mT	Intercept	$(1.80 \pm 0.05) \times 10^3$	$7.85 \times 10^{-8}$
	X Variable 1	$2.17 \times 10^{-1}$	0.21
B=500 mT	Intercept	$(1.80 \pm 0.09) \times 10^3$	$3.25 \times 10^{-7}$
	X Variable 1	$2.12 \times 10^{-1}$	0.88
B=750 mT	Intercept	$(1.80 \pm 0.06) \times 10^3$	$9.18 \times 10^{-8}$
	X Variable 1	$2.09 \times 10^{-1}$	0.27
	Intercept	$(1.80 \pm 0.06) \times 10^3$	$1.01 \times 10^{-7}$

B=1000 mT	X Variable 1	$2.03 \times 10^{-1}$	0.32
-----------	--------------	-----------------------	------

Tables 5-3, 5-4 and 5-5 indicate the statistical regression analysis used to find the coefficient parameters and p-values. The intercept p-values for AT-100, CG-100 and P-DNA are in the order of  $10^{-6}$ , which is less than 0.05 show a valuable range for analysis. The p-values indicate that there is a meaningful relationship between the resistivity and the magnetic field exposure time. The acceleration of charge carries causing an increase in temperature after magnetic field exposure. Errors in this measurement are in the order of  $10^{-9}$  based on the accuracy of the instrument.

#### 5.1.4 Temperature

The effects of magnetic fields on DNA temperature were investigated to understand ionic motion. Temperature increases as the ionic motion in a magnetic field increases the kinetic energy. The temperature variation for different magnetic fields was measured for all the three samples before and after four different magnetic field exposure times; 100 s, 200 s, 300 s and 400 s. As shown in Figures 5.22, 5.23 and 5.24, the maximum variation recorded was approximately 2.5-3.8°C (all sample was placed in cryostat cylinder to shield environment effect and temperatureAs shown as Figures 3-10, 3-11).

However this temperature was not significant enough to change the optical density and break the double-stranded DNA. Double-stranded DNA can divide into two strands at a critical temperature of approximately 95°C. The increased temperature found in this experiment was not enough to cleave the DNA stands. Maximum temperature during 400 s of magnetic field exposure for the three samples of DNA used in this work was evaluated. Temperature of AT-100, CG-100 and P-DNA increased by 2.5, 3 and 3.8°C, respectively. Such



conditions can occur when the temperature increases, causing the ionic side of DNA to move faster and faster due to the Lorentz force and hydrodynamic interactions, as described in Eq 5.8.

$$\text{Eq 5.8} \quad \mathbf{F} = (\mathbf{F}_M + \mathbf{F}_D) = \frac{d}{dt}(m\mathbf{V}), K = \frac{1}{2}mV^2 = KT$$

$F_m$  and  $F_D$  are the Lorentz and the hydrodynamic forces, respectively, of the ions exposed to a magnetic field.  $K$  is the kinetic energy while  $m$  and  $v$  are the mass and velocity of the ions respectively. The Boltzmann constant and the temperature is represented by  $K$  and  $T$ , respectively. Then, the nuclei can release energy and increase the temperature.

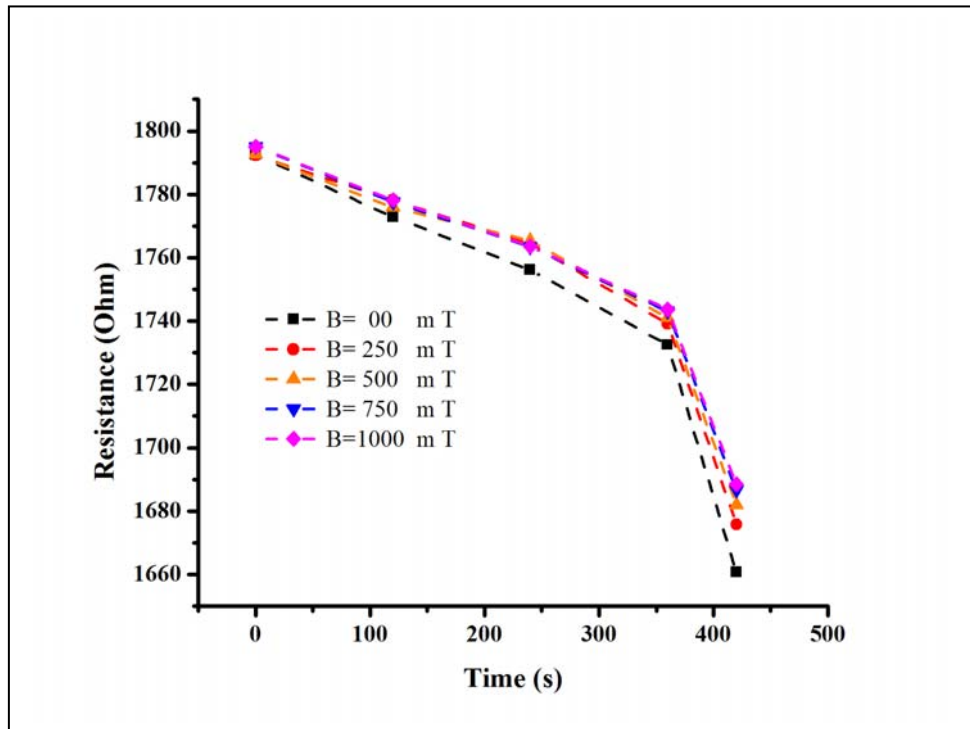


Figure 5.22 Temperature of AT-DNA exposed to magnetic fields.

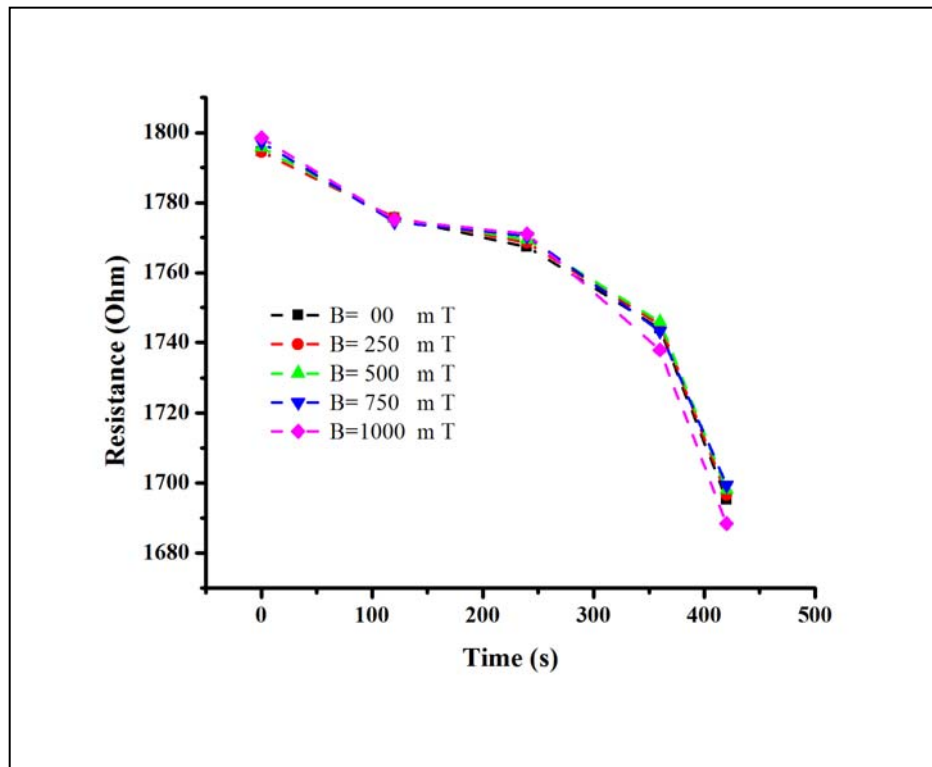


Figure 5.23 Temperature of CG-DNA exposed to magnetic fields.

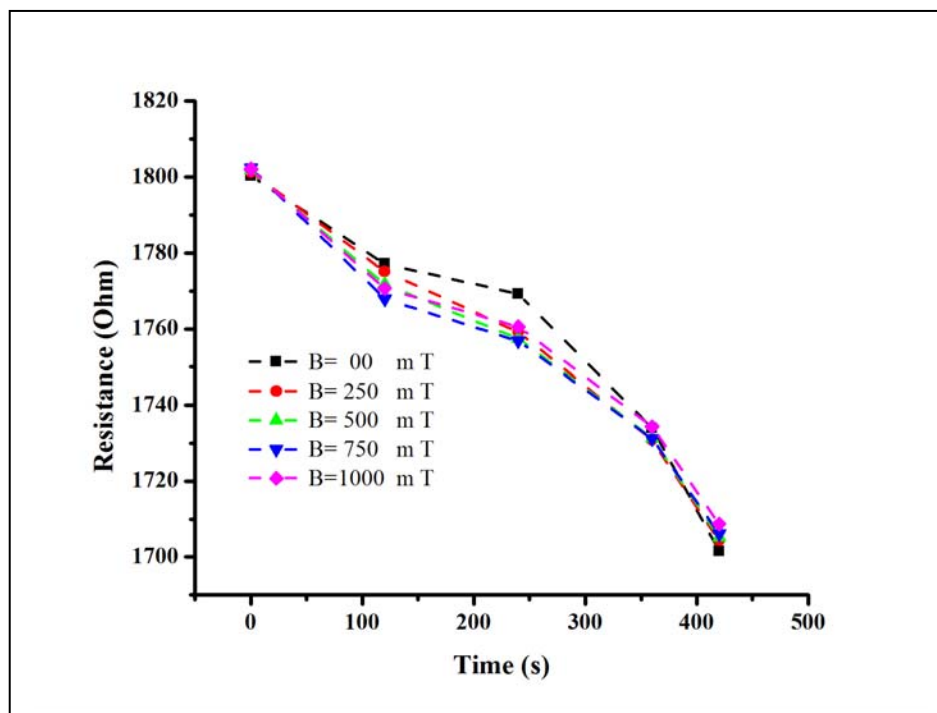


Figure 5.24 Temperature of P-DNA exposed to magnetic fields.

Table 5-6 Statistical regression analysis of the temperature of AT-100 exposed to various magnetic fields.

<b>Magnetic Field</b>	<b>Trend Line Parameter</b>	<b>Coefficients</b>	<b>p-Value</b>
B=0 mT	Intercept	$(2.39 \pm 0.01) \times 10^1$	$5.62 \times 10^{-7}$
	X Variable 1	$4.94 \times 10^{-3}$	0.29
B=250 mT	Intercept	$(2.39 \pm 0.01) \times 10^1$	$3.05 \times 10^{-7}$
	X Variable 1	$4.97 \times 10^{-3}$	0.15
B=500 mT	Intercept	$(2.39 \pm 0.01) \times 10^1$	$2.19 \times 10^{-7}$
	X Variable 1	$5.15 \times 10^{-3}$	0.10
B=750 mT	Intercept	$(2.39 \pm 0.09) \times 10^1$	$1.52 \times 10^{-7}$
	X Variable 1	$5.16 \times 10^{-3}$	0.71
B=1000 mT	Intercept	$(2.39 \pm 0.08) \times 10^1$	$1.10 \times 10^{-7}$
	X Variable 1	$5.52 \times 10^{-3}$	0.42

Table 5-7 Statistical regression analysis of the temperature of CG-100 exposed to various magnetic fields.

<b>Magnetic Field</b>	<b>Trend Line Parameter</b>	<b>Coefficients</b>	<b>p-Value</b>
B=0 mT	Intercept	$(2.43 \pm 0.03) \times 10^1$	$4.22 \times 10^{-6}$
	X Variable 1	$8.56 \times 10^{-3}$	0.43
B=250 mT	Intercept	$(2.42 \pm 0.02) \times 10^1$	$2.25 \times 10^{-6}$
	X Variable 1	$6.82 \times 10^{-3}$	0.45
B=500 mT	Intercept	$(2.43 \pm 0.04) \times 10^1$	$1.17 \times 10^{-6}$
	X Variable 1	$5.34 \times 10^{-3}$	0.30
B=750 mT	Intercept	$(2.44 \pm 0.03) \times 10^1$	$6.94 \times 10^{-6}$
	X Variable 1	$5.16 \times 10^{-3}$	0.26
B=1000 mT	Intercept	$(2.43 \pm 0.03) \times 10^1$	$4.22 \times 10^{-6}$
	X Variable 1	$8.56 \times 10^{-3}$	0.43

Table 5-8 Statistical regression analysis of the temperature of P-DNA exposed to various magnetic fields.

Magnetic Field	Trend Line Parameter	Coefficients	p-Value
B=0 mT	Intercept	$(2.40 \pm 0.02) \times 10^1$	$4.14 \times 10^{-6}$
	X Variable 1	$6.74 \times 10^{-3}$	0.82
B=250 mT	Intercept	$(2.40 \pm 0.02) \times 10^1$	$2.36 \times 10^{-6}$
	X Variable 1	$7.71 \times 10^{-3}$	0.32
B=500 mT	Intercept	$(2.39 \pm 0.02) \times 10^1$	$1.51 \times 10^{-6}$
	X Variable 1	$8.37 \times 10^{-3}$	0.16
B=750 mT	Intercept	$(2.41 \pm 0.01) \times 10^1$	$7.13 \times 10^{-7}$
	X Variable 1	$8.32 \times 10^{-3}$	0.81
B=1000 mT	Intercept	$(2.42 \pm 0.02) \times 10^1$	$1.26 \times 10^{-6}$
	X Variable 1	$9.60 \times 10^{-3}$	0.59

Table 5-6, 5-7 and 5-8 show the statistical regression analysis of the temperature versus duration of magnetic field exposure to 250, 500, 750 and 1000 mT. These data are also shown in Figures 5.22, 5.23 and 5.24.

The p-values in the table show that there is a meaningful relationship between the temperature and the magnetic field exposure time. Intercept p-values for AT-100, CG-100 and P-DNA are in the order of  $10^{-6}$ . Error values in these measurements are in the order of  $10^{-2}$  based on the accuracy of the instrument.

## CHAPTER VI: CONCLUSIONS AND FUTURE WORKS

### 6.1 Introduction

The effects of magnetic fields of different strengths on plant based DNA strands and oligonucleotide DNA were investigated in this work. DNA and oligonucleotides of A-T and C-G were exposed to magnetic fields of different strengths (0, 250, 500, 750 and 1000 mT) prior to characterizations done using UV-Vis and Raman spectroscopy techniques along with investigation on the resistivity and temperature profiles. The results were analysed from the biological and Physics perspectives.

#### 6.1.1 Biological perspective

Analysis done from the biological perspectives based on the effects of magnetic field strengths on DNA showed these results:

- ❑ The effect of magnetic fields on DNA purity is not significant.
- ❑ Magnetic field exposure increases the extinction coefficient of DNA strands and decreases the extinction coefficient of oligonucleotide DNA.
- ❑ Magnetic field exposure decreases the optical density of the three types of DNAs used in this work.
- ❑ Magnetic field exposure increases the wavelength of the DNA absorption peak.

A significant observation obtained from these results showed that the magnetic field exposure increased the DNA temperature and altered the extinction coefficient. This significant influence of magnetic field resulted in significant changes on DNA structure. Exposure to external magnetic field not only broke the double-strand DNA into single strands but also cut

double- and single-stranded DNA into smaller lengths. However, these effects did not change the purity of the DNA.

#### 6.1.2 Physics perspective

Analysis done from the Physics perspectives based on the effects of magnetic field strengths on DNA showed these results:

- ❑ Magnetic fields strength above 750 mT increased the band gap of DNA.
- ❑ Magnetic fields strength above 750 mT changed the real part of the refractive index of DNA by increasing and decreasing the index for wavelengths below and above the absorption maximum respectively. Magnetic field strengths above 750 mT decreased the imaginary part of the refractive index of DNA.
- ❑ Magnetic field strengths above 750 mT significantly affected the hydrogen bonds in the DNA helix.
- ❑ Resistivity of the three types of DNAs exposed to magnetic field decreased.
- ❑ The variation of DNA temperature exposed to external magnetic field ranged from about 2-3.5°C in 10 minutes.
- ❑ The effect of magnetic field effect on the band gap of DNA became significant above 750 mT.

The results generally indicated that the effect of exposing DNA strands and oligonucleotides to magnetic fields became significant for field strengths above 750 mT. Band gap and refractive index changed because the electronic orbital overlap decreased as a result of breakage of the DNA strands and the splitting of energy levels after exposure to magnetic field. Results from Raman spectroscopy, resistivity measurements and temperature monitoring were

comparable to those from UV-Vis spectroscopy for increasing magnetic field intensities. Resistivity of the three types of DNAs exposed to magnetic fields decreased due to division of the DNAs into smaller parts with cleavage occurring at the ionic part. The ionic part increased conductivity and decreased resistivity. Magnetic field increased charge acceleration and the resulting collisions increased the temperature. The DNA temperature variation as a result of exposure to magnetic field was approximately 2 to 3.5°C within 10 minutes. The effect of the magnetic field was evident in the Raman spectra as observed by the disappearance or reduction of the hydrogen bond peaks. This was in total agreement with the UV-Vis spectrum. Cleavage of DNA strands and the breaking of the hydrogen bonds between the two strands also corroborated with the UV-Vis and Raman spectra. Results show that the magnetic field can be a useful tool for DNA analysis and manipulation and therefore can be utilised to capture and analyse nanomaterials. The results also show that the characterization and analysis carried out can be a useful technique to evaluate environmental effect on biomolecules such as DNA. Refractive index and band gap variation not only extend the application of DNA in Physics and electronics but also opens up an avenue for possible utilizations in biomedicine.

### 6.1.3 Future works

In the past few decades, applications of DNA (both as strands and oligonucleotides) in Physics and as electronic devices have attracted significant attention. Biological applications of this smart material also increased as a result of this. The results achieved in this work, not only improved and modified the previous applications of DNA as a smart material, but also have provided a new perspective and highlighted more applications of DNA in

Physics and electronics. Temperature, resistivity and magnetic field sensors using DNA as sensing material coupled to fibre optic sensors and microarray structures are some possible interesting applications. Figure 6.1 summarises the various potential applications of DNA that can be investigated for future works based on the results and analysis done from both the Physics and biological perspectives. Potential applications of this material are in electronic devices such as sensors, arrays and other hybrid materials. The biological applications of DNA can be further improved and previous applications can be promoted to extend the capability of this material.

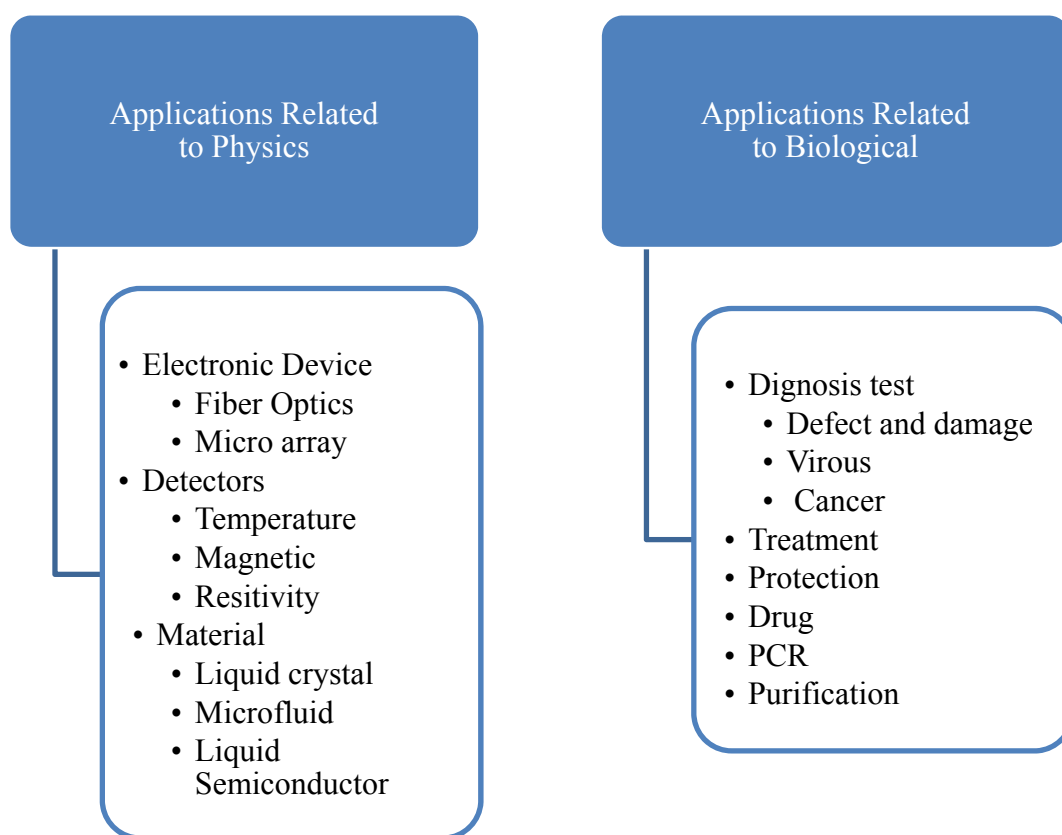


Figure 6.1 Potential applications of DNA strands and oligonucleotides in Physics and Biology

## APPENDIX A



## 6.2 Light as an electromagnetic wave motion

An electromagnetic wave (EM-wave) is built up of oscillating electric and magnetic fields. The waves oscillate in space and carries energy from one place to another. Electric and magnetic field can be described as a harmonic wave in the form:

$$\text{Eq 6.1} \quad \vec{E} = E_0 \cdot e^{i(\vec{k} \cdot \vec{r} - \omega t)}$$

$$\text{Eq 6.2} \quad \vec{B} = B_0 \cdot e^{i(\vec{k} \cdot \vec{r} - \omega t)}$$

The electric field  $\vec{E}$ , magnetic field,  $\vec{B}$  and propagation vector  $\vec{k}$ , are always mutually perpendicular).  $E_0$  and  $B_0$  represent their amplitudes,  $\vec{r}$  the position and  $\omega$  the angular frequency. If the wave is viewed at a fixed time, the relation between the spatial wavelength,  $\lambda$  and the propagation constant  $k$  can be found.

$$\text{Eq 6.3} \quad k = \frac{2\pi}{\lambda}$$

When viewing the wave at a fixed position, it is periodic in time with a period,  $T$ . The relation between the propagation constant  $k$ , period  $T$  and the wave velocity  $v$ , is:

$$\text{Eq 6.4} \quad kvT = 2\pi$$

Both  $\vec{E}$  and  $\vec{B}$  satisfies a differential equation of the form:

Eq 6.5

$$\nabla^2 E = \left( \frac{1}{c^2} \right) \frac{\partial^2 E}{\partial t^2}$$

In a direct band material, both the conduction band minimum and the valence band minimum occur at the zone centre where  $k = 0$ .

In a indirect band gap material, the conduction band minimum does not occur at  $k = 0$ , but is usually at the zone edge or close to it. The optical absorption coefficient  $\alpha \propto W_{i \rightarrow f}$  transition rate (**Fermi's golden rule**).

Where

- the matrix element  $M$ ,
- the density of states  $g(h\omega)$  (Eq 7.6) .

Eq 6.6

$$\alpha(\hbar\omega) \propto W_{i \rightarrow f} = \frac{2\pi}{h} |M|^2 g(h\omega).$$

$$M = \langle f | H' | i \rangle = \int \psi_f^*(\vec{r}) H' \psi_i(\vec{r}) d^3\vec{r}$$

Eq 6.7

$$H' = -\vec{p}_e \cdot \vec{E}_{photon}, \vec{p}_e = -e\vec{r}$$

Eq 6.8

$$\vec{E}_{photon}(\vec{r}) = \vec{E}_0 e^{\pm i\vec{k} \cdot \vec{r}}, H'(\vec{r}) = e\vec{E}_0 \cdot \vec{r} e^{\pm i\vec{k} \cdot \vec{r}}$$

Eq 6.9

$$\psi_i(\vec{r}) = \frac{1}{\sqrt{V}} u_i(\vec{r}) e^{i\vec{k}_i \cdot \vec{r}}, \psi_f(\vec{r}) = \frac{1}{\sqrt{V}} u_f(\vec{r}) e^{i\vec{k}_f \cdot \vec{r}},$$

Eq 6.10

$$\psi_i(\vec{r}) = \frac{1}{\sqrt{V}} u_i(\vec{r}) e^{i\vec{k}_i \cdot \vec{r}}$$

Eq 6.11

$$g(E)dE = 2g(k)dk, \quad g(E)dE = 2g(k)dk$$

Eq 6.12

$$g(E) = \frac{2g(k)}{dE/dk}, \quad g(k)dk = \frac{1}{(2\pi)^3} 4\pi k^2 dk \Rightarrow g(k) = \frac{k^2}{2\pi^2}$$

Eq 6.13

$$|M| \propto \int_{unit \quad cell} u_f^*(\vec{r}) x u_i(\vec{r}) d^3\vec{r}$$

Eq 6.14

$$M = \frac{e}{V} \int u_f^*(\vec{r}) e^{-i\vec{k} \cdot \vec{r}} (\vec{E}_0 \cdot \vec{r} e^{\pm i\vec{k} \cdot \vec{r}}) u_i(\vec{r}) e^{i\vec{k} \cdot \vec{r}} d^3\vec{r},$$

*Conservation of momentum demand :*

$$\hbar \vec{k}_f - \hbar \vec{k}_i = \pm \hbar \vec{k}.$$

Band gap calculation:

Eq 6.15

$$E_c(k) - E_v(k)$$

Eq 6.16

$$\alpha(\hbar\omega) \propto W_{i \rightarrow f} = \frac{2\pi}{\hbar} |M|^2 g(\hbar\omega).$$

Eq 6.17

$$g(\hbar\omega) = 0 \quad \text{for } \hbar\omega < E_g,$$

$$g(\hbar\omega) = \frac{1}{2\pi^2} \left( \frac{2\mu}{\hbar} \right)^{\frac{3}{2}} (\hbar\omega - E_g)^{\frac{1}{2}} \quad \text{for } \hbar\omega \geq E_g.$$

Eq 6.18

$$g(E) = \frac{1}{2\pi^2} \left( \frac{2m^*}{\hbar} \right)^{\frac{3}{2}} E^{\frac{1}{2}}.$$

Eq 6.19

$$\text{For } \hbar\omega < E_g, \quad \alpha(\hbar\omega) = 0.$$

$$\text{For } \hbar\omega > E_g, \quad \alpha(\hbar\omega) \propto (\hbar\omega - E_g)^{\frac{1}{2}}.$$

Eq 6.20

$$g(\hbar\omega) = 0 \quad \text{for } \hbar\omega < E_g,$$

$$g(\hbar\omega) = \frac{1}{2\pi^2} \left( \frac{2\mu}{\hbar} \right)^{\frac{3}{2}} (\hbar\omega - E_g)^{\frac{1}{2}} \quad \text{for } \hbar\omega \geq E_g.$$

Eq 6.21

$$g(E) = \frac{2g(k)}{dE/dk},$$

$$g(k)dk = \frac{1}{(2\pi)^3} 4\pi k^2 dk \Rightarrow g(k) = \frac{k^2}{2\pi^2}$$

Eq 6.22

$$E_e(k) = E_g + \frac{\hbar^2 k^2}{2m_e^*}$$

$$E_{hh}(k) = -\frac{\hbar^2 k^2}{2m_{hh}^*}$$

$$E_{lh}(k) = -\frac{\hbar^2 k^2}{2m_{lh}^*}$$

$$E_{so}(k) = -\Delta - \frac{\hbar^2 k^2}{2m_{so}^*}$$

Eq 6.23

$$\hbar\omega = E_C(k) - E_V(k)$$

$$= E_g + \frac{\hbar^2 k^2}{2m_e^*} + \frac{\hbar^2 k^2}{2m_{h(l)h}^*}$$

$$= E_g + \frac{\hbar^2 k^2}{2\mu}$$

$$\text{where } \frac{1}{\mu} = \frac{1}{m_e^*} + \frac{1}{m_{h(l)h}^*}$$

Eq 6.24

$$E_C(k) - E_V(k) = E_g + \frac{\hbar^2}{2} \left( \eta_1 \frac{k_x}{m_x^*} + \eta_2 \frac{k_y}{m_y^*} + \eta_3 \frac{k_z}{m_z^*} \right),$$

$$\eta_1, \eta_2, \eta_3 = +1 \text{ or } -1.$$

## APPENDIX B

### 7.1 Kubelka-Munk

Kubelka-Munk is a two-flux version of the radiative transfer function where the illumination and scattering is completely isotropic.

Derivation of the Kubelka-Munk theory

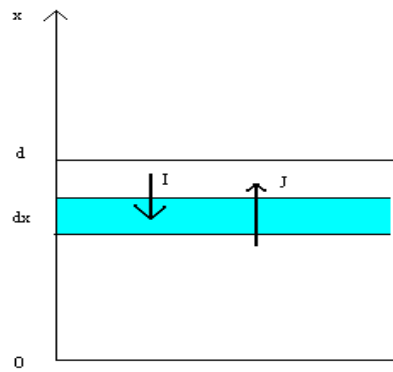


Figure 7.1 Two fluxes which are completely diffuse. One in the positive x-direction,  $J$ , and one in the negative x-direction,  $I$ .

During passage through the layer  $dx$ , some of the light will be scattered and absorbed so that  $i$  and  $j$  will be reduced at the same time. The part that was reduced from  $I$  will be added to  $J$  and vice versa. The total change in light intensity can therefore be written for both directions as.

$$\text{Eq 7.1} \quad -dI = -k_{KM}I dx + s_{KM}J dx - s_{KM}I dx$$

$$\text{Eq 7.2} \quad dJ = -k_{KM}J dx - s_{KM}J dx + s_{KM}I dx$$

$s_{KM}$  is the light scattering coefficient in  $m^2/kg$  and  $k_{KM}$  is the absorption coefficient in  $m^2/kg$ .

The mean path length for diffuse flux is 2 times the linear path length.

The Kubelka- Munk equations for diffuse light is

$$\text{Eq 7.3} \quad -dI = -k_{KM} 2I dx + s_{KM} 2J dx - s_{KM} 2I dx$$

$$\text{Eq 7.4} \quad dJ = -k_{KM} 2J dx - s_{KM} 2J dx + s_{KM} 2I dx$$

Setting  $K=2 k_{KM}$  and  $S=2 s_{KM}$  and re-arranging terms gives

$$\text{Eq 7.5} \quad -\frac{dI}{dx} = -(k + s)I + sJ, \frac{dJ}{dx} = -(K + S)J + SI$$

$$\text{Eq 7.6} \quad \frac{S + J}{S} = a, -\frac{dI}{Sdx} = -aI + J, \frac{dJ}{Sdx} = -aJ + I$$

$$\text{Eq 7.7} \quad \frac{J}{I} = r, dr = d\left(\frac{J}{I}\right) = \frac{idj - jdi}{i^2}$$

The approximation that light intensity is diffuse in both directions gives the relation for reflectance over the differential layer  $dx$ .

$$\text{Eq 7.8} \quad \frac{dr}{Sdx} = r^2 - 2ar + 1 \Rightarrow \int_{R_g}^R \frac{dr}{r^2 - 2ar + 1} = S \int_0^w dx$$

$$\text{Eq 7.9} \quad \ln \frac{(R - a - \sqrt{a^2 - 1})(R_g - a + \sqrt{a^2 - 1})}{(R_g - a - \sqrt{a^2 - 1})(R - a + \sqrt{a^2 - 1})} = 2Sd\sqrt{a^2 - 1}$$

$$\text{Eq 7.10} \quad R_\infty = \frac{1}{a + \sqrt{a^2 - 1}} = a - \sqrt{a^2 - 1} = 1 + \frac{K}{S} - \sqrt{\frac{K^2}{S^2} + 2\frac{K}{S}}$$

The reflectance for an opaque bulk can be determined by considering an infinitely thick layer,  $d = \infty$ . Solving the equation for a finite layer gives

$$R = \frac{(1/R_{\infty})(R_g - R_{\infty}) - R_{\infty}(R_g - 1/R_{\infty})\exp(Sd(1/R_{\infty} - R_{\infty}))}{(R_g - R_{\infty}) - (R_g - 1/R_{\infty})\exp(Sd(1/R_{\infty} - R_{\infty}))}$$

Eq 7.11

$R_0$  is the reflectance of the sample over an ideally black background, ( $R_g=0$ ).

If one assumes that  $R_g=0$ .

$$R_0 = \frac{\exp(Sd(1/R_{\infty} - R_{\infty})) - 1}{(1/R_{\infty})\exp(Sd(1/R_{\infty} - R_{\infty})) - R_{\infty}}$$

Eq 7.12

Solving for  $S$  and by using the relation  $K=2 k_{KM}$  and  $S=2 s_{KM}$ .

$$s_{KM} = \frac{R_{\infty}}{d(1 - R_{\infty}^2)} \ln \left( \frac{(R_{\infty} - R_g)(R_{\infty} - R_g)}{(1 - R_g R_{\infty})(R_{\infty} - R)} \right)$$

Eq 7.13

$k_{KM}$  can then be calculated using the relationship

$$\frac{k_{KM}}{s_{KM}} = \frac{(1 - R_{\infty})^2}{2R_{\infty}}$$

Eq 7.14

If the material is completely homogeneous, it is possible to use grammage,  $w$ , instead of  $d$ .

## APPENDIX C

### 8.1 Kramers-Kronig Relations

#### 8.1.1 Refractive indices

Refractive indices describe the ratio of velocity  $c$  of an electromagnetic wave to its velocity in vacuum  $c_0$ . It describes the optical response of the material to the incident EM-wave and is a property of the medium.

Eq 8.1

$$n = \frac{c}{c_0}$$

If the reflecting surface is metallic, the refraction index becomes a complex number.

##### 8.1.1.1 Pseudo refractive indices

If the material has an conductivity  $\sigma$ , the E-field creates a current density  $J$  ( $A/m^2$ ). This is described by Ohm's law.

Eq 8.2

$$\vec{J} = \sigma \cdot \vec{E}$$

With Maxwell's relations, it can be shown that the conductivity leads to a modification of equation (2.5) [2]. This leads to a differential equation described by

Eq 8.3

$$\nabla^2 E = \left( \frac{1}{c^2} \right) \cdot \frac{\partial^2 E}{\partial t^2} + \left( \frac{\sigma}{\epsilon_0 c^2} \right) \frac{\partial E}{\partial t}$$



By combining the E-field as a harmonic wave with the differential equation, it can be seen that the propagation vector,  $k$ , must be complex:

Eq 8.4

$$\vec{k} = \frac{\omega}{c} \left[ 1 + i \left( \frac{\sigma}{\epsilon_0 \omega} \right) \right]^{\frac{1}{2}}$$

The refractive index on the complex form can be derived as

Eq 8.5

$$\vec{n} = \left[ 1 + i \left( \frac{\sigma}{\epsilon_0 \omega} \right) \right]^{\frac{1}{2}}$$

The refractive index can be written in general form:

Eq 8.6

$$n = n_r + n_i$$

where the real part,  $\text{Re}(n) = n_r$  behave as the ordinary refractive index and the imaginary part,  $\text{Im}(n) = n_i$  determines the rate of absorption,  $\alpha$ , in the conductive medium.

Eq 8.7

$$\alpha = \frac{4\pi n_i}{\lambda}$$

The imaginary part, also known as extinction coefficient, is related to the damping of the oscillation amplitude of the incident field.

A non-metallic material (dielectric) is a low absorbing material and the imaginary part is small and often neglected. If the material is conductive, the imaginary part is larger and must be taken into account.

The amplitude reflectance ( $r$ ) under irradiation and energy reflectance ( $R$ ) determined directly from the specular reflection spectrum are expressed by the following equations:

$$\text{Eq 8.8} \quad r = \sqrt{R}e^{i\varphi} = \sqrt{R}(\cos \varphi + i\sin \varphi) = \frac{n-ik-1}{n-ik+1}$$

$$\text{Eq 8.9} \quad R = |r|^2 = r \cdot r^* = \frac{(n-1)^2 - k^2}{(n+1)^2 - k^2}$$

Where,  $\varphi$  is the phase change. This results because both reflection and absorption occur at the sample surface.  $r^*$  is the complex conjugate of  $r$ . Dividing Equation 9.8 into real and imaginary parts and solving for  $n$  and  $k$  yields the following equations:

$$\text{Eq 8.10} \quad n = \frac{1-R}{1+R-2\sqrt{R}\cos\varphi}$$

$$\text{Eq 8.11} \quad k = \frac{-2\sqrt{R}}{1+R-2\sqrt{R}\cos\varphi}$$

Taking the logarithm of Equation (1), gives

$$\text{Eq 8.12} \quad \ln r = \ln \sqrt{R} + i\varphi$$

However,  $\sqrt{R}$  and  $\varphi$  are not independent, but linked by Kramer's-Kronig relationship:

$$\text{Eq 8.13} \quad \varphi(\vartheta_g) = \frac{2}{\pi} \int_0^\infty \frac{\ln \sqrt{\vartheta_g R(\vartheta)}}{\vartheta^2 - \vartheta_g^2} d\vartheta$$

If the energy reflectance is measured across the entire wavenumber range, the phase change  $\varphi(\text{vg})$  can be calculated at any required wavenumber

vg using this relational expression, and then the optical constants n and k can be determined from Equations 9.12 and 9.13. Consequently, by calculating k at constant wavenumber intervals across the normal infrared range between 4600 and 400 cm<sup>-1</sup> for example, an absorbance coefficient spectrum equivalent to the transmission spectrum can be calculated from the specular reflection spectrum.

In the integration of Equation 9.13, a pole exists at  $\nu = \nu_g$  but several methods have been proposed to handle this integration. Two typical methods are the Maclaurin method and the double Fourier transform method. In the Maclaurin method, the phase change  $\phi(\nu_g)$  is given by Equation 9.14

$$\text{Eq 8.14} \quad \phi(\vartheta_g) = \frac{2\vartheta_g}{\pi} 2h \sum \frac{\text{Ln}\sqrt{R(\vartheta_i)}}{\vartheta^2 - \vartheta_g^2} \quad h = \vartheta_{j+1} - \vartheta_j$$

$j = 2, 4, 6, \dots, g-1, g+1, \dots$  (if g is an odd number)

$j = 1, 3, 5, \dots, g-1, g+1, \dots$  (if g is an even number)

The  $\nu_j$  start point is set so that  $\nu = \nu_g$  does not occur and alternate data points are used. With the double Fourier transform method,  $\phi(\nu_g)$  is determined by Equation 9.14, a double Fourier transformation which is an approximation of Equation 9.15.

$$\text{Eq} \quad 8.15$$

$$\phi(\vartheta_g) = 4 \int_0^\infty \text{Cos}(2\pi\vartheta_g)dt + \int_0^\infty \text{Ln}\sqrt{R}\text{Sin}(2\pi\vartheta)d\vartheta$$

The Maclaurin method provides better calculation accuracy, but because it is so time-consuming, the quicker double Fourier transformation method is normally used.

## APPENDIX D

### 9.1 Selection rules in Raman spectroscopy

$$\begin{aligned}\langle f | \hat{\mu} | i \rangle &= \langle f | \mu_0 + \alpha E | i \rangle = \langle f | \mu_0 + \left[ \alpha_0 + \left( \frac{\partial \alpha}{\partial x} \right)_0 x + \frac{1}{2} \left( \frac{\partial^2 \alpha}{\partial x^2} \right)_0 x^2 + \dots \right] E | i \rangle \\ &\approx \langle f | \mu_0 + \left[ \alpha_0 + \left( \frac{\partial \alpha}{\partial x} \right)_0 x \right] E | i \rangle = \langle f | \mu_0 | i \rangle + \langle f | \alpha_0 E | i \rangle + \langle f | \left( \frac{\partial \alpha}{\partial x} \right)_0 x E | i \rangle \\ &= 0 + 0 + \left( \frac{\partial \alpha}{\partial x} \right)_0 E \langle f | x | i \rangle = \left( \frac{\partial \alpha}{\partial x} \right)_0 E \langle f | x | i \rangle\end{aligned}$$

## APPENDIX E

### 9.2 The atom mass, charge and position in the DNA bases.

Table 9-1 The atom mass, charge and position in thymine.

		X Y Z			CHARGE		
	ATOMS	(Angstrom)			Nucl	Cor e	Atomic Mass
1	N	1.2529	3.6062	1.5868	7	5	14.0031
2	C	1.2918	6.3617	1.5098	6	4	12
3	N	0.0019	5.7078	1.5689	7	5	14.0031
4	C	0.0709	4.267	1.6196	6	4	12
5	C	2.44	4.2457	1.5142	6	4	12
6	C	2.494	5.6353	1.4782	6	4	12
7	H	3.3496	3.6593	1.4901	1	1	1.0078
8	O	1.326	7.5835	1.4909	8	6	15.9949
9	O	-1.0061	3.5991	1.7007	8	6	15.9949
10	H	-0.5143	5.9603	0.6947	1	1	1.0078
11	C	3.8217	6.3408	1.4082	6	4	12
12	H	4.6683	5.6218	1.3894	1	1	1.0078
13	H	3.9425	6.9996	2.2941	1	1	1.0078
14	H	3.8685	6.9586	0.4868	1	1	1.0078
15	H	1.2489	2.5967	1.6178	1	1	1.0078

Table 9-2 The atom mass, charge and position in Cytosine

	ATOMS	X Y Z			CHARGE		
			(Angstrom)		Nucl	Core	
1	N	-0.1386	-0.5262	-0.0195	7	5	14.0031
2	C	-0.0814	2.2741	-0.0169	6	4	12
3	N	-1.3083	1.5988	-0.0185	7	5	14.0031
4	C	-1.3369	0.1987	-0.0198	6	4	12
5	C	1.0882	0.1491	-0.0179	6	4	12
6	C	1.1168	1.5493	-0.0166	6	4	12
7	N	-0.0788	3.7441	-0.0185	7	5	14.0031
8	H	2.0038	-0.4047	-0.0165	1	1	1.0078
9	H	2.0542	2.0652	-0.0163	1	1	1.0078
10	O	-2.5897	-0.4909	-0.0162	8	6	15.9949
11	H	0.7882	4.2426	-0.0167	1	1	1.0078
12	H	-0.9439	4.2457	-0.016	1	1	1.0078
13	H	-0.1593	-1.536	-0.0205	1	1	1.0078

Table 9-3 The atom mass, charge and position in Adenine.

	ATOMS	X Y Z			CHARGE		
			(Angstrom )		Nucl	Core	Atomic Mass
1	N	0.0691	0.5729	-0.0164	7	7	14.0031
2	C	2.6254	3.081	0.0836	6	6	12
3	N	3.7626	2.3368	0.0662	7	7	14.0031
4	C	3.68	0.997	0.0177	6	6	12
5	N	2.5216	0.2867	-0.0192	7	7	14.0031
6	C	1.3927	0.9981	-0.0018	6	6	12
7	C	1.3884	2.4192	0.0517	6	6	12
8	N	0.1185	2.8767	0.0544	7	7	14.0031
9	C	-0.6451	1.7083	0.0159	6	6	12
10	N	2.71	4.4115	0.1268	7	7	14.0031
11	H	4.6151	0.4358	0.004	1	1	1.0078
12	H	-1.7316	1.7306	0.0104	1	1	1.0078
13	H	3.6333	4.8568	0.1491	1	1	1.0078
14	H	1.8515	4.9729	0.1385	1	1	1.0078



Table 9-4 The atom mass, charge and position in Guanine.

	ATOMS	X Y Z			CHARGE		
			(Angstrom )		Nucl	Cor e	Atomic Mass
1	N	-0.2445	1.8022	0.0362	7	5	14.0031
2	N	3.3546	3.6632	-0.0437	7	5	14.0031
3	C	3.313	2.2133	-0.0067	6	4	12
4	N	2.1226	1.5574	0.1238	7	5	14.0031
5	C	0.9818	2.2546	0.3342	6	4	12
6	C	0.9606	3.6817	0.3163	6	4	12
7	C	2.212	4.3977	0.0726	6	4	12
8	C	-0.9802	2.9325	-0.1202	6	4	12
9	N	-0.2767	4.0881	-0.0053	7	5	14.0031
10	O	2.235	5.6146	-0.0275	8	6	15.9949
11	N	4.4531	1.5025	-0.1446	7	5	14.0031
12	H	-2.0309	2.913	-0.3771	1	1	1.0078
13	H	4.433	0.4582	-0.1352	1	1	1.0078
14	H	5.3717	1.985	-0.2604	1	1	1.0078
15	H	4.2668	4.1493	-0.2006	1	1	1.0078
16	H	-0.5425	0.841	-0.0499	1	1	1.0078

## REFERENCES

- Ahmad, M., Chang, K. P., King, T. A. and Hench, L. L. (2005). A compact fibre-based fluorescence sensor. *Sensors and Actuators, A: Physical*, 119(1), 84-89.
- Ahmadi, S. M., Dehghan, G., Hosseinpourfeizi, M. A., Dolatabadi, J. E. N. and Kashanian, S. Preparation, characterization, and DNA Binding Studies of Water-Soluble Quercetin Molybdenum (VI) Complex. *DNA and Cell Biology*, 30(7), 517-523.
- Alex, Serge and Dupuis, Paul. (1989). FT-IR and Raman investigation of cadmium binding by DNA. *Inorganica Chimica Acta*, 157(2), 271-281.
- Amara, S., Douki, T., Garrel, C., Favier, A., Rhouma, K. B., Sakly, M. and Abdelmelek, H. Effects of static magnetic field and cadmium on oxidative stress and DNA damage in rat cortex brain and hippocampus. *Toxicology and Industrial Health*, 27(2), 99-106.
- Amara, S., Douki, T., Garrel, C., Favier, A., Rhouma, K. B., Sakly, M. and Abdelmelek, H. (2011). Effects of static magnetic field and cadmium on oxidative stress and DNA damage in rat cortex brain and hippocampus. *Toxicology and Industrial Health*, 27(2), 99-106.
- Arbona, J. M., Aime, J. P. and Elezgaray, J. (2012). Folding of small origamis. *The Journal of Chemical Physics*, 136, 3682472-3682479.
- Atkins, Peter William and Friedman, Ron S. (1997). *Molecular quantum mechanics*, New York: Oxford University Press, Oxford.
- Banks, D. (2006). *Microengineering, MEMS, and interfacing: A practical guide*, 199, United State: CRC Press.
- Barnothy, Madeleine F. (1964). *Biological effects of magnetic fields*, New York: Plenum Press.

- Batson, PE and Silcox, J. (1983). Experimental energy-loss function,  $\text{Im} [-1/\epsilon(q, \omega)]$ , for aluminum. *Physical Review B*, 27(9), 5224–5239.
- Blackman, CF, Benane, SG, Rabinowitz, JR, House, DE and Joines, WT. (1985). A role for the magnetic field in the radiation-induced efflux of calcium ions from brain tissue in vitro. *Bioelectromagnetics*, 6(4), 327-337.
- Bodega, G., Forcada, I., Suárez, I. and Fernández, B. (2005). Acute and chronic effects of exposure to a 1mT magnetic field on the cytoskeleton, stress proteins, and proliferation of astroglial cells in culture. *Environmental Research*, 98(3), 355-362.
- Bosch, M. E., Sanchez, A. J. R., Rojas, F. S. and Ojeda, C. B. (2007). Recent development in optical fiber biosensors. *Sensors*, 7(6), 797-859.
- Bosch, M. E., Sánchez, A. J. R., Rojas, F. S. and Ojeda, C. B. (2007). Optical chemical biosensors for high throughput screening of drugs. *Combinatorial Chemistry and High Throughput Screening*, 10(6), 413-432.
- Brandes, Rolf and Kearns, David R. (1986). Magnetic ordering of DNA liquid crystals. *Biochemistry*, 25(20), 5890-5895.
- Braun, E., Eichen, Y., Sivan, U. and Ben-Yoseph, G. (1998). DNA-templated assembly and electrode attachment of a conducting silver wire. *Nature*, 391(6669), 775-778.
- Campàs, M. and Katakis, I. (2004). DNA biochip arraying, detection and amplification strategies. *TrAC - Trends in Analytical Chemistry*, 23(1), 49-62.
- Cantor, C. R., Warshaw, M. M. and Shapiro, H. (1970). Oligonucleotide interactions. III. Circular dichroism studies of the conformation of deoxyoligonucleolides. *Biopolymers*, 9(9), 1059-1077.

- Cavaluzzi, M. J. and Borer, P. N. (2004). Revised UV extinction coefficients for nucleoside-5' monophosphates and unpaired DNA and RNA. *Nucleic Acids Research*, 32(1), 1-9.
- Chen, H., Fu, H., Zhu, X., Cong, P., Nakamura, F. and Yan, J. (2011). Improved high-force magnetic tweezers for stretching and refolding of proteins and short DNA. *Biophysical Journal*, 100(2), 517-523.
- Collings, AF and Caruso, Frank. (1997). Biosensors: Recent advances. *Reports on Progress in Physics*, 60(11), 1397-1445.
- Cuniberti, Gianaurelio, Maciá, E, Rodriguez, A and Römer, RA. (2007). Tight-binding modeling of charge migration in DNA devices. *Charge Migration in DNA*, 1-20.
- Davidson, Michael W, Strzelecka, Teresa E and Rill, Randolph L. (1988). Multiple liquid crystal phases of DNA at high concentrations. *Nature*, 331, 457-460.
- Dobson, Jon. (2008). Remote control of cellular behaviour with magnetic nanoparticles. *Nature Nanotechnology*, 3(3), 139-143.
- Dunn, David A, Lin, Vivian H and Kochevar, Irene E. (1992). Base-selective oxidation and cleavage of DNA by photochemical cosensitized electron transfer. *Biochemistry*, 31(46), 11620-11625.
- El-Bialy, N. S. and Rageh, M. M. (2013). Extremely low-frequency magnetic field enhances the therapeutic efficacy of low-dose cisplatin in the treatment of ehrlich carcinoma. *BioMed Research International*, 2013, 1-7.
- Eldashev, I. S., Shchegolev, B. F., Surma, S. V. and Belostotskaya, G. B. (2010). Influence of low-intensity magnetic fields on the development of satellite muscle cells of a newborn rat in primary culture. *Biophysics*, 55(5), 765-770.

- Elson, E. (2009). I. the little explored efficacy of magnetic fields in cancer treatment and postulation of the mechanism of action. *Electromagnetic Biology and Medicine*, 28(3), 275-282.
- Emura, R., Ashida, N., Higashi, T. and Takeuchi, T. (2001). Orientation of Bull Sperms in Static Magnetic Fields. *Bioelectromagnetics*, 22(1), 60-65.
- Epstein, J. R., Biran, I. and Walt, D. R. (2002). Fluorescence-based nucleic acid detection and microarrays. *Analytica Chimica Acta*, 469(1), 3-36.
- Faulkner, C. and Macrae, R. (2006). A DFT Study of Hydrogen Bonding Between Adenine and Thymine. *Proceedings of The Science, Engineering and Mathematics Conference*, University of Evansville, 1-11.
- Fox, M. A. (1966). Biological effects of magnetic fields. *Bulletin of Mathematical Biology*, 28(1), 137-138.
- Gamboa, O. L., Gutierrez, P. M., Alcalde, I., De la Fuente, I. and Gayoso, M. J. (2007). Absence of relevant effects of 5 mT static magnetic field on morphology, orientation and growth of a rat Schwann cell line in culture. *Histology and Histopathology*, 22(7-9), 777-780.
- Ghasemifard, Mahdi, Zavar, Matineh, Ghasemifard, Hadi and Aliabad, Hossein Asghar Rahnamaye. (2010). The effect of temperature dependences on optical properties of PMN-PZT nano-powders. *Journal of Optics*, 39(4), 157-166.
- Haber, Charbel and Wirtz, Denis. (2000). Magnetic tweezers for DNA micromanipulation. *Review of Scientific Instruments*, 71(12), 4561-4570.
- Houssier, Glaude and Kuball, Hans-G. (1971). Electro-optical properties of nucleic acids and nucleoproteins III. Kramers-Kronig relationships in linear birefringence and dichroism. Application to a DNA–proflavine complex. *Biopolymers*, 10(12), 2421-2433.

- Ichioka, S., Minegishi, M., Iwasaka, M., Shibata, M., Nakatsuka, T., Harii, K., Kamiya, A. and Ueno, S. (2000). High intensity static magnetic fields modulate skin microcirculation and temperature in vivo. *Bioelectromagnetics*, 21(3), 183-188.
- Iguchi, Kazumoto. (2001). Semiconductivity and band gap of a double strand of DNA. *Journal of the Physics Society Japan*, 70(2), 593-597.
- Iwasaka, Masakazu and Ueno, Shoogo. (1998). Optical measurements of magnetophoresis of macromolecules. *Magnetics, IEEE Transactions on*, 34(4), 2129-2131.
- Jajte, Jolanta, Zmyslony, Marek, Palus, Jadwiga, Dziubaltwska, Elzbieta and Rajkowska, Elzbieta. (2001). Protective effect of melatonin against in vitro iron ions and 7 mT 50 Hz magnetic field induced DNA damage in rat lymphocytes. *Mutation Research/Fundamental and Molecular Mechanisms of Mutagenesis*, 483(1), 57-64.
- Jangir, Deepak Kumar, Dey, Sanjay Kumar, Kundu, Suman and Mehrotra, Ranjana. (2012). Assessment of amsacrine binding with DNA using UV/visible, circular dichroism and Raman spectroscopic techniques. *Journal of Photochemistry and Photobiology B: Biology*, 14, 38-43.
- Jiang, Y. X., Lei, J. T. and Gao, X. F. (2006). Application of optical fiber DNA biosensor. *Chinese Journal of Clinical Rehabilitation*, 10(41), 152-154.
- Kawanishi, Shosuke, Hiraku, Yusuke and Oikawa, Shinji. (2001). Mechanism of guanine-specific DNA damage by oxidative stress and its role in carcinogenesis and aging. *Mutation Research/Reviews in Mutation Research*, 488(1), 65-76.
- Ke, W. Z., Yu, D. W., Gu, B. P. and Zhuang, Z. W. (2001). Raman Spectroscopic Study of Microscopic Damage on the Space Structure of DNA with Acetic Acid. *Guang Pu Xue Yu Guang Pu Fen Xi/Spectroscopy and Spectral Analysis*, 21(6), 792-793.

- Khatir, N. M., Banihashemian, S. M., Periasamy, V., Abd Majid, W. H. and Rahman, S. A. (2012). Current-Voltage Characterization on Au-DNA-Au Junctions under the Influence of Magnetic Field. *Advanced Materials Research*, 535, 1350-1353.
- Khatir, N. M., Banihashemian, S. M., Periasamy, V., Ritikos, R., Abd Majid, W. H. and Rahman, S. A. (2012). Electrical Characterization of Gold-DNA-Gold Structures in Presence of an External Magnetic Field by Means of I-V Curve Analysis. *Sensors*, 12(3), 3578-3586.
- Khatir, N. M., Banihashemian, S. M., Periasamy, V., Abd Majid, W. H. and Rahman, S. A. (2012). DNA Strand Patterns on Aluminium Thin Films. *Sensors*, 11(7), 6719-6727.
- Kim, Jiyeon, Ha, Chang Seung, Lee, Hae June and Song, Kiwon. (2010). Repetitive exposure to a 60-Hz time-varying magnetic field induces DNA double-strand breaks and apoptosis in human cells. *Biochemical and Biophysical Research Communications*, 400(4), 739-744.
- Kimura, T., Takahashi, K., Suzuki, Y., Konishi, Y., Ota, Y., Mori, C., Ikenaga, T., Takanami, T., Saito, R., Ichiishi, E., Awaji, S., Watanabe, K. and Higashitani, A. (2008). The effect of high strength static magnetic fields and ionizing radiation on gene expression and DNA damage in *Caenorhabditis elegans*. *Bioelectromagnetics*, 29(8), 605-614.
- Kirschvink, Joseph L, Kobayashi-Kirschvink, Atsuko and Woodford, Barbara J. (1992). Magnetite biomineralization in the human brain. *Proceedings of the National Academy of Sciences*, 89(16), 7683-7687.
- Lai, Henry and Singh, Narendra P. (2004). Magnetic-field-induced DNA strand breaks in brain cells of the rat. *Environmental Health Perspectives*, 112(6), 687-694.
- Lan, Guo-Yu, Chen, Wei-Yu and Chang, Huan-Tsung. (2011). One-pot synthesis of fluorescent oligonucleotide Ag nanoclusters for specific and

sensitive detection of DNA. *Biosensors and Bioelectronics*, 26(5), 2431-2435.

Lee, Byung-Cheon, Johng, Hyeon-Min, Lim, Jae-Kwan, Jeong, Ji Hoon, Baik, Ku Youn, Nam, Tae Jeong, Lee, Jung Ho, Kim, Jungdae, Sohn, Uy Dong, Yoon, Gilwon, Shin, Sanghoon and Soh, Kwang-Sup. (2004). Effects of extremely low frequency magnetic field on the antioxidant defense system in mouse brain: a chemiluminescence study. *Journal of Photochemistry and Photobiology B: Biology*, 73(1-2), 43-48.

Leszczynski, D. (2005). Rapporteur report: Cellular, animal and epidemiological studies of the effects of static magnetic fields relevant to human health. *Progress in Biophysics and Molecular Biology*, 87(2-3), 247-253.

Leuba, S. H., Wheeler, T. B., Cheng, C. M., LeDuc, P. R., Fernandez-Sierra, M. and Quiaones, E. (2009). Structure and dynamics of single DNA molecules manipulated by magnetic tweezers and or flow. *Methods*, 47(3), 214-222.

Lin-Vien, Daimay. (1991). *The handbook of infrared and Raman characteristic frequencies of organic molecules*. San Diego: Academic Press.

Lin, L. and Jiang, L. (2001). Molecule recognition and transducer technology of DNA. *Chemistry Bulletin/Huaxue Tongbao*, 64(5), 261-267.

Lindqvist, Martina and Graslund, Astrid. (2001). An FTIR and CD study of the structural effects of G-tract length and sequence context on DNA conformation in solution. *Journal of Molecular Biology*, 314(3), 423-432.

Lionnet, T., Allemand, J. F., Revyakin, A., Strick, T. R., Saleh, O. A., Bensimon, D. and Croquette, V. (2012). Single-molecule studies using magnetic traps. *Cold Spring Harbor Protocols*, 1, 133-138.



- Liu, X. and Tan, W. (1999). A fiber-optic evanescent wave DNA biosensor based on novel molecular beacons. *Analytical Chemistry*, 71(22), 5054-5059.
- Mallidis, C., Wistuba, J., Bleisteiner, B., Damm, O. S., Groß, P., Wbbeling, F., Fallnich, C., Burger, M. and Schlatt, S. (2011). In situ visualization of damaged DNA in human sperm by Raman microspectroscopy. *Human Reproduction*, 26(7), 1641-1649.
- Manosas, M., Meglio, A., Spiering, M. M., Ding, F., Benkovic, S. J., Barre, F. X., Saleh, O. A., Allemand, J. F., Bensimon, D. and Croquette, V. (2010). Chapter Thirteen-Magnetic Tweezers for the Study of DNA Tracking Motors. *Methods in Enzymology*, 475, 297-320.
- Marazuela, M. D. and Moreno-Bondi, M. C. (2002). Fiber-optic biosensors - An overview. *Analytical and Bioanalytical Chemistry*, 372(5-6), 664-682.
- Martins, S. A. M., Prazeres, D. M. F., Fonseca, L. P. and Monteiro, G. A. (2010). Optimization of DNA hybridization on aminopropyl-controlled pore-glass particles: Detection of non-labeled targets by picogreen staining. *Analytical Letters*, 43(17), 2694-2704.
- McNamee, J. P., Bellier, P. V., McLean, J. R. N., Marro, L., Gajda, G. B. and Thansandote, A. (2002). DNA damage and apoptosis in the immature mouse cerebellum after acute exposure to a 1 mT, 60 Hz magnetic field. *Mutation Research/Genetic Toxicology and Environmental Mutagenesis*, 513(1-2), 121-133.
- Mehrvar, M., Bis, C., Scharer, J. M., Moo-Young, M. and Luong, J. H. (2000). Fiber-optic biosensors - Trends and advances. *Analytical Sciences*, 16(7), 677-692.
- Minaichev, EV, Myasishcheva, GG, Obukhov, Yu V, Roganov, VS, Savel'Ev, GI and Firsov, VG. (1970). Paschen--Back Effect for the muonium atom. *Journal of Experimental and Theoretical Physics*, 58, 1586-1592.

- Miyakoshi J, Yoshida M, Shibuya K, Hiraoka M. (2000). Exposure to strong magnetic fields at power frequency potentiates X-ray-induced DNA strand breaks. *J Radiation Research*, 41(3), 293-302.
- Miyakoshi, Junji. (2006). The review of cellular effects of a static magnetic field. *Science and Technology of Advanced Materials*, 7(4), 305-307.
- Moore, R. L. (1979). Biological effects of magnetic fields: studies with microorganisms. *Canadian Journal of Microbiology*, 25(10), 1145-1151.
- Morii, Nahoko, Kido, Giyuu, Suzuki, Hiroyuki, Nimori, Shigeki and Morii, Hisayuki. (2004). Molecular chain orientation of DNA films induced by both the magnetic field and the interfacial effect. *Biomacromolecules*, 5(6), 2297-2307.
- Mosconi, F., Allemand, J. F., Bensimon, D. and Croquette, V. (2009). Measurement of the torque on a single stretched and twisted DNA using magnetic tweezers. *Physical Review Letters*, 102(7), 78301-78304.
- Nafisi, Shohreh, Kahangi, Fatemeh Ghoreyshi, Azizi, Ebrahim, Zebarjad, Nader and Tajmir-Riahi, Heidar-Ali. (2007). Interaction of zanamivir with DNA and RNA: Models for drug DNA and drug RNA bindings. *Journal of Molecular Structure*, 830(1-3), 182-187.
- Nafisi, Shohreh and Norouzi, Zeinab. (2009). A Comparative Study on the Interaction of Cis-and Trans-Platin with DNA and RNA. *DNA and Cell Biology*, 28(9), 469-477.
- Neault, J. F., Naoui, M., Manfait, M. and Tajmir-Riahi, H. A. (1996). Aspirin-DNA interaction studied by FTIR and laser Raman difference spectroscopy. *FEBS Letters*, 382(1-2), 26-30.
- Niederberger, C. (2012). Re: In situ visualization of damaged DNA in human sperm by raman microspectroscopy. *Journal of Urology*, 187(3), 995.

- Niederberger, C. (2013). Re: Oxidative DNA damage in human sperm can be detected by Raman microspectroscopy. *Journal of Urology*, 189(5), 1841.
- Nielsen, Peter E, Jeppesen, Claus, Egholm, Michael and Buchardt, Ole. (1988). Photochemical cleavage of DNA by nitrobenzamides linked to 9-aminoacridine. *Biochemistry*, 27(17), 6338-6343.
- Ohmi, Tadahiro. (1996). Total room temperature wet cleaning for Si substrate surface. *Journal of The Electrochemical Society*, 143(9), 2957-2964.
- Pan, H. and Liu, X. (2004). Apparent Biological Effect of Strong Magnetic Field on Mosquito Egg Hatching. *Bioelectromagnetics*, 25(2), 84-91.
- Peng, H. and Ling, X. S. (2009). Reverse DNA translocation through a solid-state nanopore by magnetic tweezers. *Nanotechnology*, 20(18), 185101-185116.
- Perveen, F., Qureshi, R., Ansari, F. L., Kalsoom, S. and Ahmed, S. (2011). Investigations of drug-DNA interactions using molecular docking, cyclic voltammetry and UV-Vis spectroscopy. *Journal of Molecular Structure*, 1004(1-3), 67-73.
- Peter, C., Meusel, M., Grawe, F., Katerkamp, A., Cammann, K. and Borchers, T. (2001). Optical DNA-sensor chip for real-time detection of hybridization events. *Analytical and Bioanalytical Chemistry*, 371(2), 120-127.
- Pinchuk, A. (2004). Optical constants and dielectric function of DNA's nucleotides in UV range. *Journal of Quantitative Spectroscopy and Radiative Transfer*, 85(2), 211-215.
- Piunno, P. A. E., Hanafi-Bagby, D., Henke, L. and Krull, U. J. (2000). A critical review of nucleic acid biosensor and chip-based oligonucleotide array technologies. *ACS Symposium Series*, 762, 257-291.

- Piunno, P. A. E., Watterson, J., Wust, C. C. and Krull, U. J. (1999). Considerations for the quantitative transduction of hybridization of immobilized DNA. *Analytica Chimica Acta*, 400(1-3), 73-89.
- Potenza, L., Cucchiaroni, L., Piatti, E., Angelini, U. and Dacha, M. (2004). Effects of high static magnetic field exposure on different DNAs. *Bioelectromagnetics*, 25(5), 352-355.
- Potenza, Lucia, Ubaldi, Luca, De Sanctis, Roberta, De Bellis, Roberta, Cucchiaroni, Luigi and DachÃ , Marina. (2004). Effects of a static magnetic field on cell growth and gene expression in Escherichia coli. *Mutation Research/Genetic Toxicology and Environmental Mutagenesis*, 561(1), 53-62.
- Raylman, R. R., Clavo, A. C. and Wahl, R. L. (1996). Exposure to strong static magnetic field slows the growth of human cancer cells in vitro. *Bioelectromagnetics Journal*, 17, 358-363.
- Richards, E. G. and Fasman, G. D. (1975). Handbook of Biochemistry and Molecular Biology. *Nucleic Acids*. Cleveland: *CRC Press*.
- Richter, J., Mertig, M., Pompe, W., Mönch, I. and Schackert, H.K. (2001). Construction of highly conductive nanowires on a DNA template. *Applied Physics Letters*, 78, 536-538.
- Rogers, K. R. (2000). Principles of affinity-based biosensors. *Applied Biochemistry and Biotechnology - Part B Molecular Biotechnology*, 14(2), 109-129.
- Rogers, Kim R, Apostol, Alma, Madsen, Steen and Spencer, Charles W. (2001). Fiber optic biosensor for detection of DNA damage. *Analytica Chimica Acta*, 444(1), 51-60.
- Saito, Samuel T., Silva, Givaldo, Pungartnik, Cristina and Brendel, Martin. (2012). Study of DNA-emodin interaction by FTIR and UV/Vis

- spectroscopy. *Journal of Photochemistry and Photobiology B: Biology*, 111, 59-63.
- Sakurai, T., Terashima, S. and Miyakoshi, J. (2009). Effects of strong static magnetic fields used in magnetic resonance imaging on insulin-secreting cells. *Bioelectromagnetics*, 30(1), 1-8.
- Salerno, D., Brogioli, D., Cassina, V., Turchi, D., Beretta, G. L., Seruggia, D., Ziano, R., Zunino, F. and Mantegazza, F. (2010). Magnetic tweezers measurements of the nanomechanical properties of DNA in the presence of drugs. *Nucleic Acids Research*, 38(20), 7089-7099.
- Sekino, M., Tatsuoka, H., Yamaguchi, S., Eguchi, Y. and Ueno, S. (2006). Effects of strong static magnetic fields on nerve excitation. *IEEE Transactions on Magnetics*, 42(10), 3584-3586.
- Shaw, C.P and Jirasek, A. (2009). The use of ultraviolet resonance raman spectroscopy in the analysis of ionizing-radiation-induced damage in DNA. *Applied Spectroscopy*, 63(4), 412-422.
- Silaghi, S.D. (2005). Optical characterization of DNA bases on silicon surfaces. *PhD. Dissertation*, Germany: University of Technology.
- Singh, T. B., Sariciftci, N. S. and Grote, J. G. (2010). Bio-organic optoelectronic devices using DNA. *Organic Electronics Advances in Polymer Science*, 223, 189-212.
- Slavicek, Petr, Winter, Bernd, Faubel, Manfred, Bradforth, Stephen E and Jungwirth, Pavel. (2009). Ionization energies of aqueous nucleic acids: photoelectron spectroscopy of pyrimidine nucleosides and ab initio calculations. *Journal of the American Chemical Society*, 131(18), 6460-6467.
- Strick, TR, Allemand, JF, Bensimon, D, Bensimon, A and Croquette, V. (1996). The elasticity of a single supercoiled DNA molecule. *Science New York Washington*, 1835-1837.

- Teles, FRR and Fonseca, LP. (2008). Trends in DNA biosensors. *Talanta*, 77(2), 606-623.
- Thachappillya Mukundan, Vineeth, Tran, Quang Minha Nhat and Tuona Phan, Anh. (2013). Connecting magnetic micro-particles with DNA G-quadruplexes. *Soft Matter*, 9(1), 216-223.
- Theodosiou, Eirini and Thomas, Owen RT. (2008). On the application of 'seeding' techniques in the primary separation of plasmid DNA from neutralised E. coli lysates. *Journal of Chemical Technology and Biotechnology*, 83(2), 192-200.
- Thompson, D. G., Enright, A., Faulds, K., Smith, W. E. and Graham, D. (2008). Ultrasensitive DNA detection using oligonucleotide-silver nanoparticle conjugates. *Analytical Chemistry*, 80(8), 2805-2810.
- Tombelli, S., Mascini, M., Sacco, C. and Turner, A. P. F. (2000). A DNA piezoelectric biosensor assay coupled with a polymerase chain reaction for bacterial toxicity determination in environmental samples. *Analytica Chimica Acta*, 418(1), 1-9.
- Toyama, Akira, Miyagawa, Yoko, Yoshimura, Akari, Fujimoto, Naoko and Takeuchi, Hideo. (2001). Characterization of individual adenine residues in DNA by a combination of site-selective C8-deuteration and UV resonance Raman difference spectroscopy. *Journal of Molecular Structure*, 598(1), 85-91.
- Ueno, S. (2012). Studies on magnetism and bioelectromagnetics for 45 years: From magnetic analog memory to human brain stimulation and imaging. *Bioelectromagnetics*, 33(1), 3-22.
- Villarini, Milena, Moretti, Massimo, Scassellati-Sforzolini, Giuseppina, Boccioli, Bruno and Pasquini, Rossana. (2006). Effects of co-exposure to extremely low frequency (50 Hz) magnetic fields and xenobiotics determined in vitro by the alkaline comet assay. *Science of the Total Environment*, 361(1-3), 208-219.

- Vo-Dinh, T, Alarie, JP, Isola, N, Landis, D, Wintenberg, Al L and Ericson, MN. (1999). DNA biochip using a phototransistor integrated circuit. *Analytical Chemistry*, 71(2), 358-363.
- Walt, D. R. (2000). Bead-based fiber-optic arrays. *Science*, 287(5452), 451-452.
- Wang, Hao, Lewis, James P and Sankey, Otto F. (2004). Band-gap tunneling states in DNA. *Physical Review Letters*, 93(1), 016401-016404.
- William Jr, D. (2007). *Materials Science and Engineering: An introduction*. New York: John Wiley & Sons.
- Witten, K. G., Bretschneider, J. C., Eckert, T., Richtering, W. and Simon, U. (2008). Assembly of DNA-functionalized gold nanoparticles studied by UV/Vis-spectroscopy and dynamic light scattering. *Physical Chemistry Chemical Physics*, 10(14), 1870-1875.
- Wolfbeis, O. S. (2004). Fiber-optic chemical sensors and biosensors. *Analytical Chemistry*, 76(12), 3269-3284.
- Xu, D. K., Ma, L. R., Liu, Y. Q., Jiang, Z. H. and Liu, Z. H. (1999). Development of chemiluminescent biosensing of nucleic acids based on oligonucleotide-immobilized gold surfaces. *Analyst*, 124(4), 533-536.
- Yang, Xin, Wang, Xue-Bin, Vorpagel, Erich R and Wang, Lai-Sheng. (2004). Direct experimental observation of the low ionization potentials of guanine in free oligonucleotides by using photoelectron spectroscopy. *Proceedings of the National Academy of Sciences of the United States of America*, 101(51), 17588-17592.
- Yang, Yuanlong, Celmer, Edward J, Koutcher, Jason A and Alfano, RR. (2002). DNA and Protein Changes Caused by Disease in Human Breast Tissues Probed by the Kubelka–Munk Spectral Function. *Photochemistry and Photobiology*, 75(6), 627-632.

- Yiming, Xu, Zhixiang, Zhou, Hongying, Yang, Yan, Xu and Zhiyi, Zhang. (1999). Raman spectroscopic study of microcosmic photodamage of the space structure of DNA sensitized by Yangzhou haematoporphyrin derivative and Photofrin II. *Journal of Photochemistry and Photobiology B: Biology*, 52(1-3), 30-34.
- Yousef, T. A., Abu El-Reash, G. M., El-Gammal, O. A. and Bedier, R. A. (2013). Synthesis, characterization, optical band gap, in vitro antimicrobial activity and DNA cleavage studies of some metal complexes of pyridyl thiosemicarbazone. *Journal of Molecular Structure*, 1035, 307-317.
- Yu, Q., Guan, P., Qin, D., Golden, G. and Wallace, P. M. (2008). Inverted size-dependence of surface-enhanced Raman scattering on gold nanohole and nanodisk arrays. *Nano Letters*, 8(7), 1923-1928.
- Zai Qing, Wen and Thomas G.J, Jr. (1998). UV resonance raman spectroscopy of DNA and protein constituents of viruses: Assignments and cross sections for excitations at 257, 244, 238 and 229 nm. *Biopolymers*, 45(3), 247-256.
- Zborowski, Maciej, Ostera, Graciela R, Moore, Lee R, Milliron, Sarah, Chalmers, Jeffrey J and Schechter, Alan N. (2003). Red blood cell magnetophoresis. *Biophysical Journal*, 84(4), 2638-2645.
- Zhang, G., Zhou, Y., Yuan, J. and Ren, S. (1999). A chemiluminescence fiber-optic biosensor for detection of DNA hybridization. *Analytical Letters*, 32(14), 2725-2736.
- Zhou, J. H., Feng, Y. Y., Wu, X. H., Yang, H., Xing, W. and Lu, T. H. (2005). Study on interaction between CT-DNA and cytochrome C using UV-Vis spectroscopy and electrochemistry. *Spectroscopy and Spectral Analysis*, 25(8), 1306-1308.



